ABSTRACT

POST-CRACKING TENSILE PROPERTIES OF ADVANCED CEMENTITIOUS MATERIALS AND DUCTILITY OF HIGH PERFORMANCE CONCRETE BEAMS

by
Wonsiri Punurai

In present direct tension tests, the complete stress-deformation curves, the resulting energy dissipated by damage, and the fracture energy of different types of cementitious composites, namely plain concrete, high strength concrete, normal fibrous concrete, high strength fibrous concrete, are studied and a ductility factor is calculated. It has been found that with the increasing strength of concrete due to the addition of the pozzolans such as silica fume and fly ash and when changing from normal strength to high strength, concrete ductility decreases. However, when fibers are combined with these matrices, concrete ductility increases. It is because of ductile steel fibers and the brittle plain concrete matrix affects the post-peak response of unreinforced composite specimens loaded in tension after exceeding the peak tensile strength.

With some concerns about the decrease in ductility found in unreinforced high strength concrete specimens loaded in tension, the ductility of high performance reinforced concrete beams made from pozzolanic material was also experimentally investigated. The results shows that the "brittle or ductile" behavior of cementitious composite materials, which can be observed by the post-cracking response obtained from the uniaxial direct tension test at the material level, is compatible with the"brittle or ductile" behavior exhibited by the reinforced concrete beams under flexural loading.

POST-CRACKING TENSILE PROPERTIES OF ADVANCED CEMENTITIOUS MATERIALS AND DUCTILITY OF HIGH PERFORMANCE CONCRETE BEAMS

by
Wonsiri Punurai

A Master's Thesis
Submitted to the Faculty of
New Jersey Institute of Technology
In Partial Fulfillment of the Requirements for the Degree of
Master of Science in Civil Engineering

Department of Civil and Environmental Engineering

January 2000

APPROVAL PAGE

POST-CRACKING TENSILE PROPERTIES OF ADVANCED CEMENTITIOUS MATERIALS AND DUCTILITY OF HIGH PERFORMANCE CONCRETE BEAMS

Wonsiri Punurai

Dr. Methi Wecharatana, Thesis advisor — Date
Professor of Civil and Environmental Engineering, NJIT

Dr. C.T. Thomas Hsu, Thesis Co-advisor — Date
Professor of Civil and Environmental Engineering, NJIT

Dr. Dorairaja Raghu, Committee Member — Date
Professor of Civil and Environmental Engineering, NJIT

BIOGRAPHICAL SKETCH

Author: Wonsiri Punurai

Degree: Master of Science in Civil Engineering

Date: January 2000

Undergraduate and Graduate Education:

- Master of Science in Civil Engineering,
  New Jersey Institute of Technology
  Newark, NJ, 2000

- Bachelor of Science in Civil Engineering
  Mahidol University,
  Nakhorn Pathom, Thailand 1998

Major: Civil Engineering

This thesis is dedicated to
my beloved family

ACKNOWLEDGEMENT

I would like to take this opportunity to express my sincere gratitude to my advisor, Professor Methi Wecharatana, and to my co-Advisor, Professor C.T. Thomas Hsu, for their guidance, patience and timely moral support throughout the course of this thesis work. I would also like to thank Professor Dorairaja Raghu for serving as a committee member.

I am indeed thankful Mr. Allyn Luke, assistant to the Chairman for Laboratories, Department of Civil Engineering, for his excellent technical assistance in the experiment. The help and expertise provided by Mr. Frank Johansson in developing testing setups is greatly appreciated.

I would also like to acknowledge the contributions of the following people: Dr. Walairat Bumrongjaroen, Dr. Pusit Lertwattanaruk, Dr. Rajendra Navalurkar, Mr. Insang Lee, Mr. Julio Zeballos, Mr. Zhichao Zhang. Without their contributions this work would have never been completed. I also thank to all Thai students at NJIT to keep me joyful throughout my life of studying here.

And finally, I also wish to express my special gratitude to the Royal Thai Government, Mahidol University for giving me a great opportunity to study at NJIT and to my parents, my brothers in Thailand for their support and encouragement during this research.

TABLE OF CONTENTS

TABLE OF CONTENTS
(Continued)

Chapter **Page**

TABLE OF CONTENTS
(Continued)

Chapter **Page**

LIST OF TABLES

LIST OF FIGURES

LIST OF FIGURES
(Continued)

Figure **Page**

CHAPTER 1

INTRODUCTION

1.1 General

Concrete, normal concrete in general, is a composite material, which is made up of fillers and a binder. The binder glues the fillers together to form a synthetic conglomerate. The constituents used for the binder are cement and water, while the fillers can be fine and or coarse aggregate. Concrete has many properties that make it a popular construction material. Depending on the mix, good-quality concrete has many advantages that add to its popularity. First, it is economical when ingredients are readily available. Concrete has long life and relatively low maintenance requirements, which increase its economic benefits. Concrete is not as likely to rot, corrode, or decay as other building materials. Concrete has the ability to be molded or cast into almost any desired shape. Building of the molds and casting can be done on the work-site, which reduces costs. Concrete is also a non-combustible material, which makes it fire-safe and able to withstand high temperatures. It is resistant to wind, water, rodents, and insects. Hence, concrete is often used for storm shelters. Despite its numerous advantages, concrete does have some limitations. Concrete has a relatively low tensile strength when compared to other building materials, low ductility, low strength-to-weight ratio, and is susceptible to cracking. Due to these limitations, designers have conventionally assumed zero tensile strength and have only used the compressive strength as a basis for design. Traditional normal concrete has the compressive strengths between 2,500 psi to 6,000 psi (17 to 41 MPa) with the most common near 4,000 psi (27 MPa).

However, the realization of the need in the creation of new structural forms that can carry higher loads and at the same time accomplish the aesthetic principles has led to the development of ever-higher compressive strength (more than 6,000 psi or 41 MPa according to ACI Committee 363) concrete. Such concrete is described as high-strength concrete. High strength concrete, a newly introduced material has been introduced and developed worldwide. The improvement of the compressive strength of concrete is made possible by the use of supplementary pozzolanic cementitious materials such as fly ash and micro silica either as cement replacement or additives. The addition of these micro particles helps to increase the density of the matrix, which indeed contributes to the strength development of concrete respectively. In recent years, the use of these supplementary cementitious materials has increased substantially, partly for reasons of economy and partly because of technical benefits imparted by these materials. Given that the high strength of concrete is due to the presence of a dense matrix, replacing a portion of the Portland cement with or more supplementary cementitious materials would not unduly depress the early strength of the concrete. Also, the lower chemical reactivity of supplementary cementitious materials means that a partial replacement of cement is beneficial from the standpoint of controlling the rheological properties of high-strength concrete-primarily workability at the time of compaction. In most cases, there is also the economic benefit of the price differential between cement and the supplementary cementitious material. In addition, partial replacement of cement always allows a significant reduction in the use of the water reducer, the superplasticizer in particular, which is a particularly expensive ingredient in many parts of countries. Because of all other valuable properties in addition to the compressive strength, it is sometimes logical

to describe such composites concrete by the more widely embracing term of high-performance concrete.

As the development of high strength concrete continues, concrete with compressive strength exceeding 12,000 psi (83 MPa) has been reported to be used in many transportation structures and in many high-rise buildings all over the world. Few examples of these high strength concrete structures are the long span cabled swayed bridges such as East Huntington, W.V., bridge over the Ohio River, Chicago's Water Tower Place, 311 South Wacker Drive Building, and recently the Petronas Towers in Malaysia.

From the beginning, traditional concrete has been characterized essentially by its compressive strength. As the strength of concrete increases as high as 20,000 psi (140 MPa), many other concrete properties have improved as well. One of its critical properties is the tensile behavior of concrete. The improvement of concrete compressive strength raises the question of how much do the tensile strength and the tensile properties of high strength concrete increase when compared to conventional normal concrete. One way to quantify these valuable properties is to perform the tension tests. There are three types of tests that are recommended by ASTM and widely used to evaluate the tensile strength of concrete. They are splitting tension test or sometimes called Brazillian Test, flexural test and uniaxial direct tension test. Recently, the results obtained from these tests have been reported by many researchers (Reinhardt 1986, John and Shah 1987, Remmel 1990, Wecharatana 1986, Chimamphant 1989, and Navalurkar 1996). Those results have shown that the tensile strength and properties of high strength concrete were

higher than the normal one, however, its magnitude was still not as significant when compared to other materials such as steel.

As mentioned earlier, high strength concrete has been used worldwide in view of all its valuable properties. One of its widely known characteristics is being more brittle. This behavior has been stated and recognized in a variety of the strength reduction factors provided by several codes. Knowing that typical normal strength concrete is not particularly a ductile material, high strength concrete is even less ductile (or even more brittle) than normal and lower strength concrete. This behavior may be a penalizing factor affecting the use of high strength concrete in certain structures. To help improve this particular deficit, the addition of small diameter, short, and ductile fibers into the composites has been introduced. Fibers are not added for the purpose of improving strengths, though modest increases in strengths may occur. Rather, their role is to alter the brittle behavior of matrix, or in other words to improve the ductility of matrix. The improvement of ductility of the matrix can be realized once the matrix has cracked. The randomly oriented, discrete, discontinuous fibers in the matrix will bridge across the cracks, toughening the damage composites. If the fibers are strong, appropriately bonded to the matrix, and are there in sufficient quantity, they will help to keep the crack widths small and permit the composites to carry significant stresses over relatively large strain (or deformation) in the post-cracking stage. That is, they provide some "pseudo-ductility" to the composite material after cracking occurs.

Various kinds of fibers have been introduced and used in recent years. They are steel, glass, carbon or kevlar, prolypropolyn, nylon, cellulose, and organic etc. These

types of fiber, which may come from either man-made or natural resources, vary considerably in performance and cost. Some common properties are listed in Table 1.1.

Table 1.1 Typical Properties of Fibers

Fibers	Diameter ($x10^{-6}$ m)	Specific Gravity	Modulus of Elasticity (GPa)	Tensile Strength (GPa)	Elongation At break (%)
Steel	5 - 500	7.84	200	0.5-2.0	0.5-3.5
Glass	9 – 15	2.6	70-80	2-4	2-3.5
Asbestos					
Crocidolite	0.02 - 0.4	3.4	196	3.5	2.0-3.0
Chrysotile	0.02 - 0.4	2.6	164	3.1	2.0-3.0
Fibrillated polypropylene	20 - 200	0.9	5-77	0.5-0.75	8
Aramid (Kevlar)	10	1.45	65-133	3.6	2.1-4.0
Carbon	9	1.9	230	2.6	1
Nylon	-	1.1	4	0.9	13-15
Cellulose	-	1.2	10	0.3-0.5	-
Acrylic	18	1.18	14-19.5	0.4-1.0	3
Polyethylene	-	0.95	0.3	$0.7x10^{-3}$	10
Wood Fiber	-	1.5	71	0.9	-
Sisal	10 - 50	1.5	-	0.8	3
Normal Cement Matrix For comparison	-	2.5	10-45	$3.7x10^{-3}$	0.02

Source: Bentur, A., and Mindess, S., "Introduction," Fibre Reinforced Cementitious Composites. (New York: Elsevier Science Publisher, 1990) 2-3.

In addition to these mentioned properties, fibers also differ widely in their geometries as shown in Appendix A. Common steel and glass fibers are straight and smooth, however, more complicated geometries have been developed to improve their mechanical properties when incorporating in cementitious matrix. Thus, modern fibers are varied in many shapes such as hooked or deformed ends. They may be formed as bundled filaments or fibrillated films, or in the form of mats or woven fabrics.

When fibers are combined with the cement composites in a mixer, the amount of fibers used is usually measured in terms of volume. Volume fraction is the common term used to express fiber volume per unit volume of concrete. At present, small amount of short fibers with volume fraction of less than 1% have been used in transportation structures and shortcreting. However, with the advanced processing techniques, manufacture of commercial fiber products, such as thin sheets, has increased the use of continuous and discontinuous fibers to as high as 20%. As reported in the literature, for a low volume-fraction composite, it is found that there is no significant increase in the peak load due to the presence of fibers. Only after the matrix has cracked do the fibers contribute to the matrix by bridging the cracks. Therefore, fibers improve the ductility of the composite resulting to the increase of its energy absorption capacity. In addition, there is often an improvement in impact resistance, fatigue properties and abrasion resistance. Small amounts of steel, cellulose and polypropylene fibers have been found to be very effective in reducing cracking due to restrained plastic and drying shrinkage (Shah, Sarigaphuti 1993). As the new production technologies have evolved in the development of new fibers, it appears that a large number of these products will be continue to be incorporated in concrete in the future. Since concrete is the major material

used in construction, an investigation of its properties when fibers are incorporated will be of great significance.

1.2 Objectives

In this study, the uniaxial direct tensile test results of concrete, reinforced with two types of randomly distributed short steel fibers, are reported. The series of direct tension tests are conducted to observe the post-peak behavior (the tensile softening response or hardening response) of different types of cementitious composites, namely, normal plain concrete, high strength concrete, normal fibrous concrete, and high strength fibrous concrete. High strength concrete composites are made from the addition of fine particles of silica fume, and fly ash from coal burning power plants. Two types of short steel fibers, namely harex and dramix, which are straight and hooked end steel fibers, respectively, with the volume fraction of 1% are added to normal and high strength matrices to make normal and high strength fibrous concretes. The basic parameters under investigation include: (1) fiber type; and (2) type of matrices. Emphasis is given to the "ductility", which may be extracted from the experimental results.

Citing the reports from many previous investigations, high strength concrete is brittle or less ductile. It can be developed by the use of the supplementary cementitious materials such as micro silica and fly ash, which is later known as high performance concrete. Knowing that ductility is an important property of concrete structure, in this investigation, the ductility of the high performance concrete beams made from fly ash concrete is observed. Flexural behavior of eight small-scaled under-reinforced concrete beams having the same amount of longitudinal reinforcement and confinement but

difference in the percentage replacements of fly ash in the mix proportion is evaluated in this study. Some observations are also made to discover whether or not fly ash replacement in concrete will affect the flexural behavior of reinforced concrete.

CHAPTER 2

BACKGROUND AND LITERATURE REVIEW

2.1 General

An understanding of fracture and cracking is very essential to the whole spectrum of human fabrication activities and has finally gained its rightful role in engineering research and development over the past decades. This is because of its direct engineering assessment for the improved design of structures and the prevention of sudden fractures in structures.

For a wide variety of materials with the application in engineering, cracking is the major cause of the material failure in many cases. Cracks can cause things to fail, something as small as a bone or as large as a ship. In a large structure, such as a bridge or a building, this may lead to the catastrophic failure, which can affect many people. It is known that all cracks that occur in materials are caused by tensile stresses, and the load-bearing capacity of the material primarily based on the extent of cracking developing. The study of how cracks in materials initiate and propagate is called "Fracture Mechanics". The classical concepts of fracture mechanics were firstly developed in 1920 by Griffith and have been mainly applied with a great success to metallic and ceramics. For cementitious materials such as concretes, more recent works have been carried out in the field of fracture mechanics in order to describe the crack formation and propagation, Of the more recent works carried out, they are the fictitious crack model by Hillerborg, Modeer, and Petersson (1976,1978), the crack band model by Bazant and Oh (1983), the two parameter model by Jenq and Shah (1985), and the modified strain energy model by

Wecharatana and Shah (1985). These crack models represent the general description of cracking properties of concrete and are found to have considerable theoretical and practical values when combining with nonlinear finite element analysis and other advanced numerical methods for simulating and analyzing the cracking failure behavior of complicated composite material structures such as concrete under complex loading.

2.2 Post-Peak Experiments and Techniques

With the development of the above-mentioned crack models, the interest in concrete behavior under tensile fracture, especially its post-peak response (as shown in Figure 2.1), has increased enormously. The relationship between crack width opening and the stress (or load), which can be obtained accurately only if complete load-deformation curves are available, is the most important information for generating these crack models. Direct measurement in a deformation-controlled uniaxial tension test on concrete looks to be the simplest and most accurate means to determine this relation. Various attempts have been made to carry out a uniaxial direct tension test. Among those are the direct tensile test of Rusch and Hildolf (1963), Hughes and Chapman (1966), Evan and Marathe' (1968), Heilmann, Hilsdolf, and Finsterwalder (1969). The majority agreed that they are difficulties in conducting a direct tension test, especially for the post-peak portion of the load-deformation response. It was found that without the availability of electro-hydraulic feedback control testing system, a very stiff testing machine and a special experimental testing technique, valid post-peak portion of the load-deformation responses could not be obtained. Since the difficulties were found in conducting a direct tension test for cement-based material, concrete in particular, indirect test methods have usually been devised to

determine the tensile responses for the analysis instead. One method is to produce concrete fracture by splitting cylinders, which is known as the Brazilian Test. This method, apart from its operational simplicity, has the benefit of using the same test specimens as those used to establish the compressive strength test. Another alternative approach is to obtain the tensile response values from specimens that are tested in bending. These two methods eliminate the problem encountered with test specimens subjected to the direct tensile loads. However, despite the simple procedure in carrying out these tests, the stresses that are obtained do not represent the uniaxial tensile stress state nor give an accurate value of the tensile responses of the tested material. Furthermore, it was found that the stress and strain distributions of the direct and indirect tensions are quite different. The uniaxial direct tensile test represents the real tensile strength and other real tensile properties of material at failure and does not rely on the elasticity and plasticity in order to calculate the tensile response value. Therefore, in order to obtain an accurate measurement of the tensile response of the material, the direct tensile tests are needed.

Recently, a few researchers (Petersson 1981, Hurlbut 1985, Gopalaratnum and Shah 1985, Reinhardt et.al. 1986, Wecharatana 1986,and Cintora 1987) have successfully conducted direct tension tests to monitor the post-peak responses of concrete. With the development of better testing equipments and new tensile testing technique and setup, the post-peak regime of cement-based material like concrete can be obtained. Closed-loop testing machine was a more suitable testing equipment for these tests to obtain the stable control until the complete fracture of the specimen (the separation of concrete specimen into two parts).

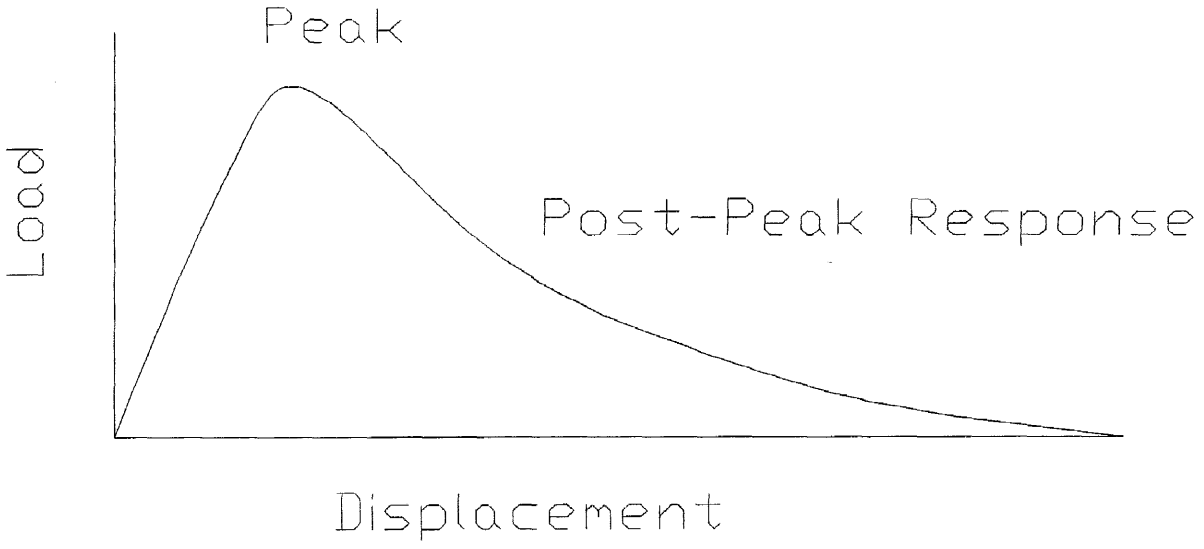

Figure 2.1 Typical Load-Displacement Curve and Post-Peak Response of Typical Concrete under Tensile Fracture

The output from high precision extensometers was used as the feedback signal to the MTS controller. The controller in turn adjusted the actuator movement accordingly, thus avoiding the abrupt failure caused by the erratic rate of crack opening. Numerous test methods using notched and unnotched specimens were conducted with this machine in order to achieve the desired post-peak responses. Hurlbut and Reinhardt held their specimen by means of gluing. Hurlbut used unnotched cylindrical specimen while Reinhardt used the notched rectangular plate specimen. The steel plates were glued to the ends of their tension specimen with high strength epoxy in order to perform the test. This method provided a homogeneous stress field throughout the length of the test specimens. However, the test results may be affected by the preparation and thickness of the adhesive used. Furthermore, the difficulty in keeping the alignment of the steel plates exactly at the centerline of the specimen often made this method extremely tedious to perform. Because of the difficulties inherent in Hurlbut and Reinhardt's physical setup, Gopalaratnum and Shah introduced different method. They clamped their specimen by means of the wedge action using steel plates by which the specimen was secured through the friction force created. However, this method was proved later to be restrictive. If the size of the specimen was increased much beyond what they used, the friction force would not be sufficient to hold the specimen, therefore resulting to slippage of the specimen. Wecharatana and Cintora tried solving this problem by introducing the self-interlock. They used a rectangular specimen tapered outward at the ends together with polyvinyl chloride (PVC) shims, which were placed internally to follow the shape of the specimen ends. Via this technique, it enabled the specimen to be loaded with a uniform stress and at

the same time provided enough pulling force without creating undesired compression at the zone in which cracking occurs.

2.3 Post-Peak Responses and Applications

With the ability of performing the complete uniaxial direct tension tests, the post-peak responses of cementitious composite materials such as concretes can be studied in greater depth. Information on the complete stress (or load)-deformation response of typical concrete subjected to uniaxial tension is now available and can be found from the literature as illustrated in Figure 2.2. It can be seen that the shape of the curves is different. This is because of the differences in testing methods and material compositions of each test series.

It is widely recognized now that the shape of the stress (or load)-deformation contains important properties of the material. Total area underneath the stress-deformation curves represents the total amount of energy absorbed in a tensile test up to the failure of the specimen. This energy can be divided into two parts, which correspond to the two curves, one in the pre-peak region including unloading branches defined as the stress-strain curve, and the other in the post peak region defined as the stress-crack width curve (as shown in Figure 2.3). In general, the area enclosed by the stress-strain curve represents an energy per unit volume, absorbed by the whole specimen. The area below the stress-crack width curve represents an energy absorbed to create the unit area of fracture surface in material, which is denoted by G_F. The peak of the stress-deformation curve demonstrates the maximum attainable tensile stress (or load) that material can carry. And finally, the shape of the descending branch in the post-peak portion

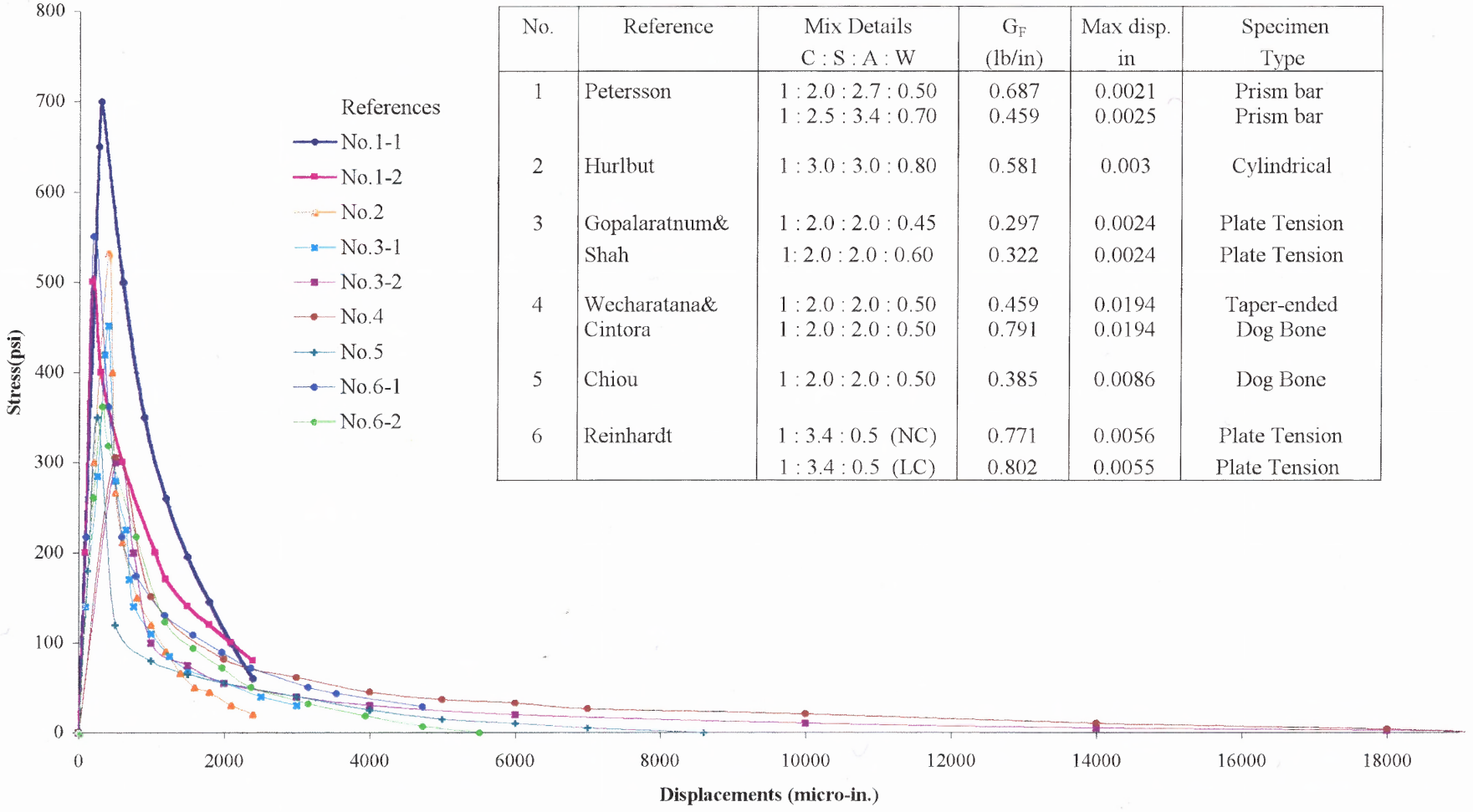

No.	Reference	Mix Details C : S : A : W	G_F (lb/in)	Max disp. in	Specimen Type
1	Petersson	1 : 2.0 : 2.7 : 0.50	0.687	0.0021	Prism bar
		1 : 2.5 : 3.4 : 0.70	0.459	0.0025	Prism bar
2	Hurlbut	1 : 3.0 : 3.0 : 0.80	0.581	0.003	Cylindrical
3	Gopalaratnum&	1 : 2.0 : 2.0 : 0.45	0.297	0.0024	Plate Tension
	Shah	1: 2.0 : 2.0 : 0.60	0.322	0.0024	Plate Tension
4	Wecharatana&	1 : 2.0 : 2.0 : 0.50	0.459	0.0194	Taper-ended
	Cintora	1 : 2.0 : 2.0 : 0.50	0.791	0.0194	Dog Bone
5	Chiou	1 : 2.0 : 2.0 : 0.50	0.385	0.0086	Dog Bone
6	Reinhardt	1 : 3.4 : 0.5 (NC)	0.771	0.0056	Plate Tension
		1 : 3.4 : 0.5 (LC)	0.802	0.0055	Plate Tension

Figure 2.2 Complete Tensile Stress (or Load)-Displacement Curves as Found from the Literature

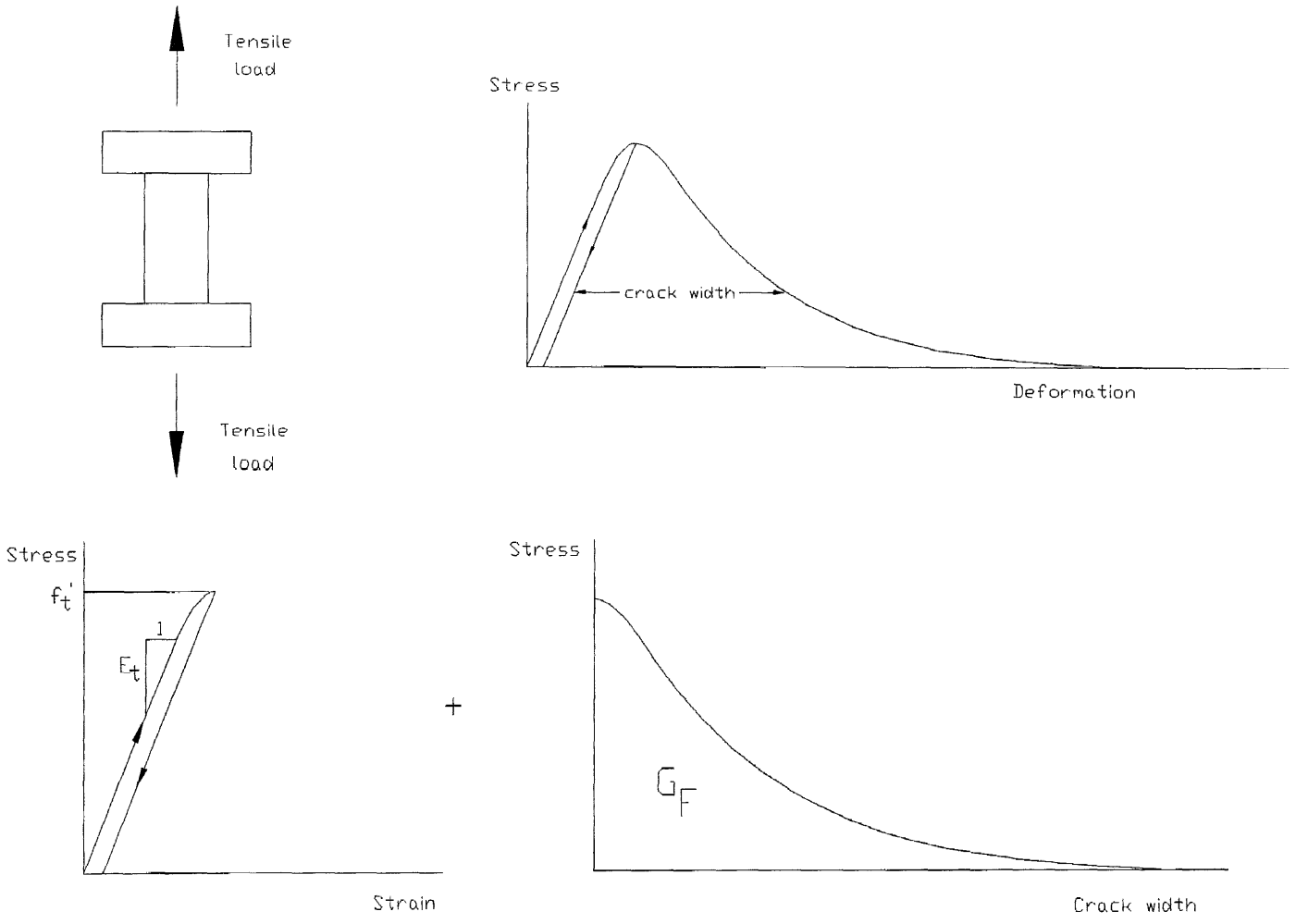

Figure 2.3 A General Description of Tensile Fracture Behavior of Concrete by Hillerborg

indicates tensile cracking property of material. By incorporating these mentioned parameters into the numerical computations, reinforced and unreinforced concrete in the cracked stage can be analyzed. Additionally, the use of these mentioned valuable properties in some previous investigations (Loland 1985, Wecharatana 1990) gives the basic information on the ductility of the material, which is one of the major concerned properties of a structural material when used in design.

Since the experimental stress-displacement relationship is very hard to obtain due to the difficulties in conducting experiment, a few equations have been proposed by some researchers in order to predict this relationship based on the existing experimental results without the need to conduct the tedious direct tension experiment. They are as follows:

1. Petersson (1981):

$$\frac{\sigma}{f_t} = 1 - \frac{\omega}{\omega_c} \qquad \text{Eq. (1)}$$

Where

σ is the tensile stress, f_t is the maximum tensile strength, ω is the crack opening displacement, ω_c is the maximum crack opening displacement.

2. Reinhardt (1986):

$$\frac{\sigma}{f_t} = \{1 + c_1\left[\frac{\omega}{\omega_c}\right]^3\}\exp(-c_2\left[\frac{\omega}{\omega_c}\right]) - \frac{\omega}{\omega_c}\left(1 + c_1^{\,3}\right)\exp(-c_2)$$

Where

σ is the tensile stress, f_t is the maximum tensile strength, ω is the crack opening displacement, ω_c is the maximum crack opening displacement. C1 and C2 are empirical constants and equal to 3 and 6.93 for normal plain concrete.

3. Gopalaratnum and Shah (1985):

$$\frac{\sigma}{f_t} = \exp(-k\omega^{\lambda}) \qquad \text{Eq. (3)}$$

Where

σ is the tensile stress, f_t is the maximum tensile strength, ω is the crack opening displacement (micro-inch), k and λ are constants which equal to 1.544×10^{-3} and 1.01 for concrete.

4. Wecharatana and Cintora (1987):

$$\frac{\sigma}{f_t} = \frac{A}{\zeta}(1 - e^{-B\zeta^{c}})(1-\zeta)^{D} \qquad \text{Eq. (4)}$$

Where

A, B, C, and D are empirical constants which for concrete are 0.0052, 400, 1.75 and 0.5, respectively.

It should be noted that these reported empirical models are for mortar and concrete, and which were in good agreement with their observed experimental results only. For other cementitious composites, different sets of constant or other formulations have to be developed or obtained experimentally. As, new cement-based composite materials like high strength concrete (HSC), fiber reinforced concrete (FRC) were introduced, however the theoretical modeling that can be used for predicting not only the tensile behavior of normal concrete but also that of other types of cementitious matrix materials is lacking. Due to the fact that scarce information has been reported in the literature and the theoretical model cannot be developed without the availability of these existing experimental results, one of the objectives of this study has thus been to experimentally determine the complete stress-displacement curves of all different types of cementitious composite materials. At present investigations, a series of direct tension

test were carried out on different types of cement-based composites, namely, plain concrete, high strength concrete, normal fibrous concrete, and high strength fibrous concrete, for the study of fracture and structural behavior, such as ductility.

As mentioned earlier, the ductility of material, has by now mainly characterized by "traditional" mechanical quantities obtained from the material tests such as compressive strength test and tensile test, which provide the material behavior under load on plain specimens only. In this study, this structural behavior of the reinforced concrete specimens will also be investigated. Eight small-scaled under-reinforced concrete beams having the same amount of longitudinal reinforcement but different in the cementitious matrix compositions in the mix proportion were tested to failure to study their ductility behavior.

CHAPTER 3

MATERIALS AND EXPERIMENTAL METHODS

In this study, experiments were set up in two series of investigations: (1) the post-cracking tensile properties of different types of cementitious composites as mentioned earlier in chapter 1; (2) the ductility of the high performance concrete structure made from the high performance fly ash concrete. Four different tests were designed so as to yield the basic parameters under the objectives of this investigation. They are uniaxial direct tension test (tapered specimen), flexural beam test (rectangular beam specimen), compression test, and splitting tensile test (3x6 in cylinder specimen). All details of the experiments will be discussed in the following.

3.1 Tension Softening Behavior

In this study, experimental programs were conducted for the purpose of studying the post cracking tensile properties of different types of cementitious composites, namely, normal plain concrete, high strength concrete, normal fibrous concrete, and high strength fibrous concrete. A series of uniaxial direct tension tests were carried out to study the effects of varying the fiber type and matrix type on the tensile behavior. Compression tests were used to evaluate traditional properties such as compressive strength (f_c'), etc. Details of these tests are discussed below.

3.1.1 Materials

In this study, materials used for the process of producing different types of cementitious composites, namely, normal plain concrete, high strength concrete, normal fibrous concrete, and high strength fibrous concrete, consisted of Portland cement type I, local siliceous sand, crushed limestone, silica fume, fly ash, steel fibers and water. Silica fume and fly ash were used as an additive and a supplementary material in order to make high strength concrete. Two types of short steel fibers, namely harex and dramix, which were straight- and hooked-end steel fibers respectively, with the volume fraction of 1% were added to normal and high strength matrices in order to make normal and high strength fibrous concretes, respectively. All mentioned material properties are summarized as follows:

Cement: The Portland cement type I with the specific gravity of 3.15 was used throughout the experiments.

Coarse Aggregate: Crushed limestone coarse aggregate size 3/8" was used.

Fine Aggregate: local siliceous sand (river sand) passing through sieve No.4 (opening size 4.75 mm) was used in this experiment.

Silica Fume: Silica fume used in this study was in the powdered form with 96% of SiO_2. Its particle size was of the range between 1 to 5 microns.

Fly Ash: ASTM Class F wet bottom fly ash, industrial by-product collected from a cold-fired boiler from a power plant, was used in this study. 94.6% of its particles were smaller than 5.5 microns.

Dramix steel fibers: Hooked-end steel fibers with a diameter of 0.02 in (0.5 mm) and a length of 1.2 in (30 mm) were used. The fibers had a density of 490 lb/ft^3 (or 7.8 g/cm^3) with an aspect ratio (l/d) of 60. The fiber volume fraction of 1% was used throughout the study.

Harex steel fibers: These fibers have an arc cross-section with the dimensions of 0.09x0.01 in (2.2 x 0.25 mm) and are 1.25 in (or 32 mm) in length. These fibers had a density of 490 lb/ft^3 (or 7.8 g/cm^3). The fiber volume fraction of 1% was used throughout the study.

Water: Tap water was used throughout this experimental program.

3.1.2 Mix Proportions

The matrix mix proportions for the four different kinds of concrete are listed in Table 3.1.The ratio of water to cementitious materials was kept constant at 0.5 while the ratio of fine and coarse aggregate to cementitious material were 2 and 3, respectively. In the high strength concrete mixes, silica fume and fly ash were used to improve the matrix properties, including interfacial bonding. Silica was used as an additive material while fly ash was used as a supplementary material. In the case where fly ash was used, a fraction of cement was substituted with fly ash on an equal mass basis.

Table 3.1 Matrix Mix Proportions

Group	Fiber used	Fiber type	V_f (%)	Compositions* C: S: A: W	Pozzolanic Additives (%)	No. of Specimen
Normal Strength	Nil	Plain Concrete	Nil	1: 2: 3: 0.5	-	4
High Strength Concrete	Nil	Plain Concrete	Nil	Same	MS-08[₮]	4
	Nil	Plain Concrete	Nil	Same	MS-10	4
	Nil	Plain Concrete	Nil	Same	FA-25[T]	4
	Nil	Plain Concrete	Nil	Same	FA-35	4
Normal Fibrous Concrete	Harex	Steel fiber	1	Same	-	4
High Strength Fibrous Concrete	Dramix	Steel fiber	1	Same	FA-25	4

* C = Cement; W = Water; S = Fine Aggregate; A = Coarse Aggregate

[₮] MS-10 – Silica Fume, with 10% addition of cement used.

[T] FA-25 – Fly Ash, with 25% replacement of cement used

3.1.3 Specimens Configuration and Fabrication

For present direct tension tests, end-tapered specimens (as shown in Figure 3.1) of dimensions 3.25 x 1.75 x 12 in. (95 x 44 x 305 mm.) developed by Wecharatana (1986) and Cintora (1987) were used. All mixes were prepared in a conventional blade-type concrete mixer. For normal and high strength plain concretes, the mixer was first loaded with the fine aggregate, cement together with the addition of fly ash or silica fume, and then mixed for 5 minutes. After that, the coarse aggregate was loaded into the mixer and mixed for another 5 minutes. Water, then, was added into the mixer and mixed for 5 or 10 more minutes to produce a uniform mixture. However, special attention had to be given in the case where the fibers were used. About one third of fibers had to be separated and added in the stage of mixing cement and fine aggregate. Then, the remaining fibers were gradually added into the mix until a uniform mixture was produced. Occasionally manual dispersion may be required in some cases because fibers tended to gather into balls when added without being separated. A tilting drum mixer during mixing would also improve fiber dispersion.

All end-tapered specimens were casted in plexi-glass mold, which were prepared and lubricated with oil before the mix was ready to pour. For different types of concrete, three 3x6 in. controlled compression cylinders were also casted in the plastic mold. These specimens were then vibrated on a vibrating table to expel the air in order to obtain a well-compacted specimen. The specimens were covered with the wet towels after casting and demolded twenty-four hours later. After demolding, they were transferred to a curing room for twenty-eight days. Twenty-four hours before testing, all specimens were taken out from the curing room and notched by a circular diamond blade saw.

3.1.4 Test Setup and Experimental Procedure

Test setup and procedure of testing can be categorized into two different types, uniaxial direct tension test (end-tapered specimen) and compression test (3x6 in. standard cylinder specimen).

3.1.4.1 Uniaxial Direct Tension: The test setup and techniques used in this study have been developed from the work of earlier researchers: Wecharatana (1986), Cintora (1987), and Navalurkar (1996), at the New Jersey Institute of Technology. End-tapered specimens of dimensions 3.25 x 1.75 x 12 in. (95 x 44 x 305 mm.) were clamped within the steel box-shaped grips with the dimension of 6 x 4 x 5 in. (150 x 100 x 125 mm.) by means of wedge action and loaded under MTS closed-loop deformation control. The wedge action was provided by employing PVC shims (as shown in Figure 3.1) with a slope of 0.4166 to fit the specimen within the steel grips. Loads were transferred to the upper grip via a universal joint connected through the top of MTS testing machine, then to the specimen and the PVC shims. Another universal joint was used at the bottom end to avoid creating the moment and to allow free rotation of the specimen. Two small side notches of 0.5 in. were saw cut at the mid length of each specimen in order to prevent the random distribution of cracks along the specimen and to force a single crack to propagate across the notches while the specimen was loading. Two extensometers with a maximum travel of 0.2 in. (5 mm.) were placed over the notches to measure displacements. As deformations across the notches were measured, the output signal from the extensometers mounted across each notch was electronically averaged and fed back to a data acquisition board to be stored, and simultaneously to the servo controller to control the loading. All

signals of load, deformation were recorded directly onto the computer disk where data manipulation and plotting could be done later. In the data manipulation process, the uniaxial deformations were converted to strains by dividing the deformations with the gage length of 1 in. as well as the stresses were obtained from the ratios of the loads to the net cross sectional area of 3.97 in^2.

In this study, all specimens were loaded with a monotonically increasing displacement at the constant rate of $6.7x10^{-8}$ in. per second under a 5-kip MTS hydraulic servo-controlled testing system. Once the first transverse crack was observed, a complete record of the load-displacement response can be obtained. During the tests, Optical observations of specimen cracks were also recorded using a digital camera. The total time of testing a specimen was approximately 3 to 4 hours. The schematic details of the complete direct tension test set up are shown in Figure 3.1 and Figure 3.2.

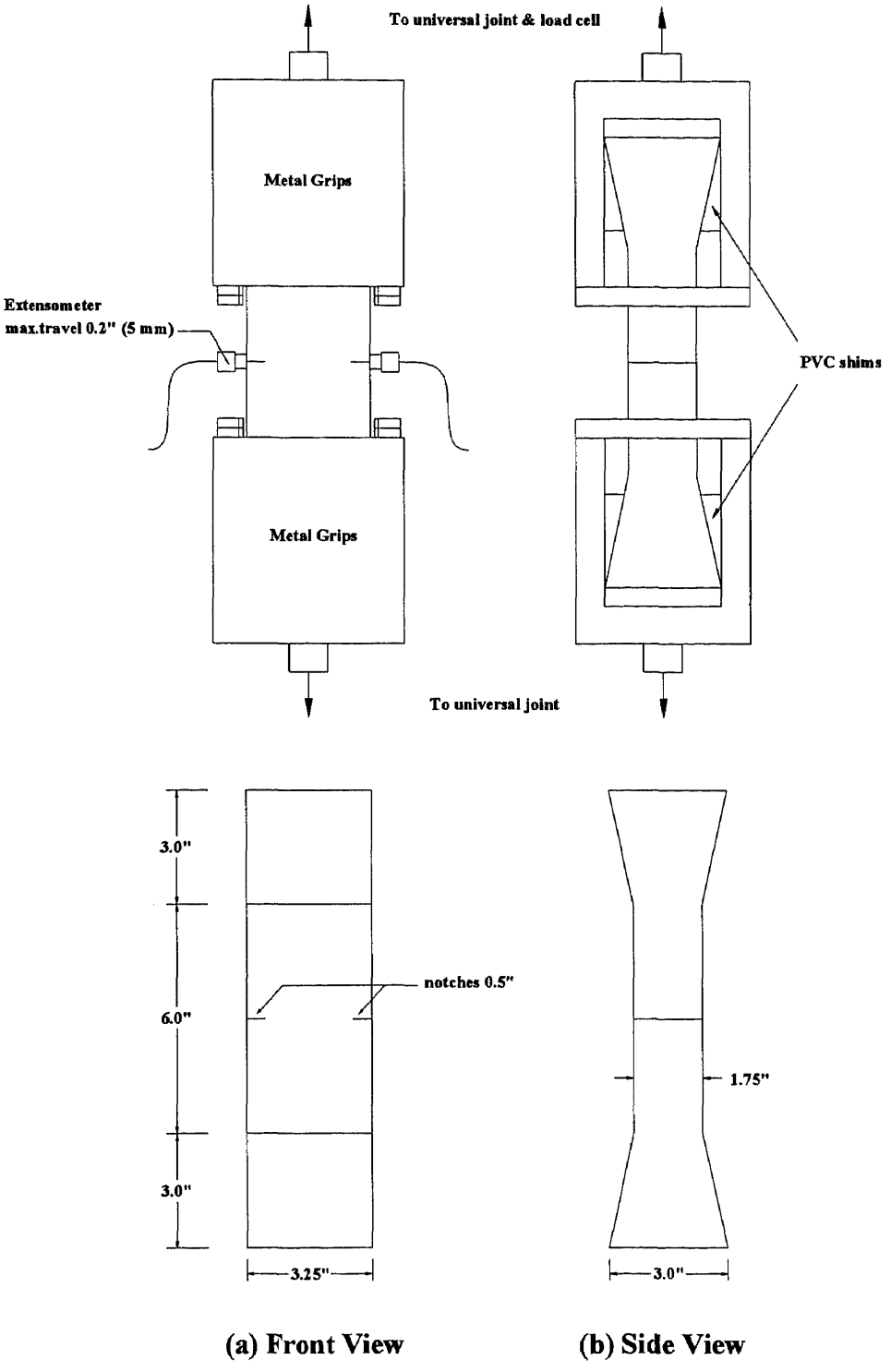

Figure 3.1 Schematic Details of Direct Tension Test Setup and Test Specimen

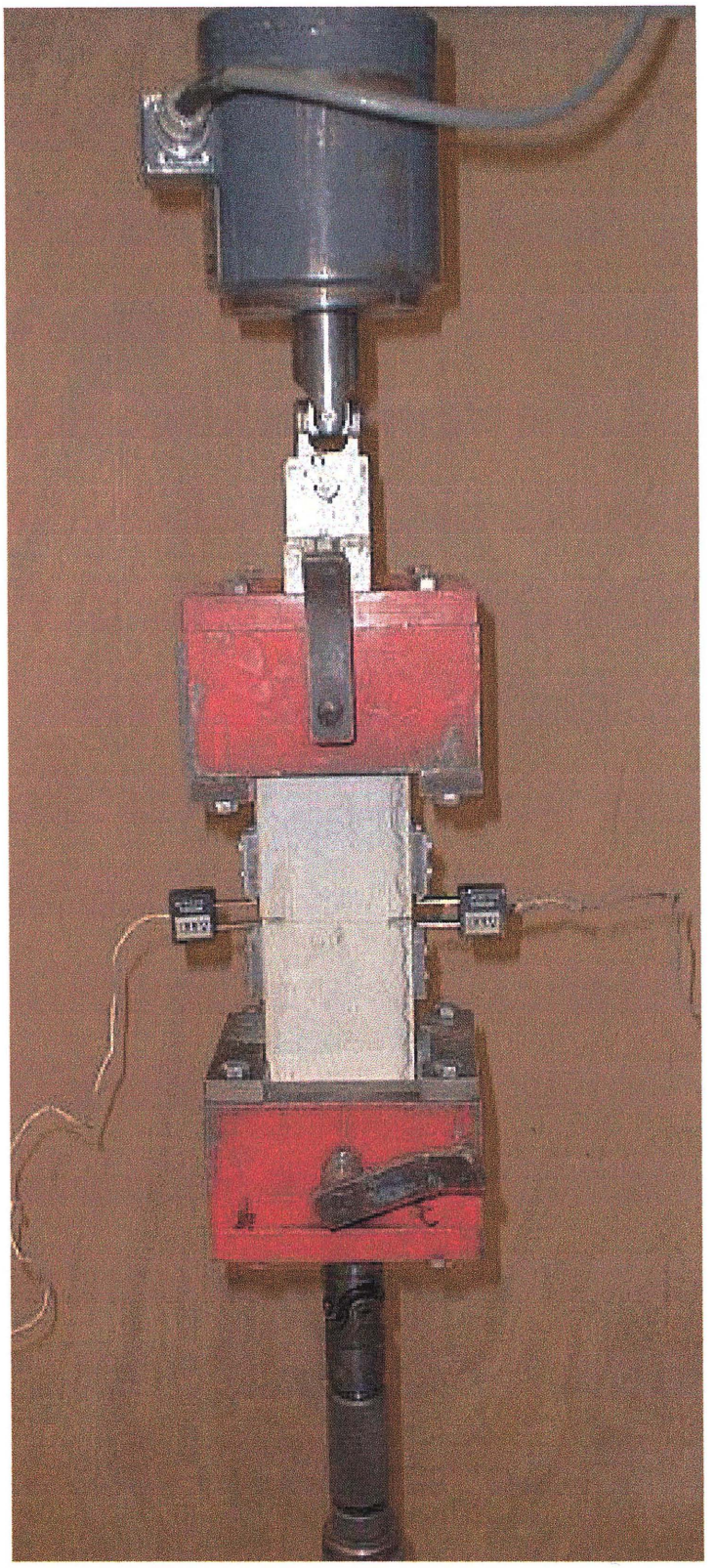

Figure 3.2 Picture of Direct Tension Test showing the Specimen within the Metal Grips connected to 5-kip MTS Load Cell

3.1.4.2 Compression: Information about the compressive properties of concrete is always important and needed in practical design. The 3 x 6 inches (76 x 152 mm) cylinders made from the same mix proportion used for tension were tested in uniaxial compression under MTS closed-loop deformation control to obtain the stress-strain behavior, the compressive strength (f_c'), and the modulus of elasticity (E_c). The tests were conducted at the deformation rate of 4.167×10^{-7} in. per second or the strain rate of 0.0001 in/in per second. It took approximately 2 to 3 minutes to reach the peak load and around 20 minutes to complete the entire test. Two strain gages with the gage length of 4 in. were mounted onto the specimen in order to measure the axial deformations. When the specimen was loaded, the deformations measured by two gages were sent back as the output signal to the MTS controller to constantly adjust the applied load. All signals of load, deformation and stroke were recorded directly onto the computer disk where data manipulations of stress-strain responses were done automatically by means of data acquisition via microcomputer.

Prior to testing, all cylinders were carried out from the curing room and allowed to dry at room temperature for about twenty-four hours. After that, all specimens were capped with sulfur based capping compound before testing. The average axial compression value of three specimens from each series was used to calculate f_c', the compressive strength of concrete. Details of the test set up are shown in the Figures 3.3 and 3.4, respectively.

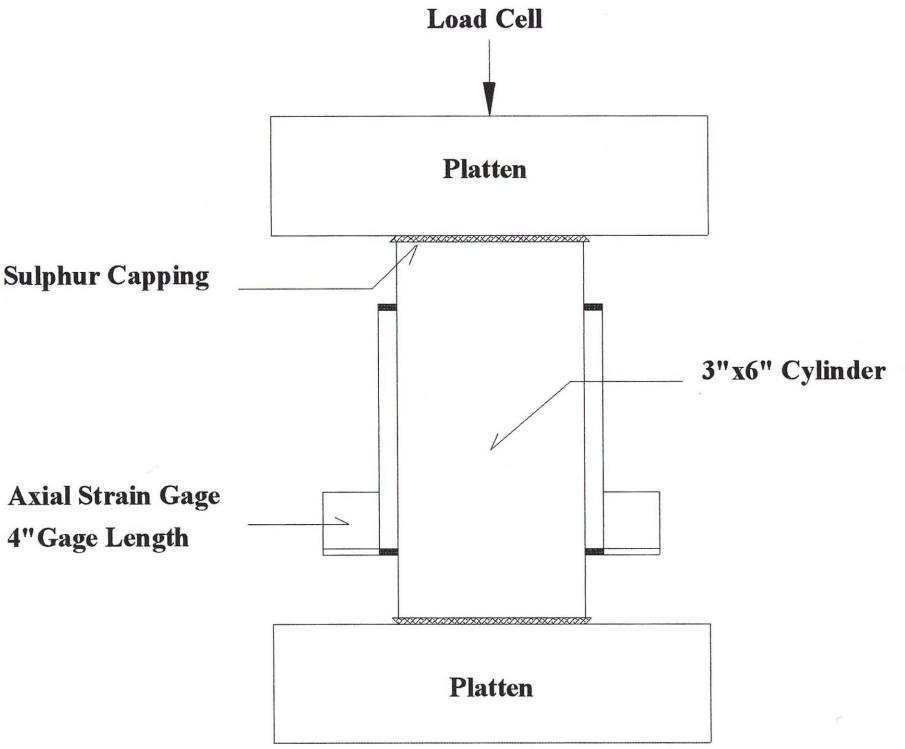

Figure 3.3 Compression Test Setup used in this study

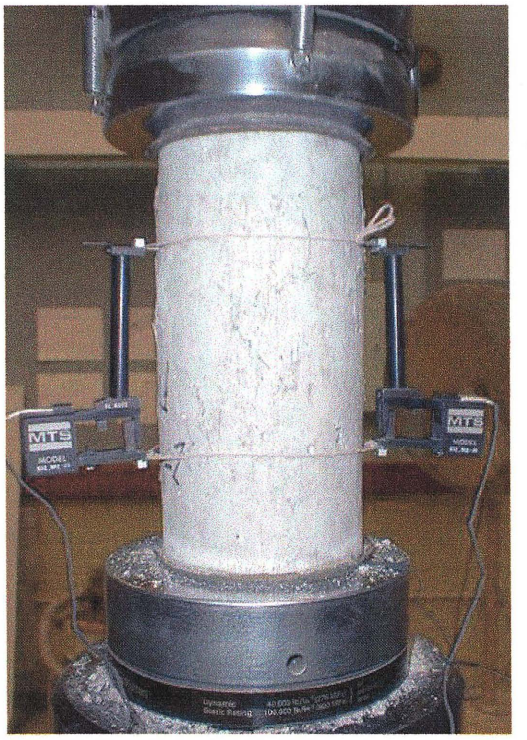

Figure 3.4 Picture of Compression Test Setup

3.2 Ductility of High Performance Reinforced Concrete Beams

Experiments were setup with the objective of investigating the overall flexural behavior and ductility of the high performance concrete beams made from high performance fly ash concrete. The effect of fly ash replacement on these two properties was observed.

Eight small-scaled under-reinforced concrete beams having the same amount of longitudinal reinforcement and confinement reinforcement but different in the percentage replacements of fly ash in the mix proportion were used in this study. Three 3x6 in. cylinders each were used for evaluating the concrete compressive strength and splitting tensile strength, respectively. All tests were performed under the MTS closed loop testing machine. Details of test specimen are discussed below.

3.2.1 Test Specimen

3.2.1.1 Materials: Materials used in the concrete of this study consisted of standard Portland cement type I, crushed limestone, siliceous sand (river sand), fly ash, and water.

Cement: A standard Portland Cement Type I.

Coarse Aggregate: Crushed limestone coarse aggregate size 3/8" was used for casting concrete.

Fine Aggregate: local siliceous sand (river sand) passing through sieve No.4 (opening size 4.75 mm) was used in this experiment.

Fly Ash: ASTM Class F wet bottom fly ash, industrial by-product collected from a cold-fired boiler from a power plant, was used in this study. This fly ash was the same as the one used for uniaxial direct tension test as mentioned in the previous chapter. The characteristics including size distribution and chemical composition, of this fly ash are shown in Appendix A.

Water: Tap water was used throughout this experimental program.

3.2.1.2 Specimen Configuration and Fabrication: The model beam test specimens used in this study were 3 x 3 in. (75 x 75 mm) in cross section and 16 in. (400 mm) long reinforced with two No. 2 tension reinforcement bars (6.25 mm diameter). The steel stress-strain curve is shown in Figure 3.5. By keeping the water to cementitious materials ratio to be constant at 0.5, the beams were mixed and casted in four different series of mix proportion and in accordance with ASTM C-109. Specimens from series A are the control while the others are specimens with the replacement of fly ash. Table 3.2 shows the material compositions of each mix series.

Table 3.2 Material Compositions

Test Series	Mix Proportion (By weight)					Total Specimen
	Cement	Fly Ash (Class F)	Water	Sand	Aggregate	
A	1	0	0.5	2	3	2
B	0.9	0.1	0.5	2	3	2
C	0.8	0.2	0.5	2	3	2
D	0.7	0.3	0.5	2	3	2

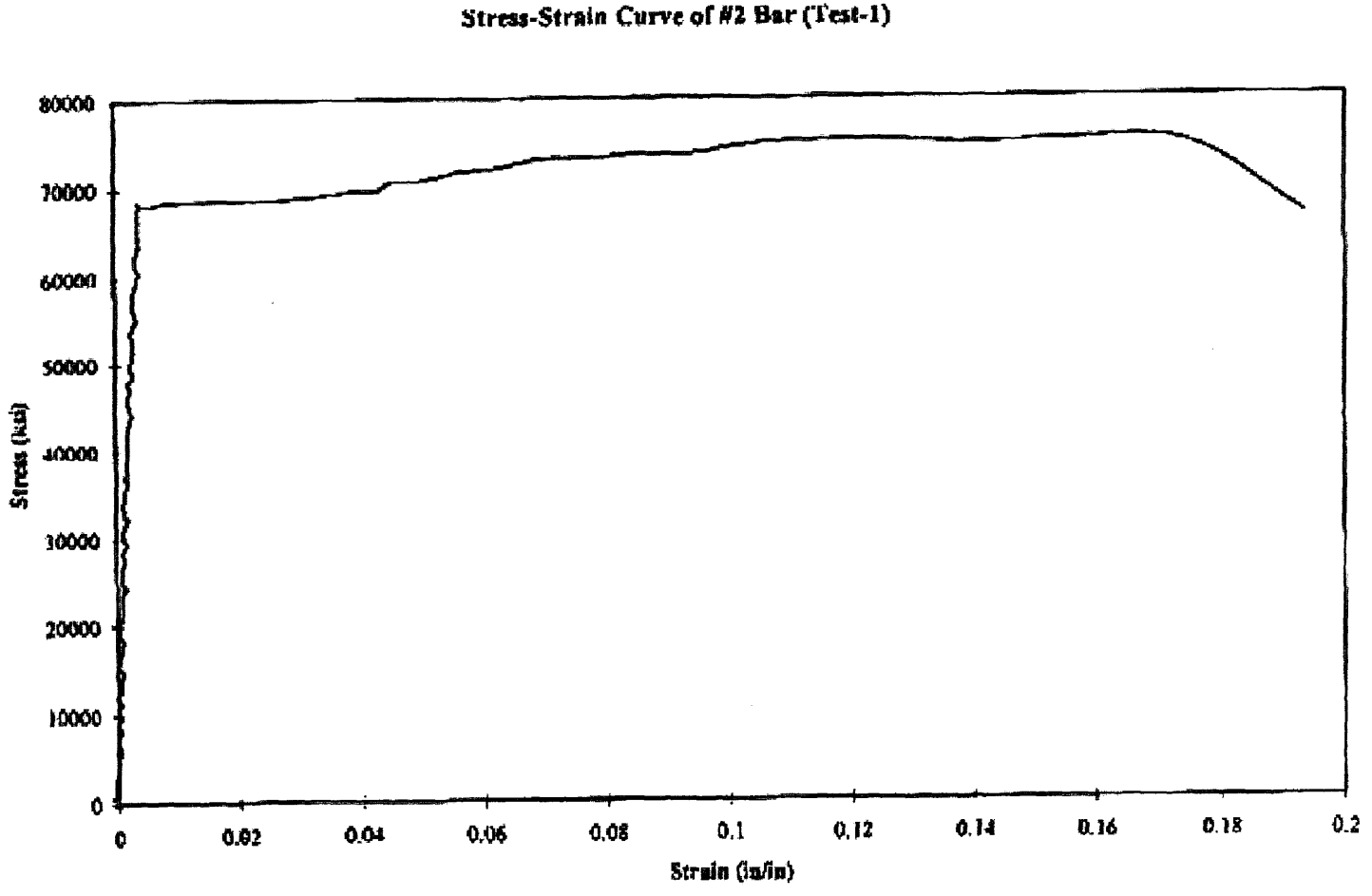

Figure 3.5 Experimental Stress-Strain Curve in Tension for Steel

3.2.2 Test Setup and Experimental Procedure

A beam from each series was tested under three-point loading test. At the age of 28 days, it was tested as a simply supported beam by applying a concentrated load at the top of the mid-span of the member. The beam span between two supports was 12 in.. Each beam was loaded monotonically using a 100 kips MTS servo-controlled closed-loop hydraulic testing machine. The displacement rate of $1x10^{-5}$ in. per second was used throughout the test. As the applied loads were increased from zero to the maximum load and then to failure, load-point deflections measurements off a reference bar were recorded at mid-span immediately under the load using Linear Variable Differential Transducer (LVDT). The total time of testing a specimen was approximately half an hour. The test data comprising of load and deflection were recorded using DAS 8 PGH data acquisition board and Labtech Notebook Program. The beam test setup, load arrangement, beam cross-section, and reinforcement details are shown in Figure 3.6 and Figure 3.7.

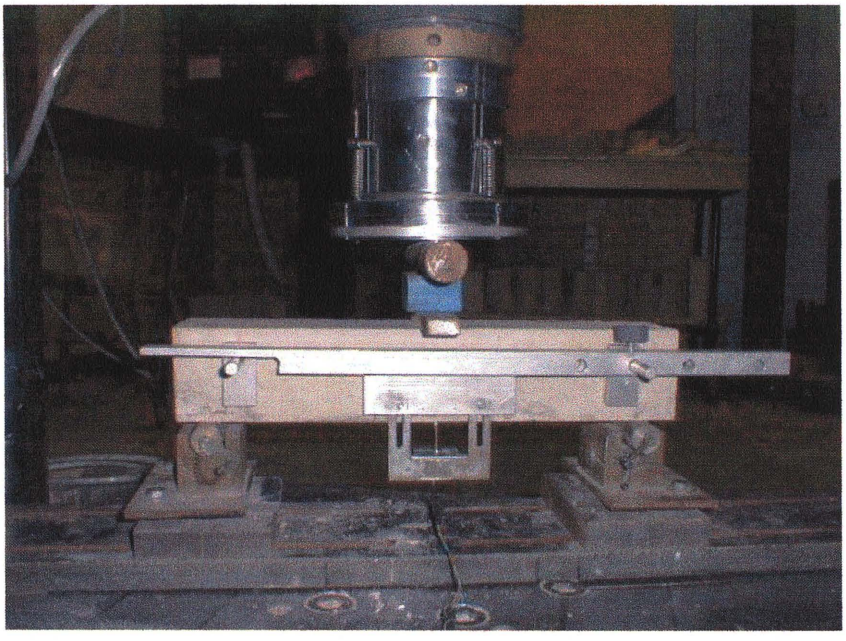

Figure 3.6 Picture of Beam Test Setup

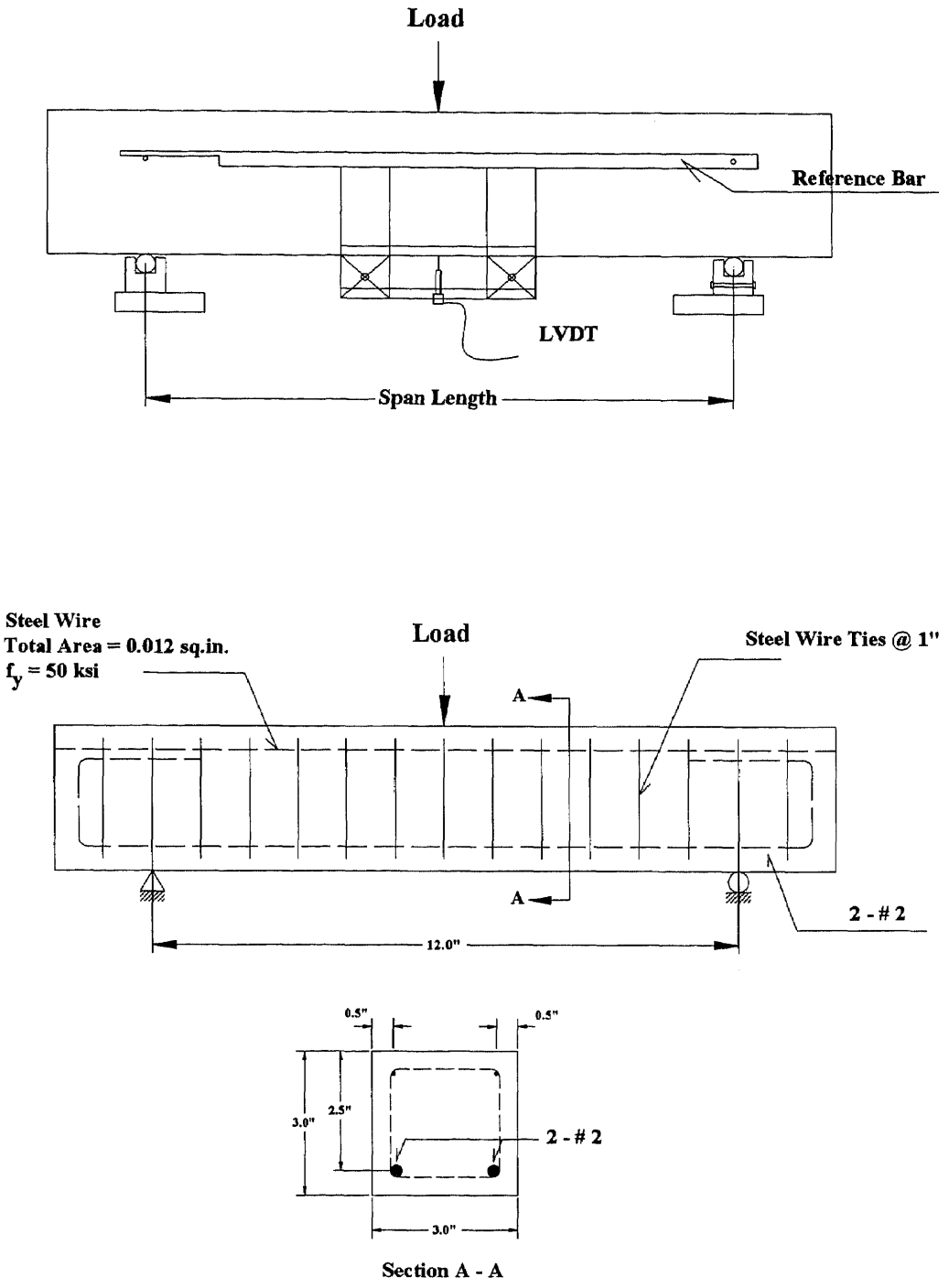

Figure 3.7 Loading Arrangement and Cross Section of Beam Specimens

For each series of beam test, three 3 x 6 in. cylinders each were also tested in uniaxial compression and splitting-cylinder tests to determine concrete compressive strength and split cylinder tensile strength, respectively.

For uniaxial compression test, the procedure and test setup used were the same as the one mentioned earlier in test series 1. For each specimen, It took approximately 2 to 3 minutes to reach the peak load and around 20 minutes to complete the entire test The observed parameters from this testing were the stress-strain behavior, the compressive strength (f_c'), the modulus of elasticity (E_c). The data used in the strength analysis was obtained from the average of the three specimens. Details of the test set up are shown in Figures 3.3 and 3.4.

For splitting-cylinder test, the concrete 3 x 6 in. standard cylinder specimen was placed in the 100-kip MTS servo-controlled closed-loop hydraulic testing machine, the same machine that was used for the beam-bending test. Load was applied uniformly along two opposite lines on the surface of the cylinder through two plywood pads as shown in Figure 3.8. Below the region of the load application, there was a nearly uniform tensile region existed such that an indirect tensile strength of concrete could be measured.

All tests were performed at the deformation rate of 0.05 in. per second, which is in accordance with ASTM C496 until the failure of specimen where the cylinder usually spliced neatly into halves (as shown in Figure 3.9). The total time of testing a specimen was approximately 10 to 15 minutes. For each specimen, ultimate magnitude of compressive load was recorded where data manipulation of splitting tensile strength was computed as:

$$f'_t = \frac{2 * P}{\pi * L * D} \qquad \text{Eq. (5)}$$

Where

f'_t = splitting tensile stress, psi.

P = total load at failure, lb.

L = length of concrete cylinder, in.

D = diameter of concrete cylinder, in.

The average value of three specimens from each series was also used to study the influence of fly ash replacement on splitting tensile strength of concrete.

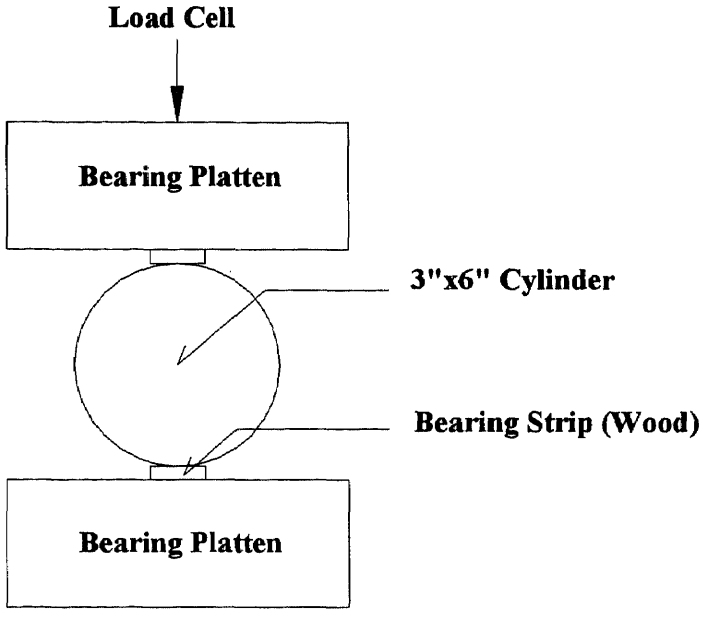

Figure 3.8 Front View of Splitting Tensile Test Specimen

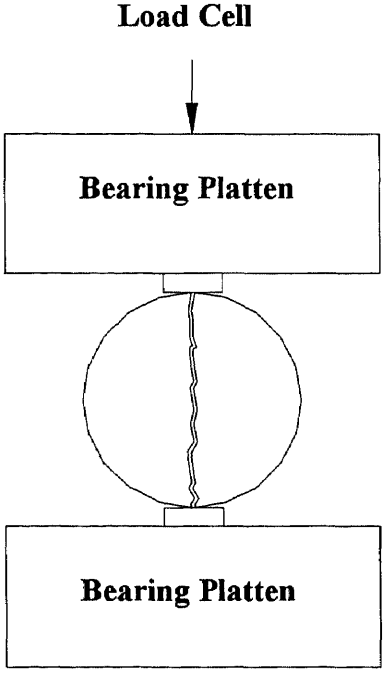

Figure 3.9 Front View of Cylinder after Testing

CHAPTER 4

EXPERIMENTAL RESULTS AND DISCUSSIONS

4.1 Post Cracking Tensile Properties of Cementitious Composite Materials

Experimental study of the uniaxial direct tension test was conducted in order to understand the general tensile properties of different cement-based composites including seven different mixes as mentioned in Table 3.1 of the previous chapter. Tapered specimens (see Figure 3.1) were used to study the post-peak load (or stress)-displacement relationships.

Table 4.1 and Figure 4.1 present the average tensile properties of different cement-based composites obtained from the tension test series of seven different mixes. Values reported in the table include the peak stress and strain in tension (f_t', ε_{tp}), and in compression (f_c',ε_{cp}); initial tangent modulus of elasticity in tension (E_t) and in compression (E_c); the peak displacement, ω_c; the fracture toughness G_{IC}; and finally the fracture energy G_F. The peak displacement value, ω_c, refers to displacement at the point where the specimen has no capability in carrying any tensile forces (zero load). For these mentioned values, stresses were calculated based on the net cross-sectional area of the notched tension specimens while the fracture toughnesses and fracture energies were calculated as the total area underneath the stress-deformation and the stress-crack width curves, respectively. Some discussions related to the overall responses are discussed in the following.

4.1.1 Load displacement Relationship

The load versus deformation relationships for different types of cementitious composites, namely, normal plain concrete, high strength concrete, normal fibrous concrete, and high strength fibrous concrete with the differences in mix compositions as mentioned in Table 3.1 are shown in Figure 4.1. The matrices of the four series of concrete are slightly different in compositions. Their cylindrical compressive strengths are presented in Table 4.1 whereas the average tensile stresses versus the deformation curves are shown in Figure 4.1. "Deformation" hereby refers to the average displacement measured across the notched by the extensometers during testing. Response for each of the specimens tested can be found in Appendix B.

During testing, a few features could be observed from these responses. For plain concrete, either normal or high strength, the specimen behaved elastically at the beginning of the loading at which the deformation across the notch increased linearly with the deformation up to about 60% of the maximum attainable load (linear-elastic response stage). Then the deformation with respect to the applied load increased more rapidly (the non-linear prepeak section). The load kept increasing until it reached the maximum tensile load. At this point a crack could be visible at the critical section of the specimen (see Figure 4.2). After the peak load, the load decreased gradually with increasing deformations as a major crack developed within the specimen to which it was completely separated into two parts where the load reached zero. It was also observed that the crack always occurred across the notch either starting from one side to the other side or from both sides simultaneously. For the normal and high strength fibrous concretes, the same behavior was also observed except that the presence of larger

Table 4.1 Average Material Properties of the Various Mixes Tested

Materials	Vf 1%	Matrix Compositions C: S: A: W	Pzzolanic Additives (%)	Tension Tests						Compression Tests		
				Strength f_t' (psi)	Initial Modulus E_t (x10^6 psi)	Strain at Peak Stress ε_{tp} (in/in)	Fracture Toughness (G_{IC}) lb/in	Fracture Energy (G_F) lb/in	Peak Disp. ω_p (in.)	Strength f_c' (psi)	Initial Modulus E_c (x10^6 psi)	Strain at Peak Stress ε_{cp} (in/in)
Normal Strength	Nil	1:2:3:0.5	-	349.248	1.139	0.00044	1.297	1.255	0.0195	5301	4.99	0.00174
High Strength	Nil	Same	MS-08	522.738	1.89	0.000299	0.772	0.703	0.0144	7321	5.585	0.001491
Concrete	Nil	Same	MS-10	527.122	1.992	0.000337	0.497	0.470	0.0088	7832	5.181	0.001463
	Nil	Same	FA-25	427.937	1.391	0.00039	0.879	0.834	0.0127	6585	5.481	0.001593
	Nil	Same	FA-35	440.637	1.572	0.00035	0.510	0.476	0.0079	6853	5.531	0.001495
Normal Fibrous Concrete	Harex	Same	-	514.448	1.271	0.000503	12.265	12.188	0.2558	5382	5.232	0.002594
High Strength Fibrous Concrete	Dramix	Same	FA-25	577.815	1.653	0.000412	51.327	50.609	0.2151	7181	5.392	0.00317

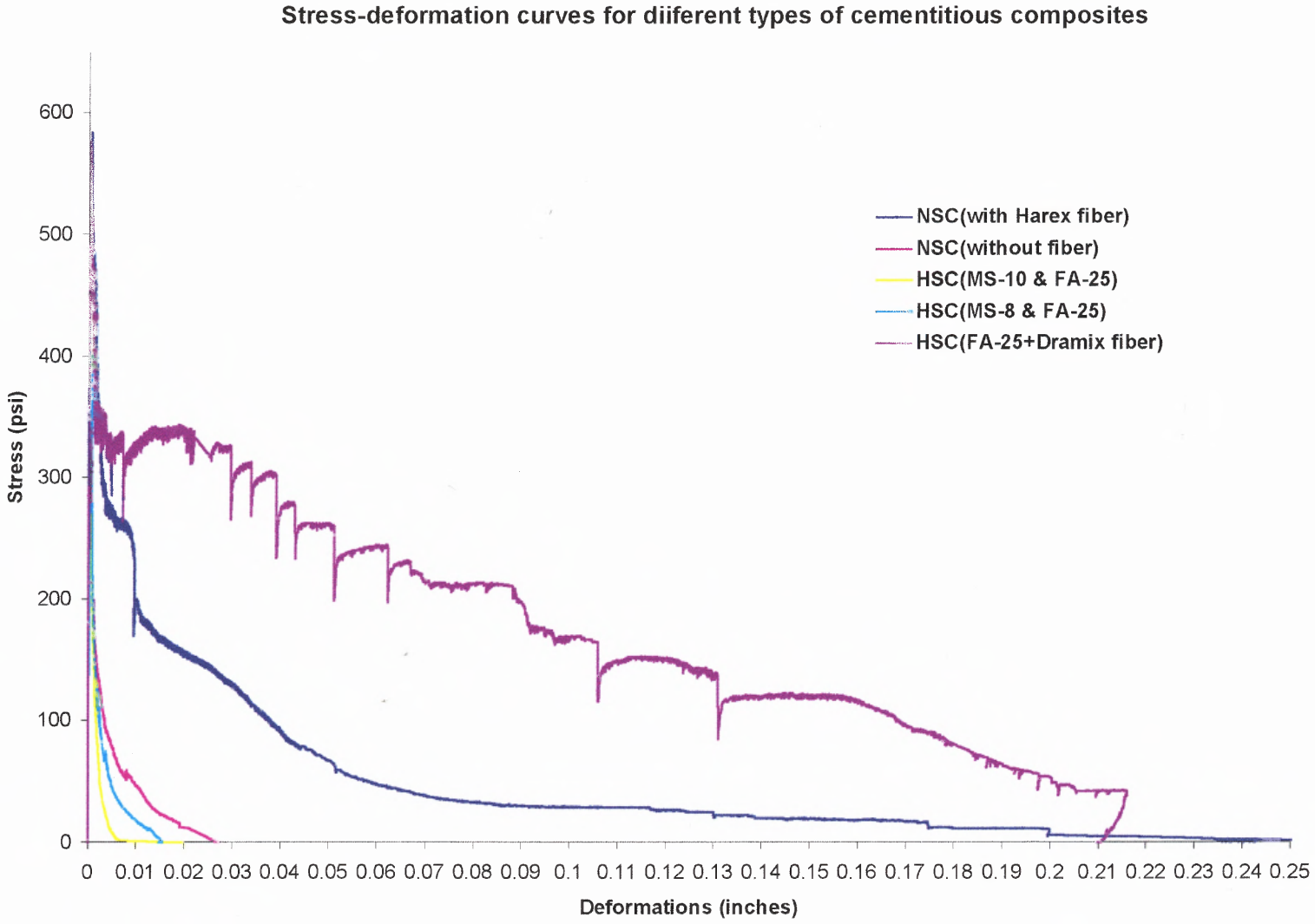

Figure 4.1(a) Stress-Deformation Curves for Different Types of Cementitious Composites

deformations occurred after the peak load along with the development of multiple cracks within the specimen (Figure 4.1(c)). This phenomenon continues progressively until the failure of the specimen.

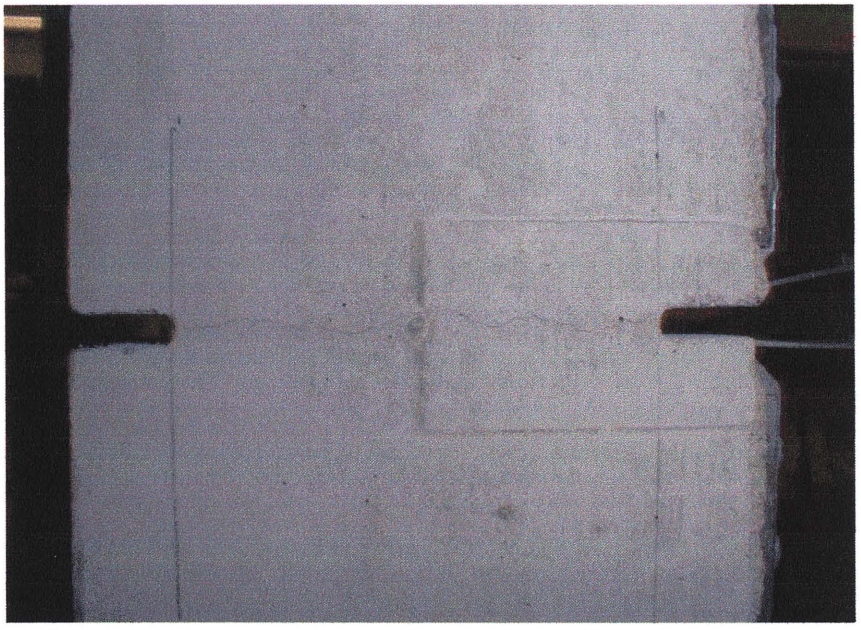

Figure 4.1(b) A Visible Crack developed at the Critical Section of the Specimen

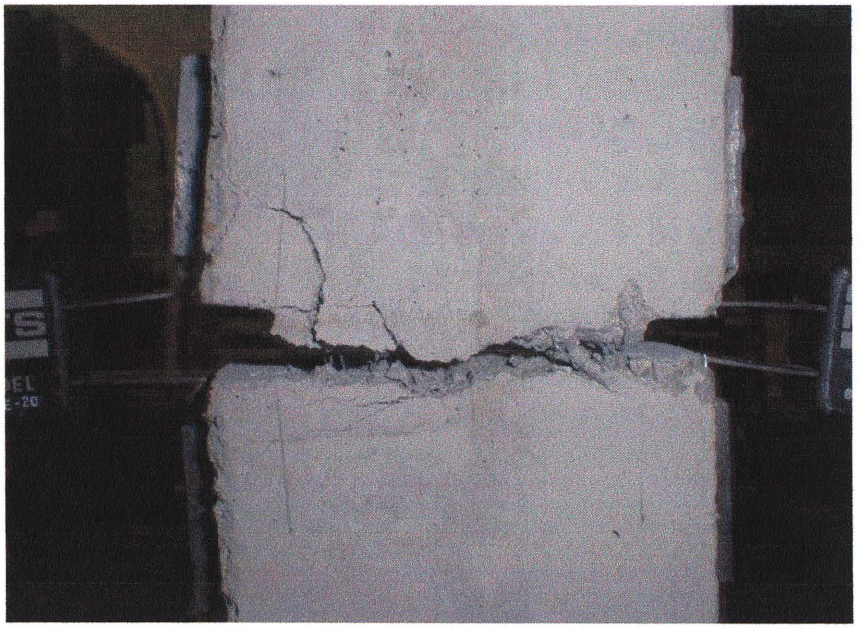

Figure 4.1(c) The Development of Multiple Cracks at Critical Section of the Specimen

4.1.2 Properties of the Plain Matrix and Effect of Fiber Reinforcement

4.1.2.1 Properties of the Plain Matrix: The matrices used for the four different types of concrete are slightly different in the mix proportion so the effects of the matrix variation on the tensile behavior can be investigated. Silica fume and fly ash are the key ingredients in the process of producing the dense matrices in high strength concretes. As can be observed from Table 4.1 and Figure 4.1, the tensile responses of the high strength matrices produced from these two ingredients are quite different. However, but enlarging the scale around the pre-peak and post-peak regions, appreciable differences in the tensile strength and post-peak stress displacement relationship can be noticed.

Figure 4.2 (a) illustrates the influence of fly ash on the tensile behavior of the matrix. The three curves shown represent the tensile stress-displacement response obtained from specimens, which have different amount of fly ash replacement in the mix proportions. It can be seen that the replacement of cement by fly ash in the composite has influence on the tensile strength and the post-peak section. Replacing a certain amount of cement by fly ash in concrete can increase the tensile strength. However, it can decrease the tensile stiffness of the composite to a certain degree. This can be seen by the lesser in the ability to sustain the applied load at any same level of displacement as illustrated by the steeper the slope of the post peak section as shown in Figure 4.2 (a). The same behavior was also found for the case of silica fume as shown in Figure 4.2 (b). These results clearly indicate that the tensile behavior of composite depends on the matrix types and mixes.

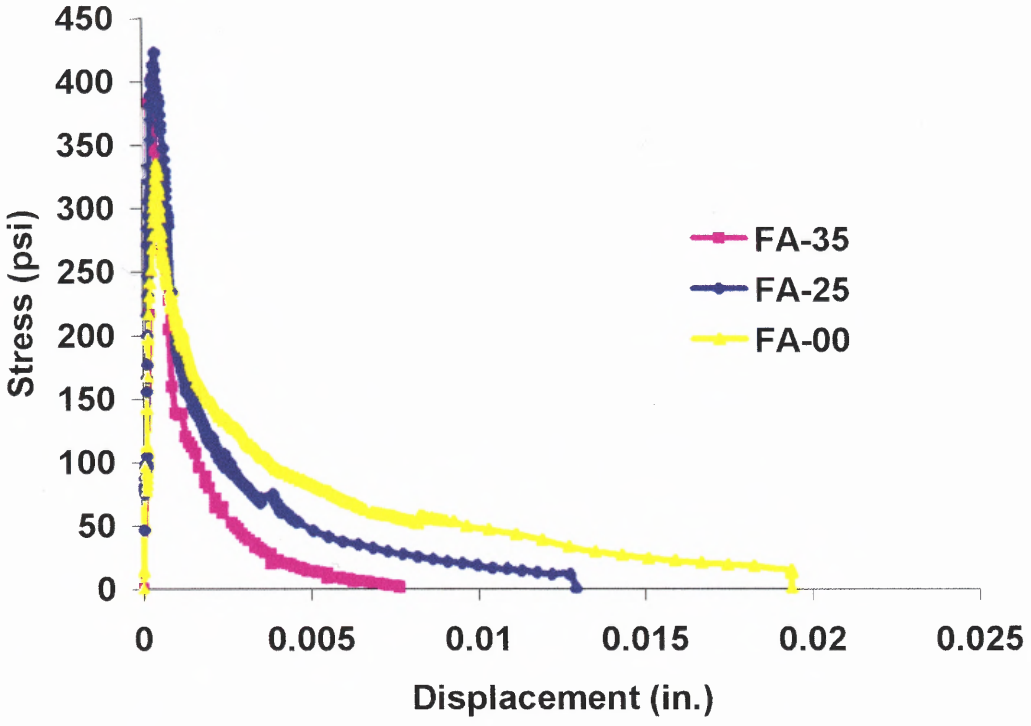

Figure 4.2(a) Stress-Deformation Curves for Concrete Matrices with and without Fly Ash (FA-35 = 35 Percent Cement by Weight Replaced by Fly Ash)

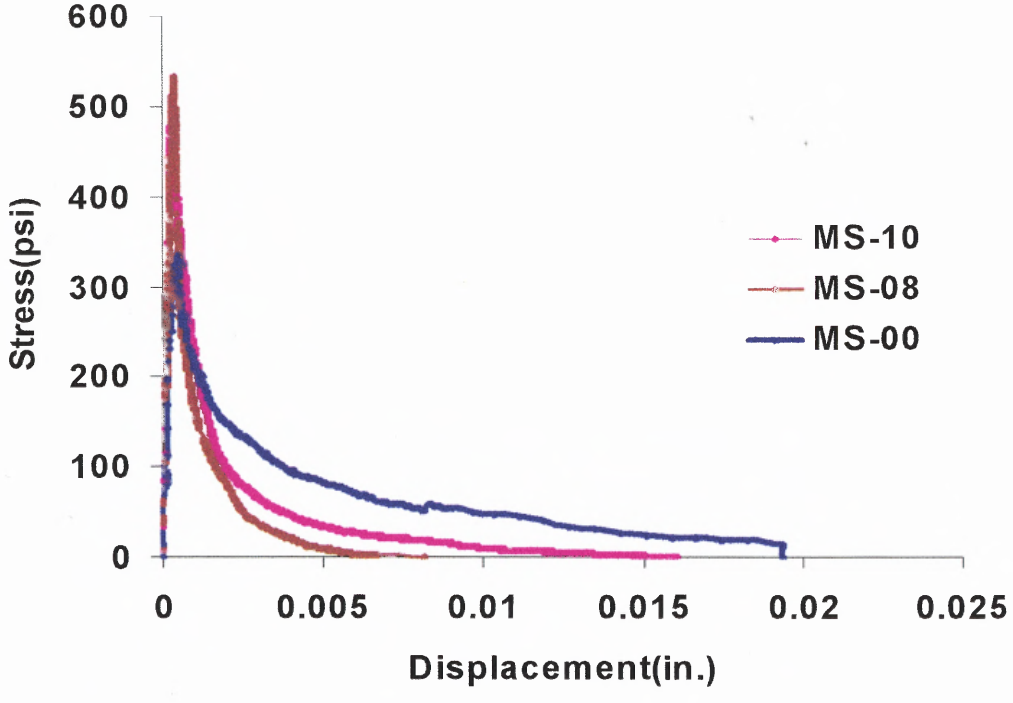

Figure 4.2(b) Stress-Deformation Curves for Concrete Matrices with and without Silica Fume (MS-10 = 10 Percent Addition of Cement by Weight by Silica Fume)

4.1.2.2 Effect of Fiber Reinforcement: The test results for normal and high strength concrete specimens incorporating two types of steel fibers, the Dramix and Harex steel fibers are shown in Figure 4.1 and Table 4.1. As mentioned, although the matrices of the composites used are different for the same fiber volume fraction of 1 percent, their tensile behavior tends to be similar, which makes it possible to have a reasonable comparison. It can be observed that by incorporating small amount of fiber for the normal and high strength cement based matrices, the overall tensile properties of the matrix enhance. The strength improvements due to fibers were formed to be 47% and 35% for normal and high strength concrete, respectively. In the Dramix fiber case, the larger value of strain capacity and peak stress of the composites can be found (Figure 4.3). The Harex steel fiber shows the same tendency to these reinforcing effects, but not as significant as in the case of Dramix in both the ultimate stress and the strain capacity since there are no hooked ends on Harex Fiber.

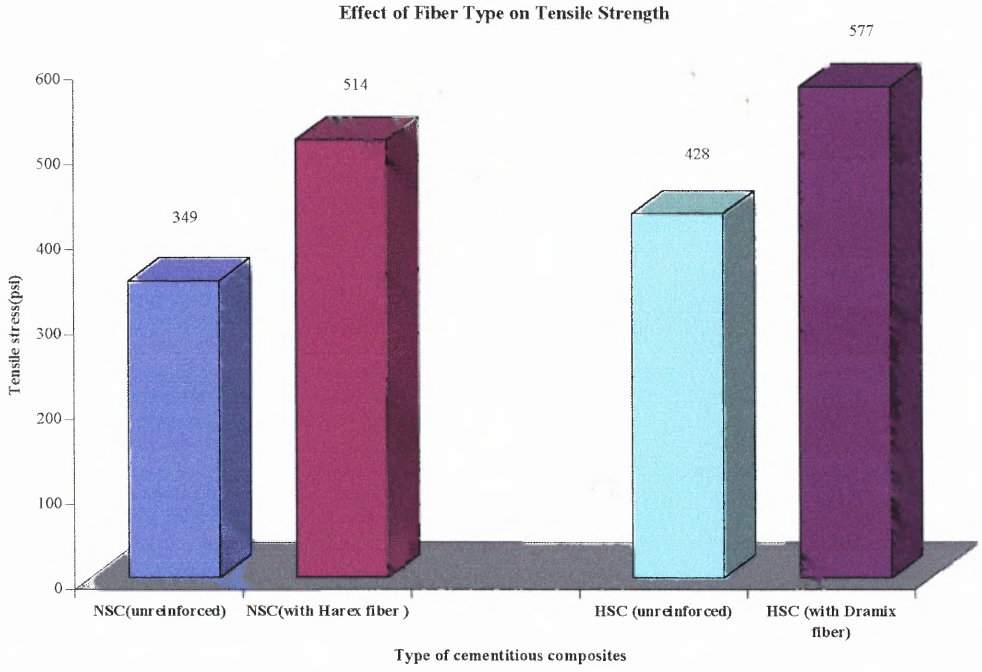

Figure 4.3 Effect of Fiber Type on Tensile Strength

4.1.3 Tensile Modulus of Elasticity

In fracture based-studies, the initial Young's modulus of elasticity under tension is an essential parameter for several theoretical models such as the ones developed by Reinhardt, Bazant and Oh, Gopalaratnum and Shah and etc. From the opening displacements measured over the cross-section at the notch by means of two extensometers within the gage length of 1-inch in this experimental study, the values of initial tangent modulus of elasticity of various cementitious composites can be calculated as shown in Table 4.1.

It can be observed from Table 4.1 that the tensile modulus of elasticity in tension varies with different mixes and depends on characteristic of the cement-based matrix. It seems that the stiffer the matrix, the higher the tensile modulus of elasticity. The presence of fibers in the matrix has little effect on the tensile modulus of elasticity. This can be explained by comparing the tensile moduli of steel fibers and concrete matrix. In general, the tensile modulus of steel fibers is 200 GPa or $29x10^6$ psi whereas that of cement matrix is 10-45 GPa (as mentioned earlier in Table 1.1). If the fibers do have the effect on the tensile modulus of elasticity of the composites, the tensile modulus of elasticity of high strength and normal fibrous concrete obtained from the experiment tests should be equal or much higher than that obtained from the plain high and normal strength concretes. However, the results of tensile modulus of elasticity of high strength and normal fibrous concretes in Table 4.1 do not show any effect of fibers as expected. The tensile modulus of elasticity of the fibrous concretes is almost the same as that of the plain concretes.

It is also noted from the results shown in Table 4.1 that the initial tangent modulus of elasticity in tension is not comparable to that in compression for every type of cementitious composites. This observed response contradicts the discussions with Gopalaratnum's work, which concluded that the modulus of elasticity for typical normal concrete in tension was comparable to the one obtained in compression.

Another interesting evidence can also be found from Table 4.1. that tensile modulus of elasticity of the composites (E_t) tends to increase proportionally with the increasing of the compressive modulus of elasticity (E_c) and the 28-day compressive strength (f_c'). The same bahavior was also found from available test data reported by other investigators (Gopalaratnum and Shah 1985, Chimamphant 1989, and Wecharatana 1990). Based on the results in this study, there exists a linear relationship between the ratios of the initial tangent modulus in tension over the one in compression versus the 28-day compressive strength as shown in Figure 4.4.

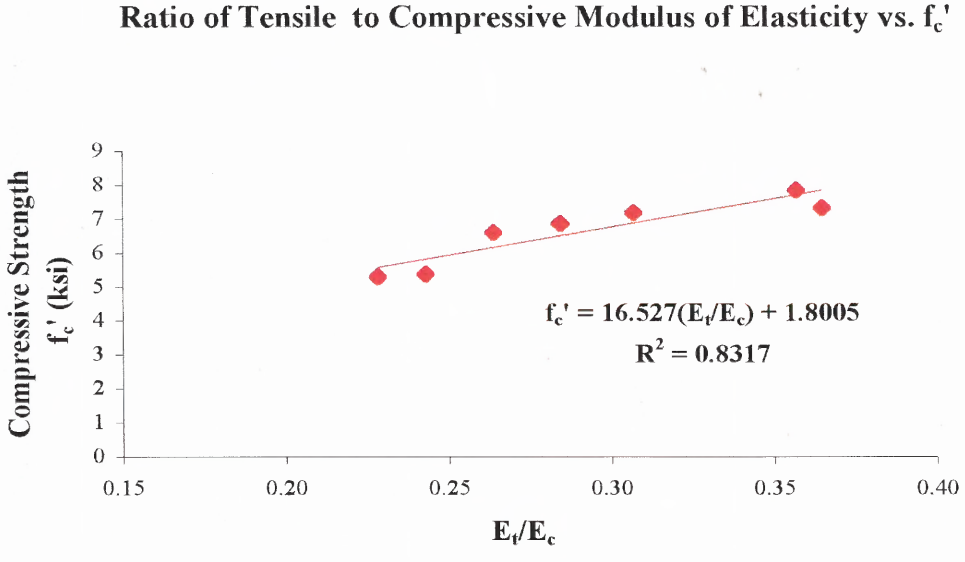

Figure 4.4 A Linear Relationship between the Ratios of the Initial Tangent Modulus in Tension (E_t) over the One in Compression versus the 28-Day Compressive Strength (Based on the Experimental Results in This Study)

This relationship provides a simple mean in obtaining the initial tangent modulus in tension, which can lead to a promising theoretical model for fracture studies of concrete and other types of cementitious composites without the need to conduct the tedious and time-consuming direct tension test. Since scarce information has been reported by other investigators for the evaluation of this modulus ratio, comparison of the linear relationship was made with the only one experimental data found in the literature as shown in Table 4.2. The comparison turns out to be quite satisfactory.

Table 4.2 A Comparison of the Initial Tangent Modulus of Elasticity in Tension Computed from the Linear Relationship with Experimentally Results Obtained by Chimamphant

Author	Materials	f_c' at 28 days	E_c ($x10^6$ psi)	E_t ($x10^6$ psi)	E_t(theoretical) ($x10^6$ psi)
Chimmaphant (1989)	Normal Concrete	5.142	2.044	0.564	0.413
	Silica Fume Concrete.	9.526	4.524	2.844	2.115

4.1.4 Stress vs. Strain-Crack width Relationships

It is postulated by the author that the accurate value of fracture energy can be obtained from the stress-crack width relationships, therefore an attempt was made to plot the relationship between the stress and crack width. To calculate the crack widths from the measured average displacements at any stress level obtained from the load-displacement relationships, it was assumed in this study that the crack width was zero at the peak stress level. Beyond this, the uncracked parts of the specimen gradually unloaded with the unloading modulus, which is equal to the initial tangent tensile modulus of elasticity. An average plots between the stress and crack width for all types of cementitious composites used in this study is presented in Figure 4.5(a).

In some preliminary investigations, the normalized stress-crack width relationship was also used as an invaluable parameter in support of the theoretical model and was sometimes used to characterize the fracture behavior of materials. Therefore, in this study an attempt was made to plot this relationship. The maximum peak stress and crack widths based on calculation method as mentioned earlier were used to normalize the stress-crack width relationship. An average normalized stress-crack width relationship is presented in Figure 4.5(b).

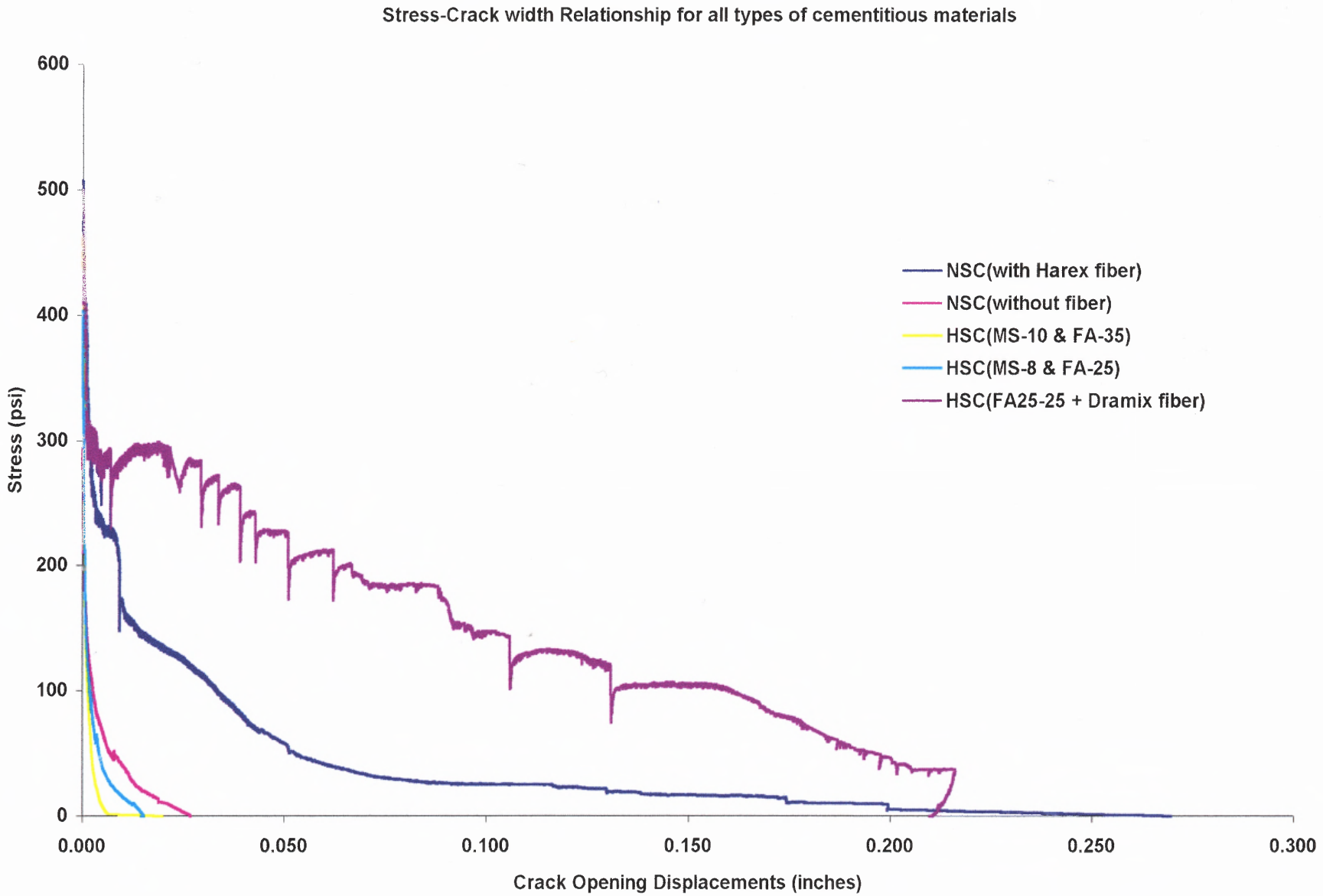

Figure 4.5(a) Stress-Crack Width Relationship for All Types of Cementitious Materials

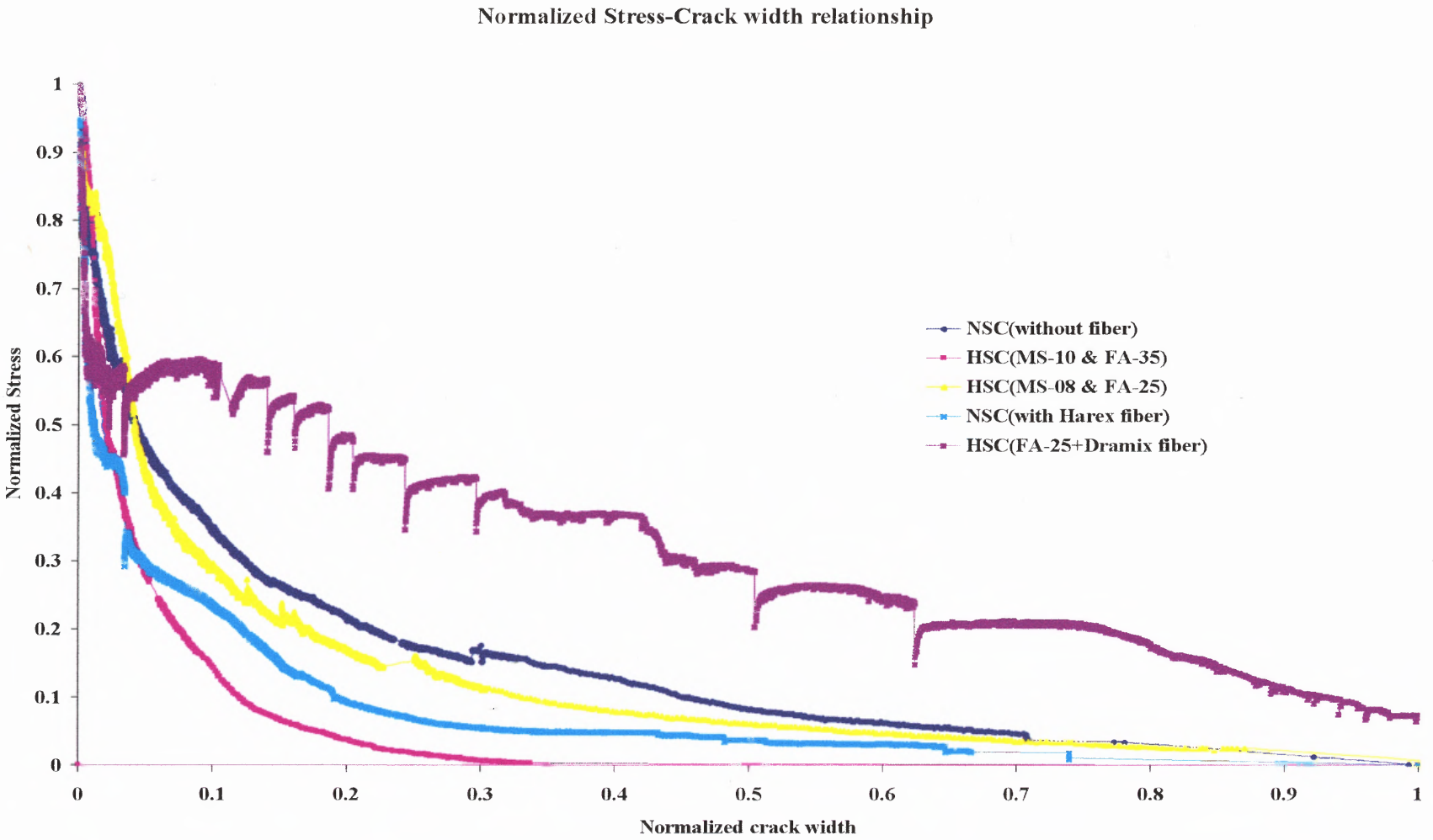

Figure 4.5(b) An Average Normalized Stress-Crack Width Relationship

4.1.5 Tensile Fracture Energy

Fracture energy has been widely used as a critical nonlinear fracture parameter for concrete in many proposed models. It is the amount of energy absorbed to create the unit area of fracture surface in a material. For a given material, if the accurate value of fracture energy is provided, the mode of fracture can be foreseen.

As found from the literature, fracture energy was usually taken as the total area under the load deformation curves (which was defined here in the present study as the fracture toughness). However, due to the fact that the presence of the crack can be seen experimentally in this study once the peak stress level is reached, the tensile fracture energies of the present study, G_F, will be calculated as the total area under the stress-crack width relationship. It is also equal to the total area under the curve of load-deformation curve subtracted the area in front of the unloading line taken from the peak load. The method of calculation for this area was mentioned earlier in section 4.1.4.

Fracture energies for the different types of cementitious mixes tested were summarized in Table 4.1. It can be seen that the fracture energy of the normal strength cement-based composites is 1-2 times higher than the high strength one. Among the high strength composites, the concrete made of the 25 percent replacement of cement by weight absorbed the most energy. For the fibrous composites, an appreciable larger amount of fracture energy was found. The differences in type and configuration of fibers result in the considerable difference in fracture energy. As can be seen from Table 4.1, the fracture energy of high strength fibrous composites made of hook-ended fibers (Dramix) is about 50-60 times higher than the one without fibers while the normal fibrous

composites made of straight-ended (Harex) is just 12-15 times when compared to the normal one without fibers.

Among all the data yielded in this study, the relationships between the fracture energy and other properties of the composites are also plotted. Figures 4.6(a) through (c) demonstrate the relationship between the fracture energy (G_F), compressive strength (f_c'), tensile strength (f_t'), and the peak displacement of unreinforced cement-based composites, respectively. As shown in these Figures, the relationships between the fracture energy, compressive, tensile strength, and the peak displacement are not quite conclusive. The data, however, indicate certain trends towards increasing fracture energy for decreasing the strengths and towards increasing fracture energy for increasing the peak displacements. Based on these observations, it might be concluded that the fracture energy increases with the decreasing of the strengths while it increases with the increasing of the peak displacement of the composites.

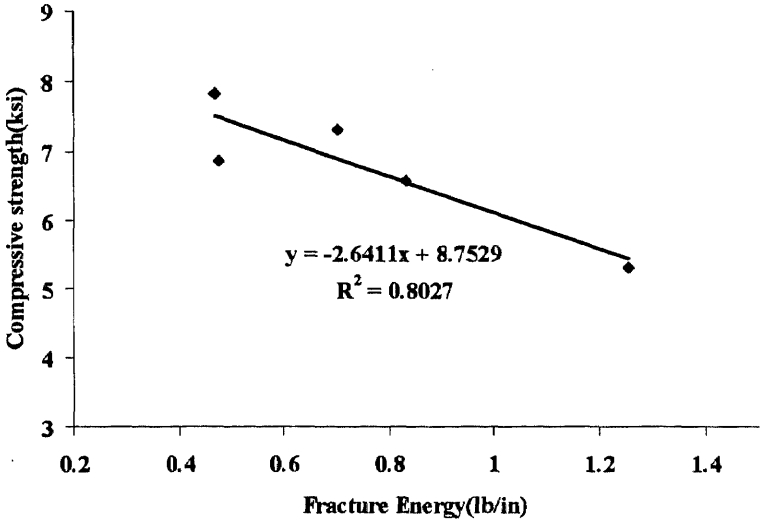

Figure 4.6(a) The Relationship Plotted between the Fracture Energy and the Compressive Strength of the Unreinforced Cement-Based Composites

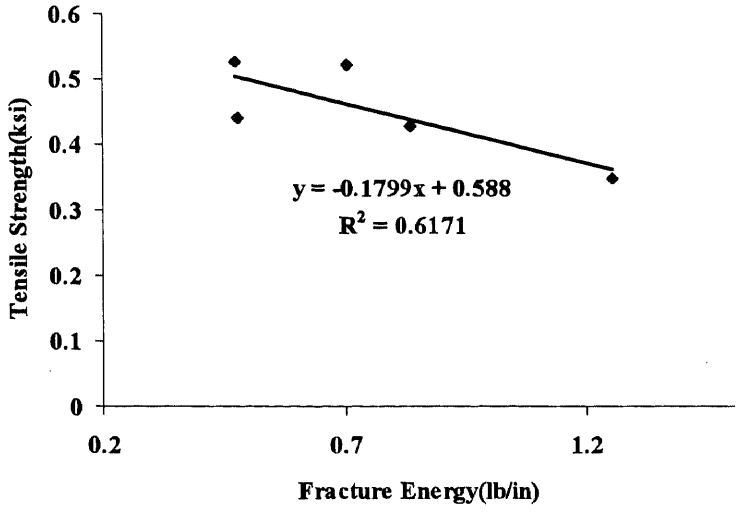

Figure 4.6(b) The Relationship Plotted between the Fracture Energy and the Tensile Strength of the Unreinforced Cement-Based Composites

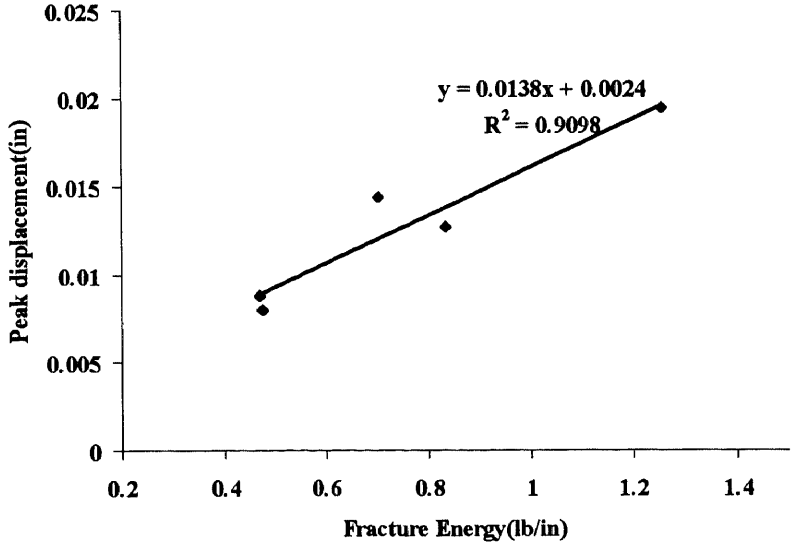

Figure 4.6(c) The Relationship Plotted between the Fracture Energy and the Peak Deformation of the Unreinforced Cement-Based Composites

The presence of fine pozzolans such as silica fume and fly ash in the cement matrix increases the strength of the matrix but at the same time tends to decrease the fracture energy of concrete. In the case of high strength concrete, it should be noted that fly ash concrete gives higher values of fracture energy and peak displacement than that of silica fume. This is interesting because the fly ash used in this study has almost the same particle size as silica fume (between 1 to 5 microns), but incorporating fly ash in concrete tends to give better improvements than silica fume. This seems that the characteristic of particles also plays an important role on the bond property and cracking behavior of concrete. This observation confirms the conclusion made by Montgomery and Diamond in 1984.

Finally, the values of fracture energies obtained from this study was compared to those reported by other researchers. It should be noted that the fracture energy calculated based on assumption used in this study (total area below the stress-crack width relationship) is not much different from the one calculated based on conventional assumption as found in the literature (about 0.5 to 1% lesser), therefore the comparison to the values reported by other investigators can still be justified. Since some reported values have already been given in the previous chapter (Chapter 2), so they will not be shown again here. From the comparisons, the fracture energy was found not to be dependent a material property. For materials of the same strength, variation of fracture energy remains. It was observed that specimen configurations and matrix mix compositions might have influence on the measured fracture energy.

4.1.6 Ductility by Means of Tension Softening

It is believed that material characteristic such as the brittle or ductile nature of the composite is well demonstrated within the non-linear region of the load-deformation response prior to the peak load. Materials that fail in tension at relatively low values of strain are classified as "brittle" materials. Examples are glass, ceramic, stone, and cast iron. These materials fail at the fracture or ultimate stress at point B of the diagram in Figure 4.7 with only little elongation after the proportional limit (point A in Figure 4.7)

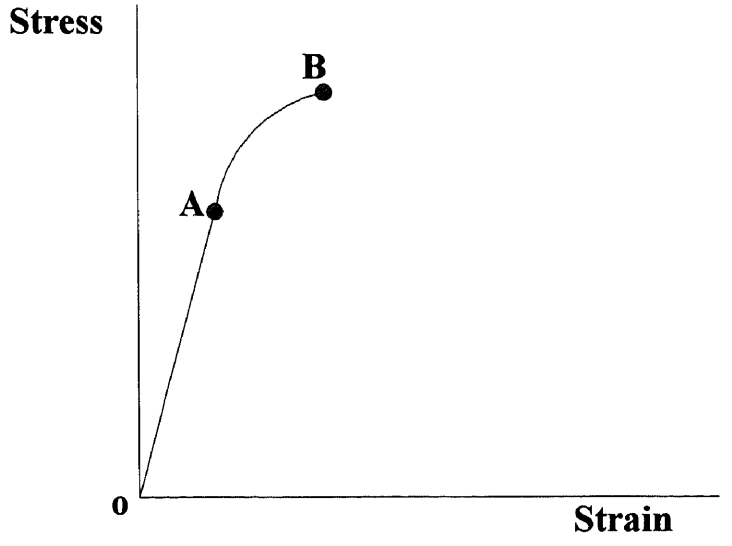

Figure 4.7 Typical Stress-Strain Diagram for a Brittle Material

At present study, the ductility index of the cementitious composite is proposed. The concept of ductility index is derived from the ratio of the tensile strain at peak load over the strain at the proportional limit. This ratio represents the ability of material to elongate after the proportional limit up to the first crack of fracture. The ductility indices for different types of cementitious composite materials are summarized in Table 4.3.

Table 4.3 Ductility Index of Cementitious Composite Materials

Materials	V_f (1%)	Matrix Compositions C: S: A: W	Pozzolanic Additives	Average Strain		Ductility Index
				At tensile peak load	At proportional limit	
Normal Strength	Nil	1:2:3:0.5	-	0.000440	0.000163	2.699
High Strength Concrete	Nil	Same	MS-08	0.000299	0.000163	1.834
	Nil	Same	MS-10	0.000340	0.000153	2.222
	Nil	Same	FA-25	0.000390	0.000173	2.254
	Nil	Same	FA-35	0.000350	0.000156	2.244
Normal Fibrous Concrete	Harex	Same	-	0.000510	0.000168	3.036
High Strength Fibrous Concrete	Dramix	Same	FA-25	0.000412	0.000108	3.815

It can be observed that the high strength concrete with the addition of silica fume of 8% by weight has the lowest ductility of 1.83 whereas the high strength hook-ended fibrous concrete has the highest index of 3.82. It seems that the more brittle (or less ductile) the material behaves, the lower the ductility number is. The addition of fiber to the normal and high strength concretes increases the ductility of the matrices. Some fibers may be more efficient than others depending on the configuration of the fibers. As shown in Table 4.3, the addition of hooked-ended fibers results in the higher percentage of increase in ductility of the matrix when compared to the straight-ended fiber.

4.2 Flexural Behavior and Ductility of High Performance Concrete Beams

In test series 2, the experiments to investigate the flexural characteristics and ductility of high performance concrete beams made from fly ash concrete were conducted. Eight small-scaled under-reinforced concrete beams having the same amount of longitudinal reinforcement and confinement reinforcement but different in the percentage replacements of fly ash in the mix proportion were tested under three-point loading test. Six standard 3 x 6 in. cylinders of fly ash concrete were also tested in compression and splitting-tensile tests. The results, dealing with the load-deflection, compression strength, splitting tensile strength of the reinforced concrete beam specimens obtained from the tests are discussed in the following.

4.2.1 Load-Deflection Behavior of High Performance Concrete Beams

A comparison of typical load-deflection diagrams for eight beam specimens is shown in Figure 4.9. All beam specimens have the same amount of longitudinal reinforcement and confinement reinforcement but the percentage replacements of fly ash in the mix proportion were varied as indicated in Table 3.2. From Figure 4.9, each beam was designated by a letter and 3 numerals, such as A001. The first letter, A, B, C, or D, indicates a beam specimen from test series (as shown in Table 3.2) The first and second numerals indicate the proportion of fly ash in the mix: 00, 10, 20, 30 percent by weight, respectively. The final numerals: 1 and 2 indicate the specimen number.

During testing, all beams reached tensile steel yielding with visible deflections prior to the crushing of concrete, which were corresponding to the current strength method. The concrete cracked in tension near the mid-span of the beam under a relatively

small load. As the load on each beam was increased beyond cracking, the tensile steel reinforcement yielded, whereupon the beam underwent large deflection with further increasing in load. All beam specimens were tested to failure in this study. Based on the observations during testing and the final failure modes of the specimens, one can conclude that control specimens A001 and A002 show a successful ductile failure with a complete "plastic" hinging rotation occurred near the mid-span of the beam (see Figure 4.8).

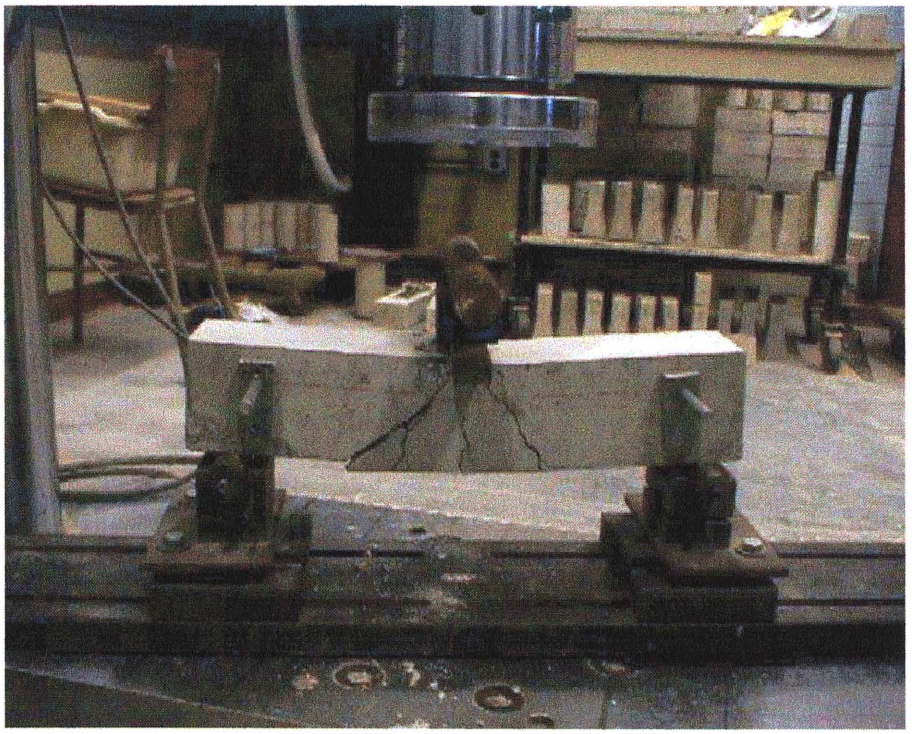

Figure 4.8 A Ductile Failure Mode with a Complete "Plastic" Hinging Rotation Occurred near the Mid-Span of Beam.

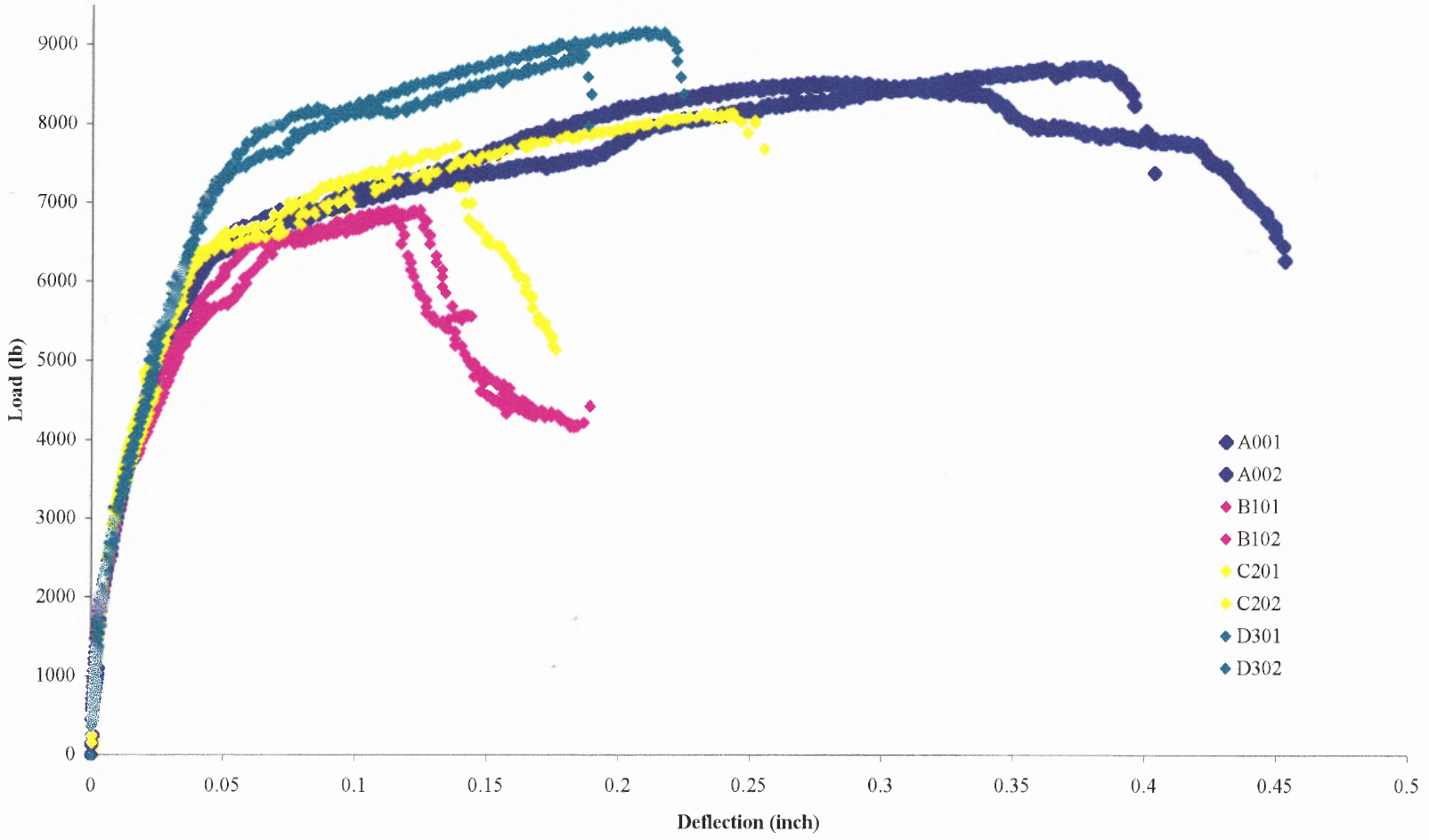

Figure 4.9 Comparison of Load-Deflection Diagram for Eight-Beam Specimens Different in Percentage Replacement of Fly Ash

Specimens C201, D301, and D302 also demonstrated an almost complete ductile failure with less obvious hinging region near the mid-span of the beam. For specimens B101, B102, and C202, however, they did not arrive at a successful ductile failure. Although specimens B101, B102, and C202 experienced tension steel yielding after concrete cracking, these beams failed and collapsed suddenly due to shear diagonal tension prior to a complete development of hinging rotation near the mid-span of the beam. Thus, the load-deflection diagrams of specimens B101, B102, and C202 were incomplete even though some test results of three specimens could still be found useful for this study.

4.2.1.1 Ultimate Loading Capacity vs. Fly Ash Replacement: It can be seen from the results of these tests that the percentage replacement of fly ash does affect the flexural behavior of reinforced concrete beams. The substitution of fly ash varying from 10% up to 30% was found to be the controlling factor in determining the shape of the load-deflection curve. Figure 4.9 shows that at the same deflection, from zero level up to the stage of steel yielding, members with the 30% replacement of cement by fractionated fly ash resulted in the highest load carrying while the other members, which were with 10% and 20% replacements, gave no significant difference from the control member. It is interesting to note that with 10% replacement of cement by the fly ash used in this study, the load was shown to be lower than any other specimens, even the control one that contains 0% percent replacement of fly ash in its mix proportion.

Table 4.4 presents the ultimate loading capacity (P_u) of all beams tested to failure. They show similar results to the load at steel yielding. The average ratio of P_u (experimental) vs. P_u (theoretical) is 1.633, and the standard deviation of all 8 tests is 0.162.

Table 4.4: Ultimate Loading Capacity and Deflection at Ultimate

Beam Specimen	Experimental		Theoretical[Ŧ] P_u (kips)	$\frac{P_u \text{ (exp.)}}{P_u \text{(theo.)}}$	Ductile Failure Mode
	P_u (kips)	Δ_u (in.)			
A001	8.711	0.38	4.979	1.750	Complete*
A002	8.516	0.34	4.979	1.710	Complete
B101	6.954	-	4.910	1.416	Incomplete
B102	6.904	-	4.910	1.406	Incomplete
C201	8.145	0.24	4.991	1.632	Complete
C202	7.725	-	4.991	1.548	Incomplete
D301	9.17	0.22	5.011	1.830	Complete
D302	8.877	0.19	5.011	1.772	Complete
			Average	1.633	
			Standard deviation	0.162	

* "Complete" ductile failure indicates that the "plastic" hinge has been fully developed at the hinging region

Ŧ Theoretical Ultimate loading was completed by the present ACI strength Method with the load and resistance factors equal to 1 and ignoring the compression bar at the top of the beam.

4.2.1.2 Ductility vs. Fly Ash Replacement: It is also observed from Figure 4.9 that members with higher percentage replacement of fly ash exhibited slightly less deflection than those members with lower percentage of fly ash replacement at the same load level

up to the stage of steel yielding. However, the deflection at the steel yielding seems to be independent of the percentage replacement of fly ash. For every test specimen, the deflection at steel yielding, Δ_y, is about 0.05 in.

Table 4.4 also gives the values of deflections at ultimate load, Δ_u. They are 0.38 in., 0.34 in., 0.24 in., 0.22 in., and 0.18 in. for test specimens A001, A002, C201, D301, D302, respectively. Thus, the experimental ductility indexes: Δ_u / Δ_y (as defined by ACI committee 363) for these under-reinforced concrete beams is 7.6, 6.8, 4.8, 4.4, and 3.6 respectively. Based on these results, one can conclude that the concrete beams with fly ash replacement suffer a loss in ductility as compared to the control beams. These findings are obviously to be critical as the ductility behavior of reinforced concrete structure is vital to the structural integrity and safety. More research on this subject should be done in the near future.

Past research (Hsu and Hsu, 1994) revealed that compressive strength and stress-strain behavior of concrete, amount of longitudinal reinforcement, spacing of confinement reinforcement for any reinforced concrete members were the major parameters that controlled the shape of the load-deflection curves. In this study, since the combination of confinement spacing and longitudinal reinforcement amount were kept to be the same for every test members and no modification of the mix was made except the replacement of cement by fly ash in concrete; it was evident that the difference in ultimate loading capacities and load-deflection curves might be resulted from the influence of compressive strength and its stress-strain behavior of fly ash concrete. Thus, the influence of fly ash on compressive strength will be discussed in the following.

4.2.2 Influence of Fly Ash Replacement on Compressive Strength of Concrete

On the day that the beams were tested, the 3 x 6 in. cylinders were also tested in uniaxial compression under closed-loop strain control using a 100 kips MTS hydraulic testing machine to determine their concrete compressive strengths.

The tabulated results for the compressive strength are obtained from the average of three cylinders for each series of beams. They are presented in Table 4.5.

Table 4.5 Compressive Strength of Four Different Fly Ash Concretes

Specimen	Fly Ash Replacement (%)	Sample No	Compressive Strength (f_c') at 28 day (psi)	Average (psi)
Series A	0	1	5801	
		2	5376	
		3	5518	5565
Series B	10	1	4952	
		2	4669	
		3	4527	4716
Series C	20	1	5659	
		2	6084	
		3	5518	5754
Series D	30	1	6084	
		2	6017	
		3	6225	6109

As expected, the difference in compressive strength can be observed from Table 4.5. The results show that the compressive strengths at the age of 28 days were higher for all levels of fly ash replacement when compared to the control cylinder, except for the 10% fly ash replacement. Replacing 10% of the weight of cement with fly ash lowered the 28-day compressive strength but about 15% of the control strength while 20% and 30% replacements of fly ash increased the strength slightly about 3% and 10%, respectively. One can also observe here that using fly ash as a partial replacement, in the

amount of at least 20% of the weight of cement, would produce the same compressive strength as the control concrete. These results are in good agreement with the results from Jaturapitakkul (1993), and Wang (1992) for fly ash that has the same size distribution and chemical composition as the fly ash used in this study.

4.2.3 Influence of Fly Ash Replacement on Splitting Tensile Strength of Concrete

In addition to compressive strength, tensile strength by splitting test was also determined. The fly ash concrete with 0%, 10%, 20% and 30% replacement of cement by weight of cementitious materials were tested for their strength. The results obtained from the test are shown in Table 4.6. The results show that the splitting tensile strength of fly ash concrete behaves the same way as the compression strength does. It is also seen from the results obtained from both tests that the splitting tensile strength of fly ash concrete increases with the increase of the compressive strength.

Table 4.6 Splitting Tensile Strength of Four Different Fly ash Concretes

Specimen	Fly Ash Replacement (%)	Sample No	Splitting Tensile Strength (f_t') at 28 day (psi)	Average (psi)
Series A	0	1	799	
		2	874	
		3	877	850
Series B	10	1	669	
		2	619	
		3	616	635
Series C	20	1	913	
		2	912	
		3	914	913
Series D	30	1	1006	
		2	912	
		3	885	934

A typical way to express the splitting tensile strength of concrete is as a percentage of its compressive strength. From Tables 4.5 and 4.6, the results yield an average value for the splitting tensile strength of 15% of the compressive strength. The maximum and minimum values are 13.5 % and 16 % respectively, with standard deviation of 1.256%.

CHAPTER 5

SUMMARY AND CONCLUSIONS

The results obtained from all of the experimental tests conducted in this study lead to the following conclusions.

1. The post-peak behavior of different types of cementitious composite materials under a tensile load obtained from uniaxial direct tension tests is dependent on testing techniques. However, it provides the complete descriptive information of fracture and structural behavior of all types of cementitious composites when subjected to the tensile loading. The stress in cement-based materials increases linearly with deformation up to about 60% of the maximum attainable stress. Then the deformation increases nonlinearly with respect to the stress until the maximum stress is reached where the crack is formed. Finally, a gradual steep fall of stresses occurs with increasing deformation until a certain deformation is reached where the two parts of the specimen are formed. The same behavior is also found when small amount of steel fibers is incorporated into the cement-based matrix, however the presence of the larger deformations occurs after the peak load along with the multiple cracks, developed until the failure of the specimen. This is primarily a result of the type and shape of the fibers.

2. It is evident from the results that the "brittle or ductile" behavior at the material level of cementitious composite materials, which can be explained by the post-cracking response obtained from the uniaxial direct tension test, is also compatible with the observed ductile behavior exhibited by the reinforced concrete structural members under

flexural loading. The higher the strength of the matrix, the lesser the ductility of the composite is.

3. Based on study of the reinforced concrete beams with fly ash replacement, there was a loss in flexural ductility of the fly ash concrete when compare to those of the control concrete beams. Thus, more research on reinforced concrete structures with different fly ash replacements is needed to be conducted.

4. The present experimental results obtained from the direct tension tests could be useful for the theoretical modeling of the fracture behavior of cementitious composites. They can also be used to determine the coefficients needed in many proposed fracture formulas, if any exists. For the ductility and brittle manner of materials and structures that were found experimentally in this study, further investigations of these behaviors are recommended for larger sizes of test specimens so that the research results can be used for structural design in practice.

APPENDIX A

PROPERTIES OF MATERIALS

Table A.1 Chemical Composition of Fly Ash used in this study

Parameter	Composition (%)
Loss on Ignition	2.67
Moisture	0.18
Sulfur Trioxide	3.81
Silicon Dioxide	38.93
Aluminum Oxide	24.91
Iron Oxide	12.89
Calcium Oxide	6.85
Potassium Oxide	2.10
Phosphorous Anhydride	0.07
Magnesium Oxide	1.55
Barium Oxide	0.61
Sodium Oxide	1.31
Manganese Oxide	0.05
Titanium Dioxide	1.57
Strontium Oxide	0.34

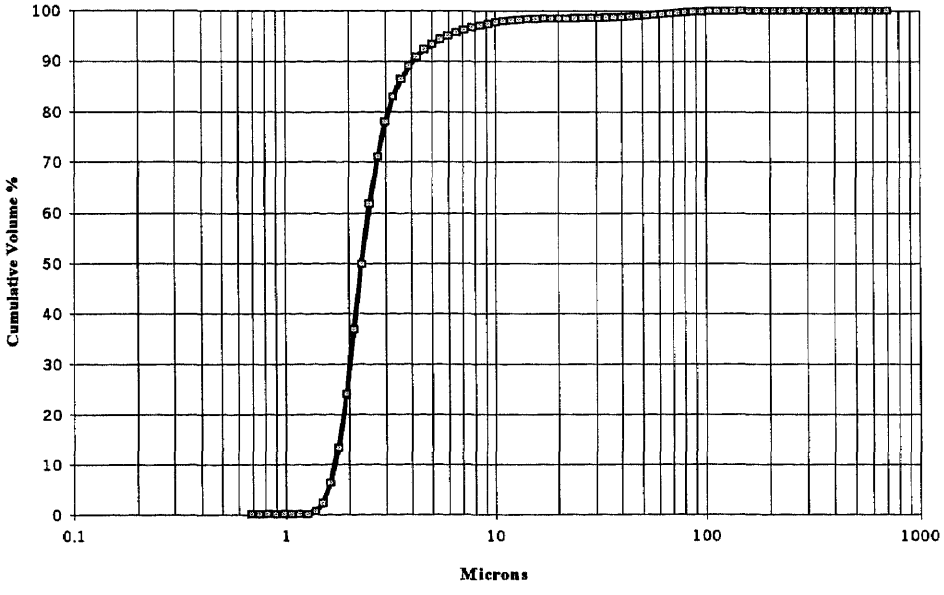

Figure A.1: Particle Size Distribution of Mercer Fly Ash

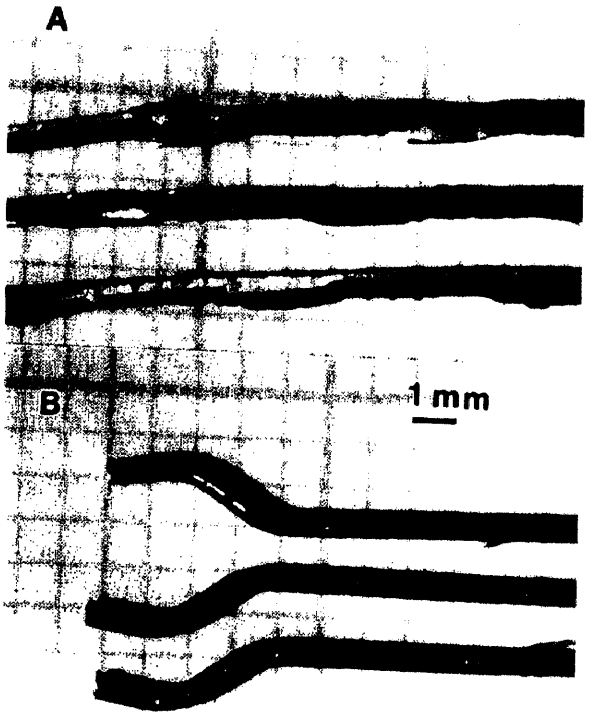

Source: Bentur, A., and Mindess, S., "Structure of Fibre Reinforced Cementitious Materials," Fibre Reinforced Cementitious Composites. (New York: Elsevier Science Publisher, 1990) 16-17.

Figure A.2: Various Shapes of steel fiber. A, Straight; B, Hooked

APPENDIX B

EXPERIMENTAL RESULTS OF DIRECT TENSION TESTS

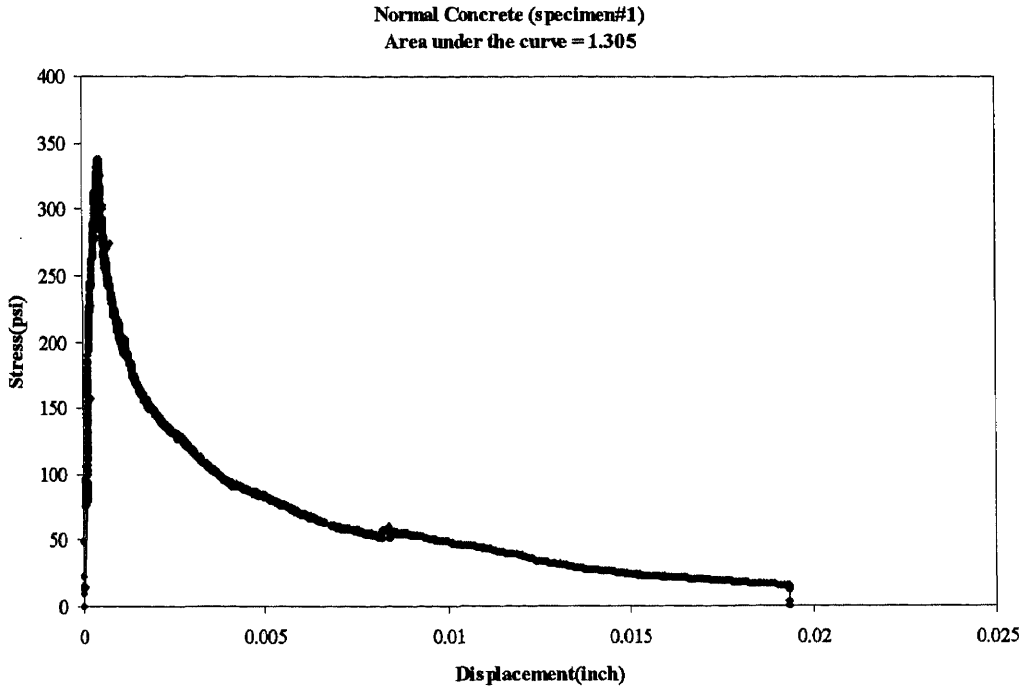
Normal Concrete (specimen#1)
Area under the curve = 1.305
Stress(psi)
400
350
300
250
200
150
100
50
0
0
0.005
0.01
0.015
0.02
0.025
Displacement(inch)

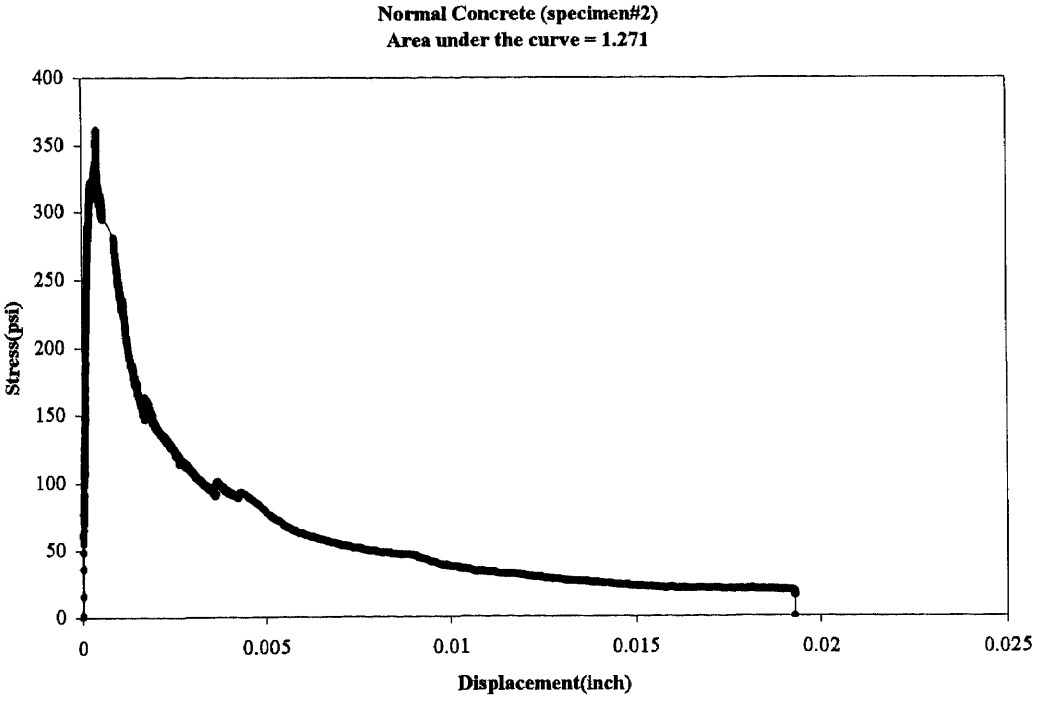
Normal Concrete (specimen#2)
Area under the curve = 1.271
Stress(psi)
400
350
300
250
200
150
100
50
0
0
0.005
0.01
0.015
0.02
0.025
Displacement(inch)

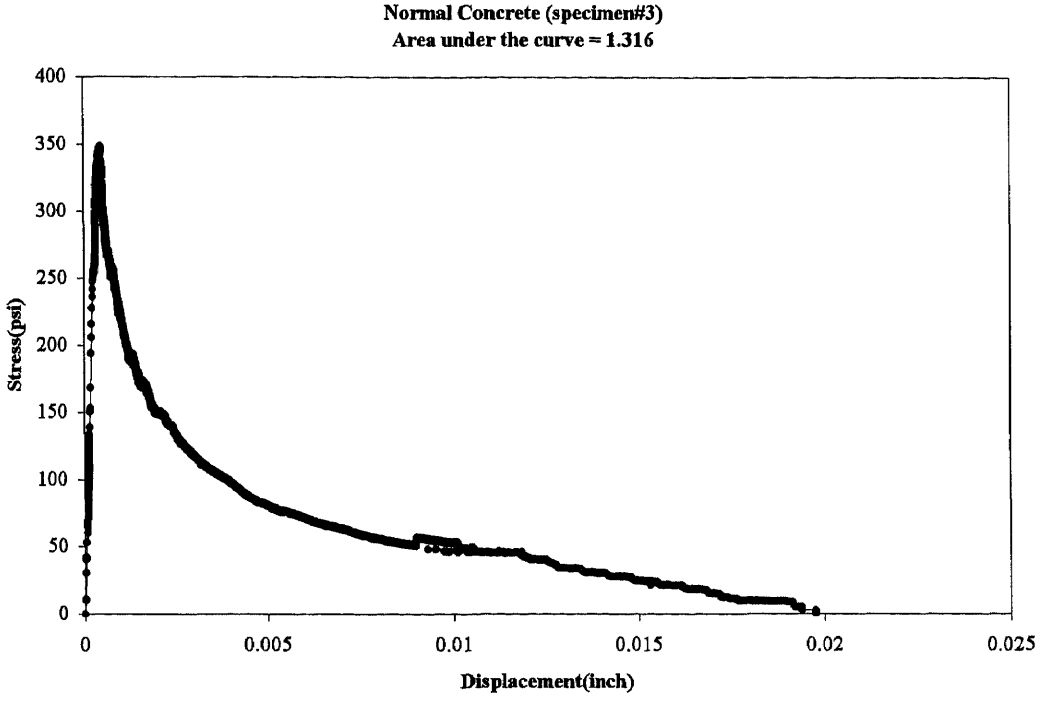
Normal Concrete (specimen#3)
Area under the curve = 1.316
Stress(psi)
400
350
300
250
200
150
100
50
0
0
0.005
0.01
0.015
0.02
0.025
Displacement(inch)

High Strength Concrete (MS-08, specimen#1)
Area under the curve = 0.735

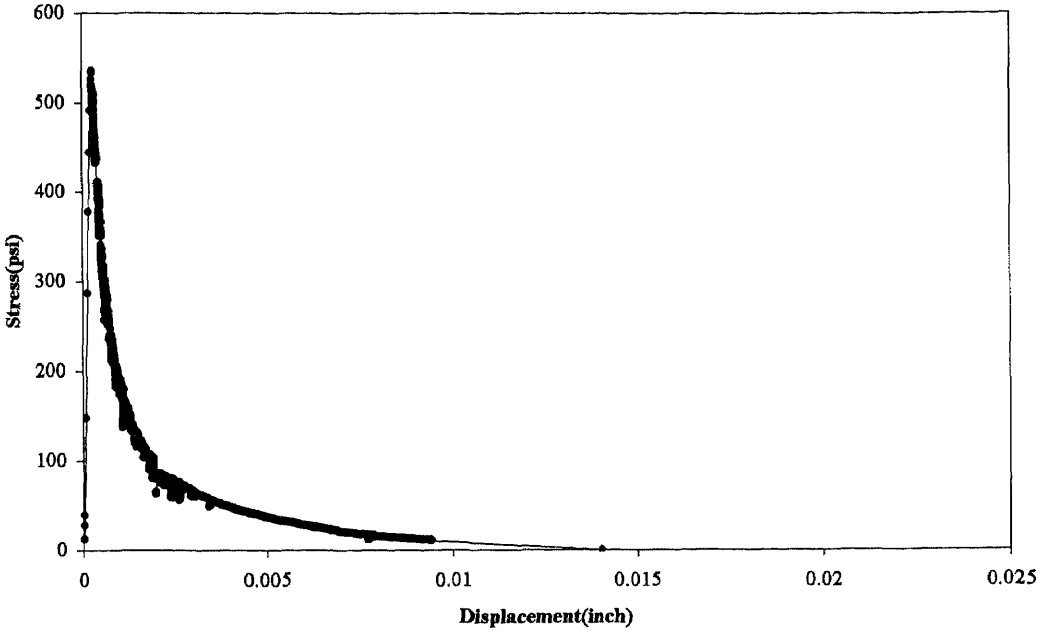

High Strength Concrete (MS-08, specimen#2)
Area under the curve = 0.823

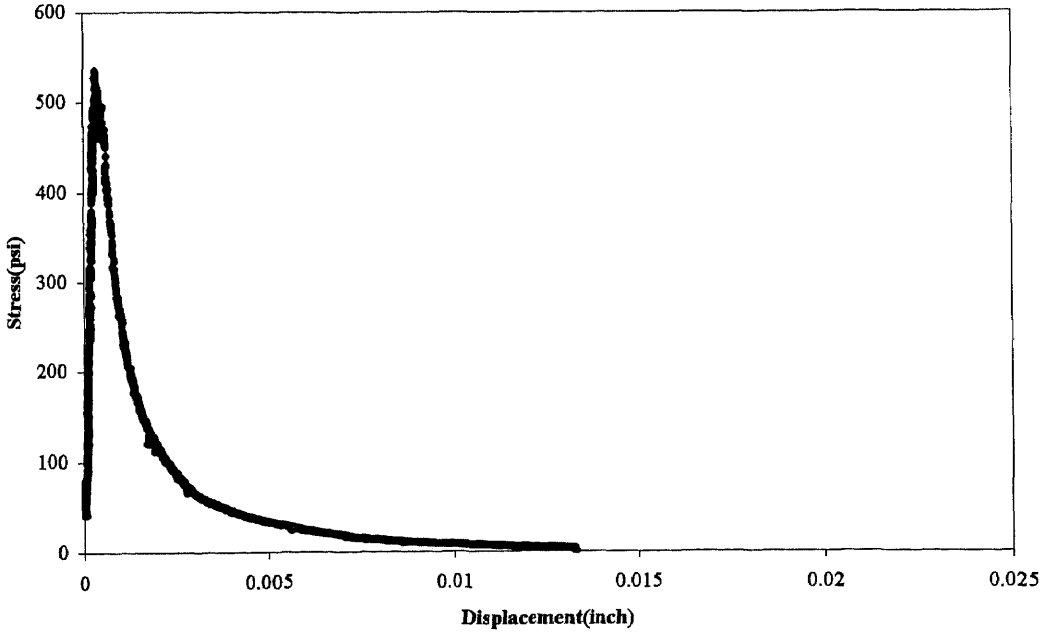

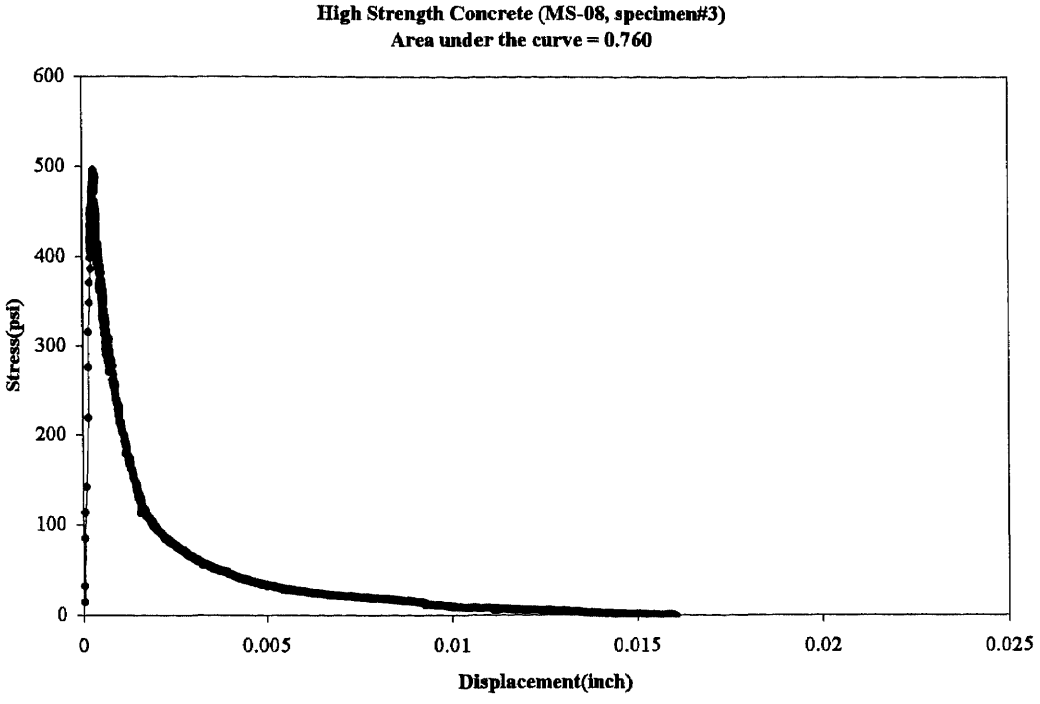
High Strength Concrete (MS-08, specimen#3)
Area under the curve = 0.760
600
500
400
300
200
100
0
Stress(psi)
0
0.005
0.01
0.015
0.02
0.025
Displacement(inch)

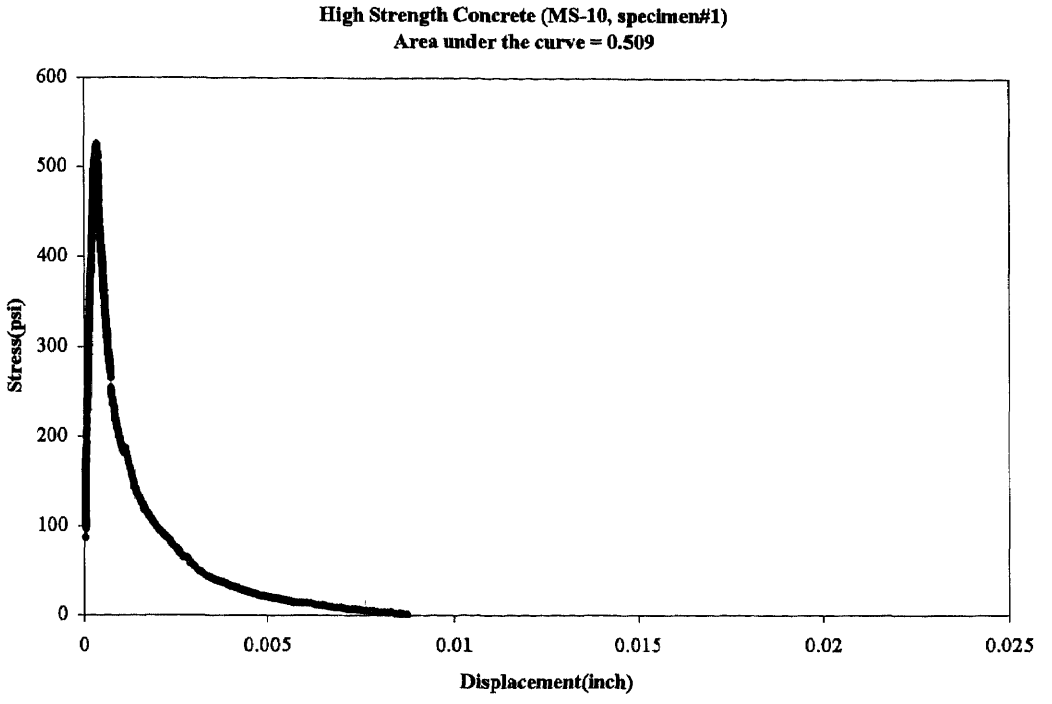
High Strength Concrete (MS-10, specimen#1)
Area under the curve = 0.509
Stress(psi)
600
500
400
300
200
100
0
0
0.005
0.01
0.015
0.02
0.025
Displacement(inch)

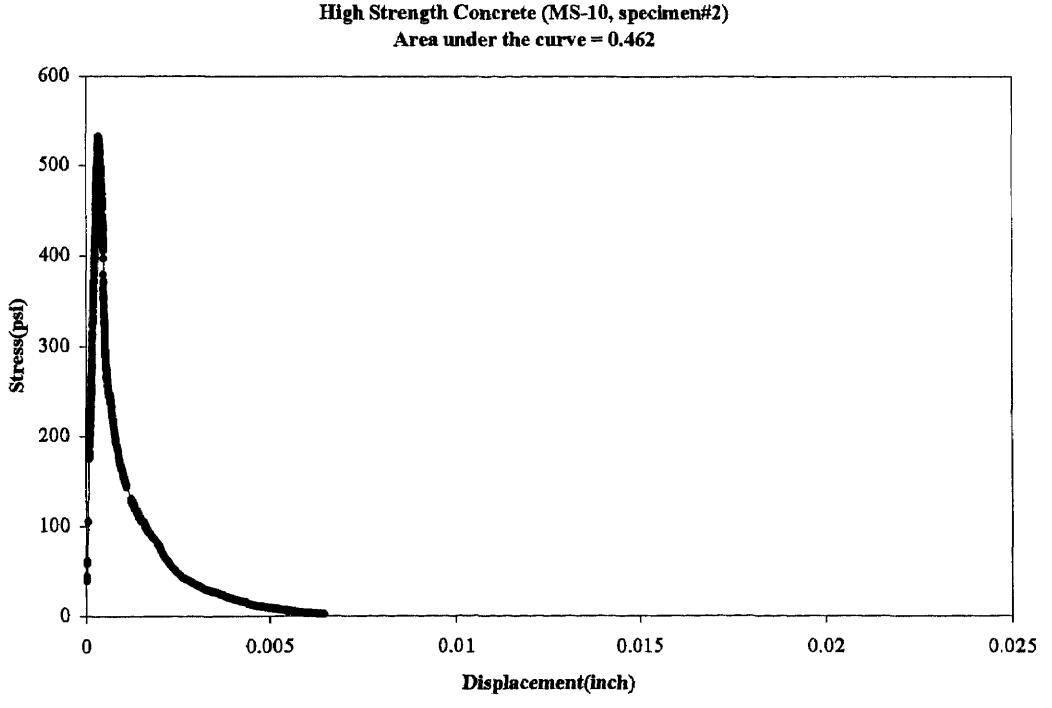
High Strength Concrete (MS-10, specimen#2)
Area under the curve = 0.462
Stress(psi)
600
500
400
300
200
100
0
0
0.005
0.01
0.015
0.02
0.025
Displacement(inch)

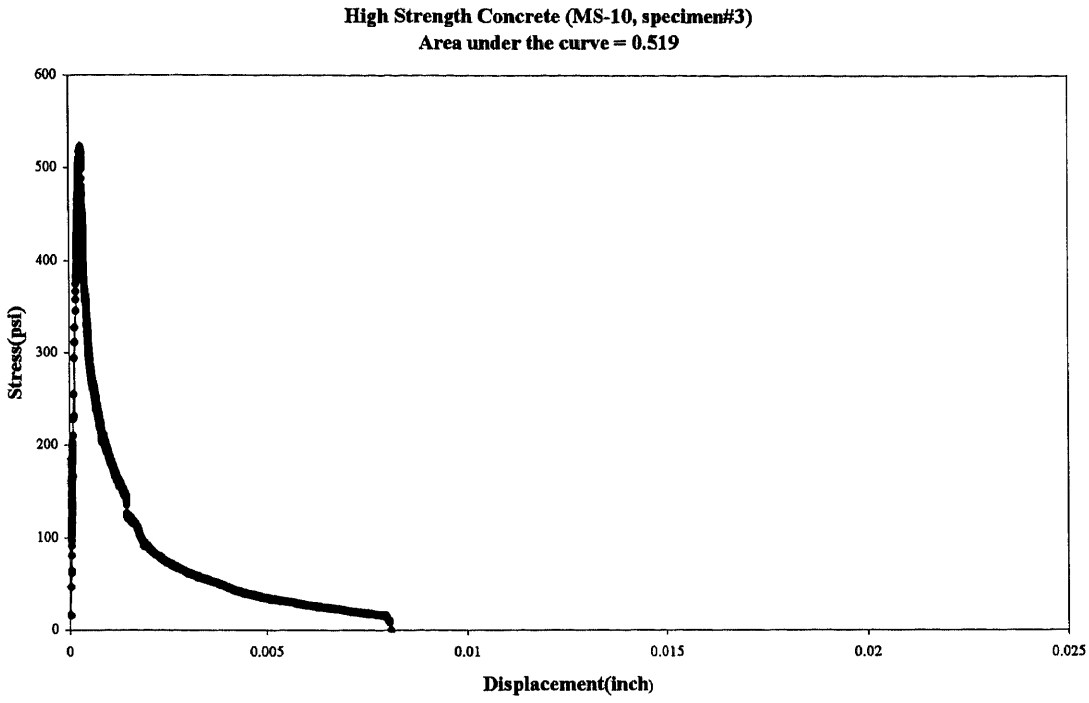
High Strength Concrete (MS-10, specimen#3)
Area under the curve = 0.519
Stress(psi)
600
500
400
300
200
100
0
0
0.005
0.01
0.015
0.02
0.025
Displacement(inch)

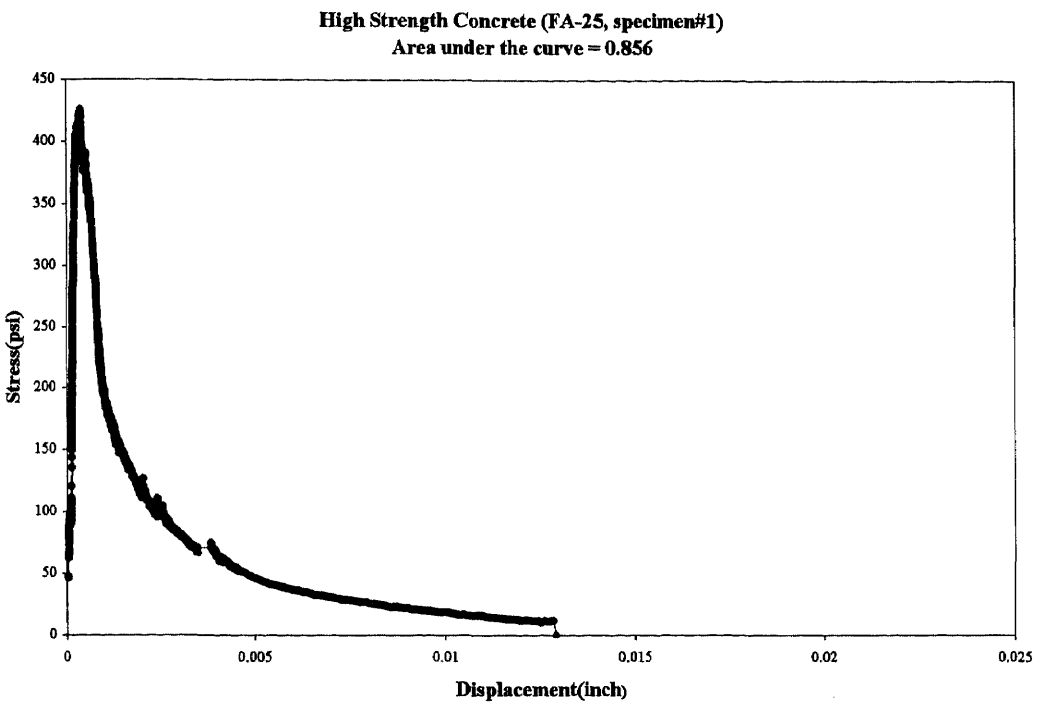
High Strength Concrete (FA-25, specimen#1)
Area under the curve = 0.856
Stress(psi)
450
400
350
300
250
200
150
100
50
0
0
0.005
0.01
0.015
0.02
0.025
Displacement(inch)

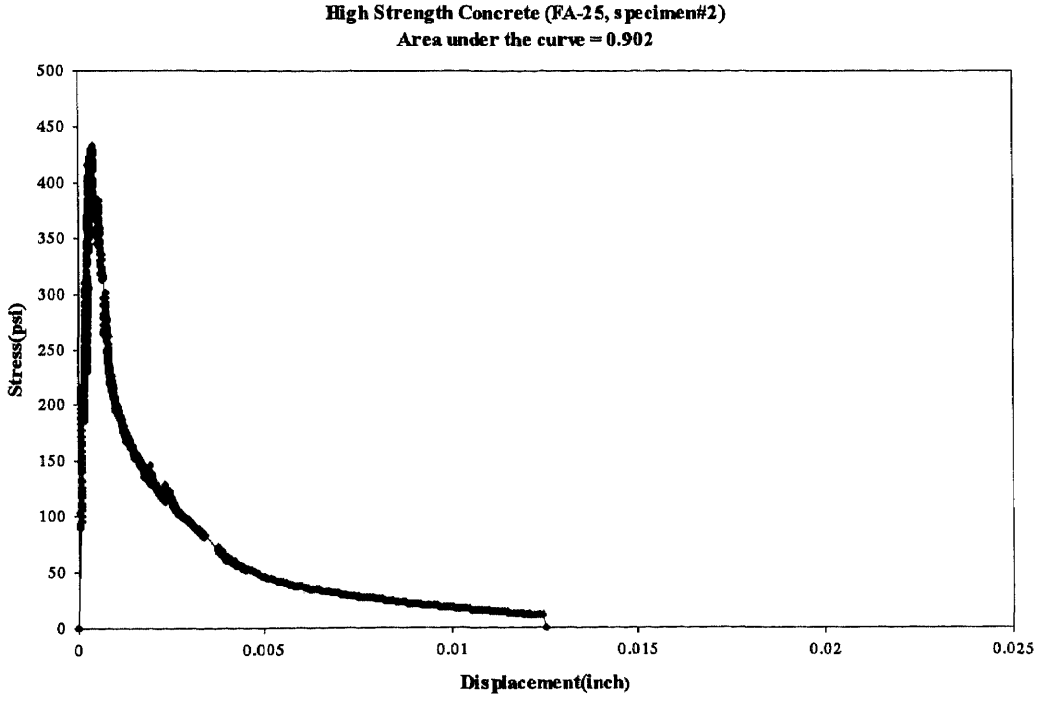
High Strength Concrete (FA-25, specimen#2)
Area under the curve = 0.902
Stress(psi)
500
450
400
350
300
250
200
150
100
50
0
0
0.005
0.01
0.015
0.02
0.025
Displacement(inch)

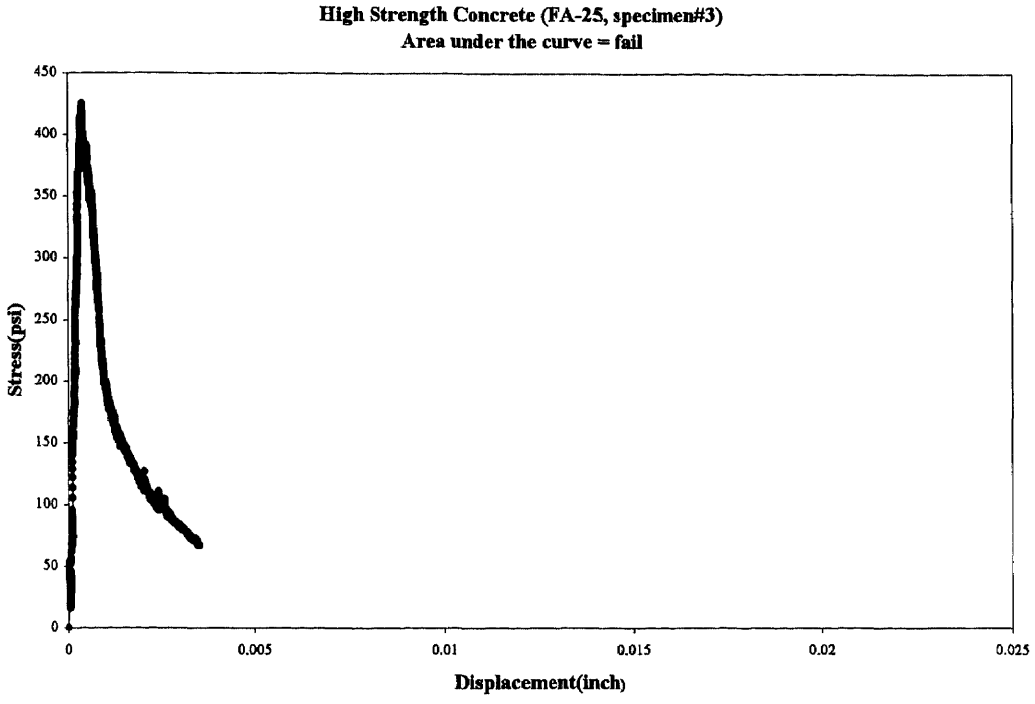
High Strength Concrete (FA-25, specimen#3)
Area under the curve = fail
Stress(psi)
450
400
350
300
250
200
150
100
50
0
0
0.005
0.01
0.015
0.02
0.025
Displacement(inch)

High Strength Concrete (FA-35, specimen#1)
Area under the curve = 0.497

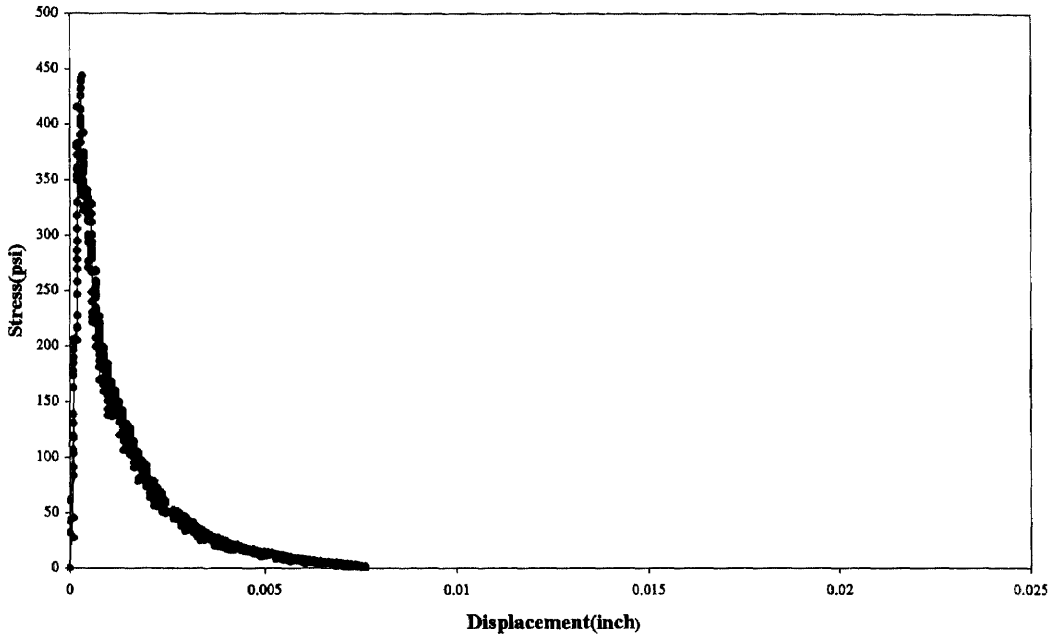

High Strength Concrete (FA-35, specimen#2)
Area under the curve = 0.516

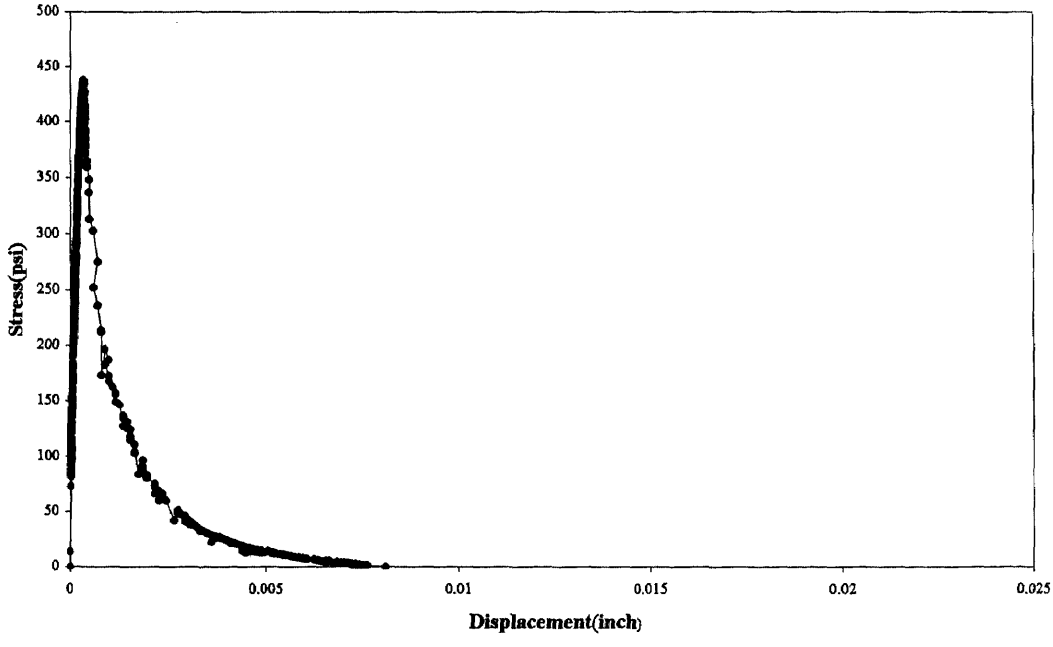

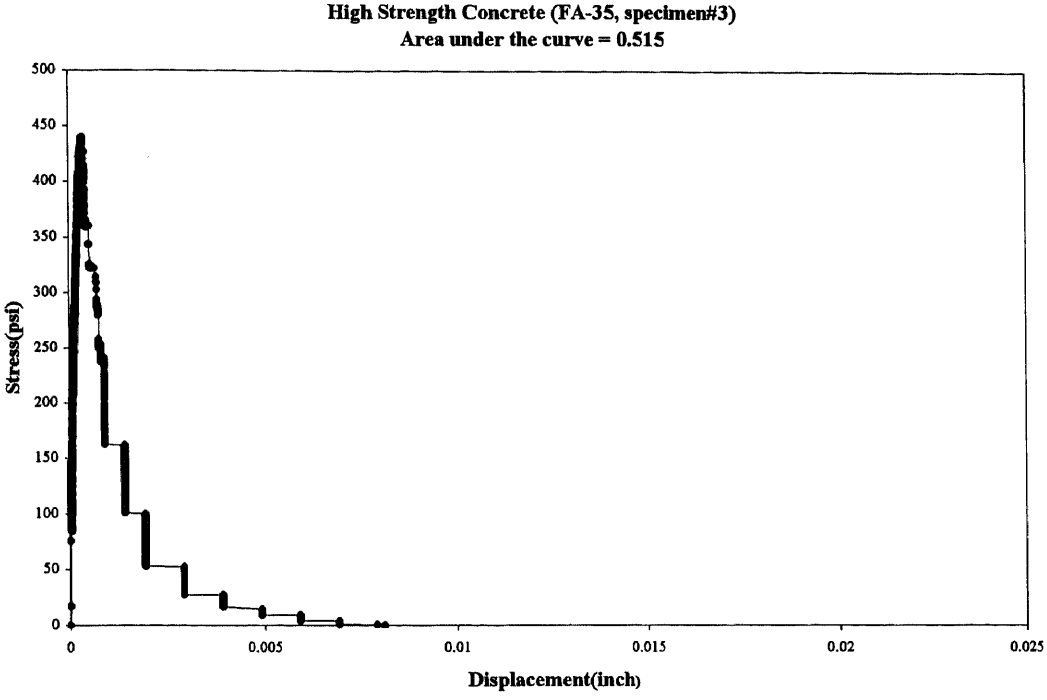
High Strength Concrete (FA-35, specimen#3)
Area under the curve = 0.515
Stress(psi)
500
450
400
350
300
250
200
150
100
50
0
0
0.005
0.01
0.015
0.02
0.025
Displacement(inch)

Normal strength fibrous concrete (specimen#1)
Area under the curve = 12.422

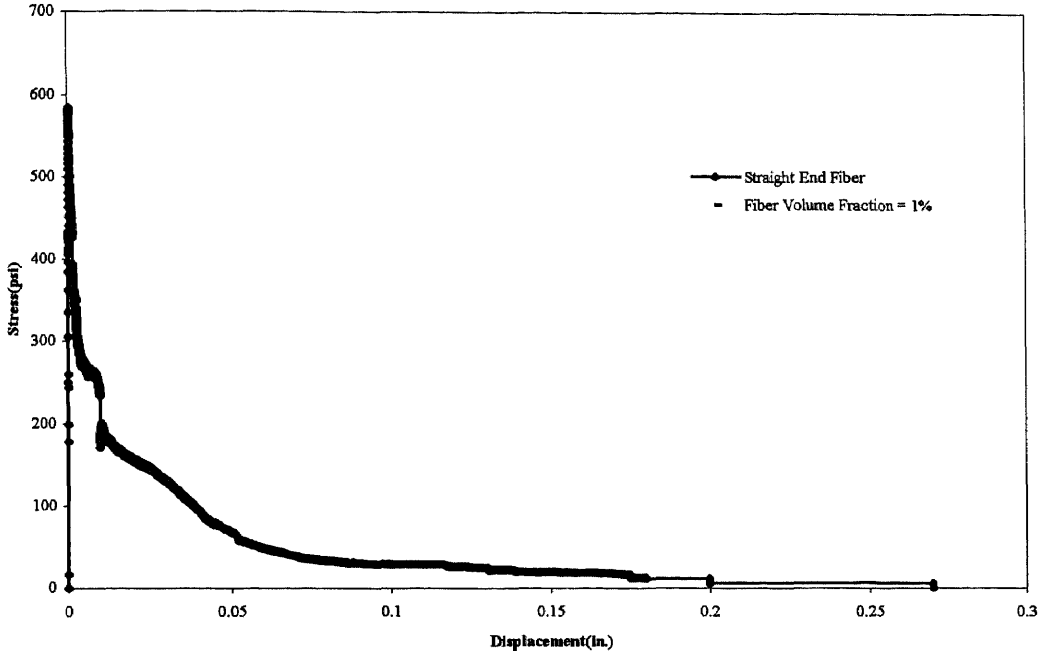

Normal strength fibrous concrete (specimen#2)
Area under the curve = 12.186

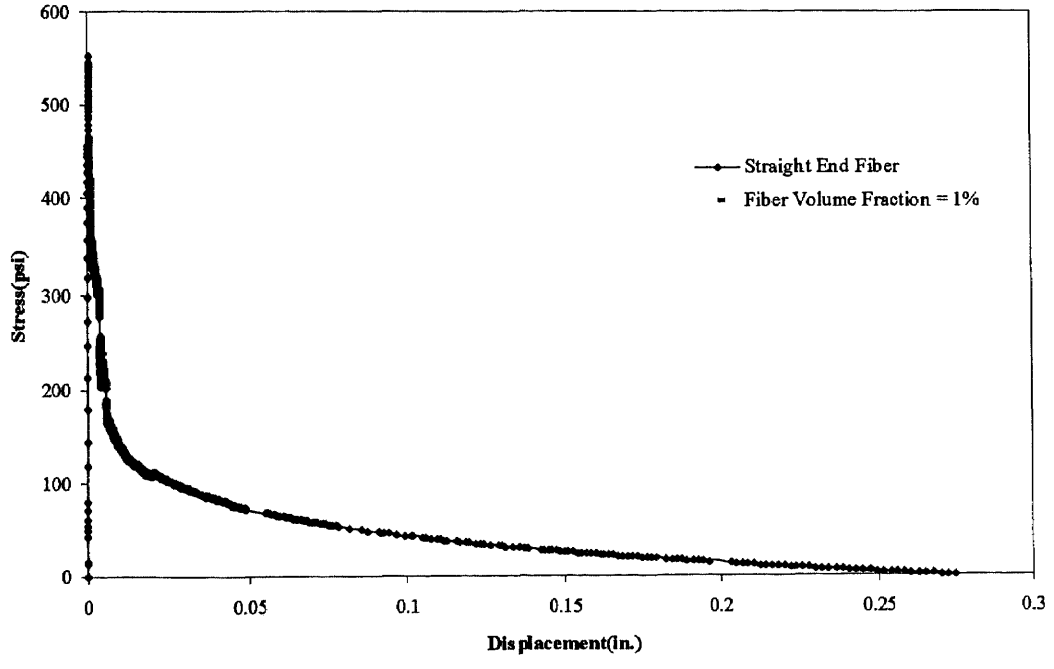

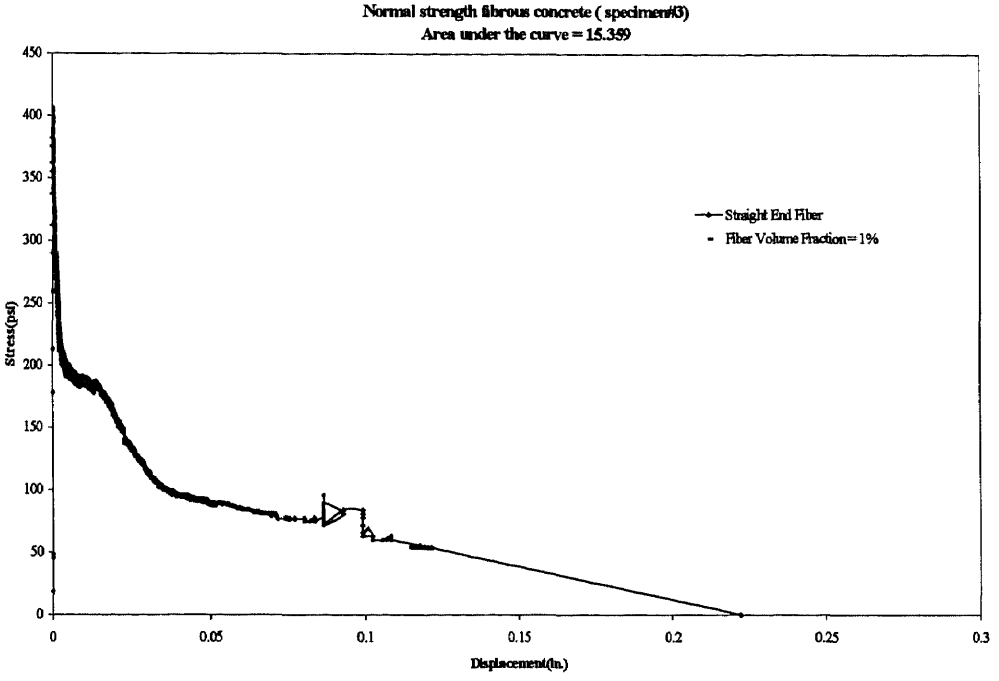
Normal strength fibrous concrete (specimen#3)
Area under the curve = 15.359
Straight End Fiber
Fiber Volume Fraction = 1%
Stress(psi)
Displacement(In.)
450
400
350
300
250
200
150
100
50
0
0
0.05
0.1
0.15
0.2
0.25
0.3

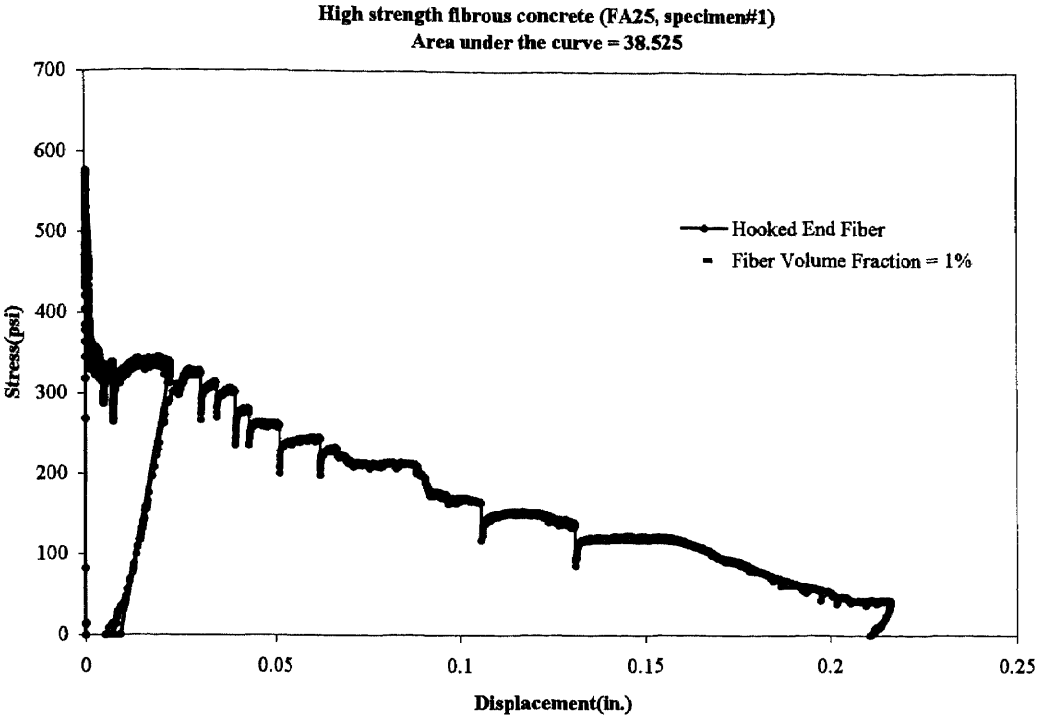
High strength fibrous concrete (FA25, specimen#1)
Area under the curve = 38.525
Stress(psi)
Displacement(in.)
Hooked End Fiber
Fiber Volume Fraction = 1%
0
100
200
300
400
500
600
700
0
0.05
0.1
0.15
0.2
0.25

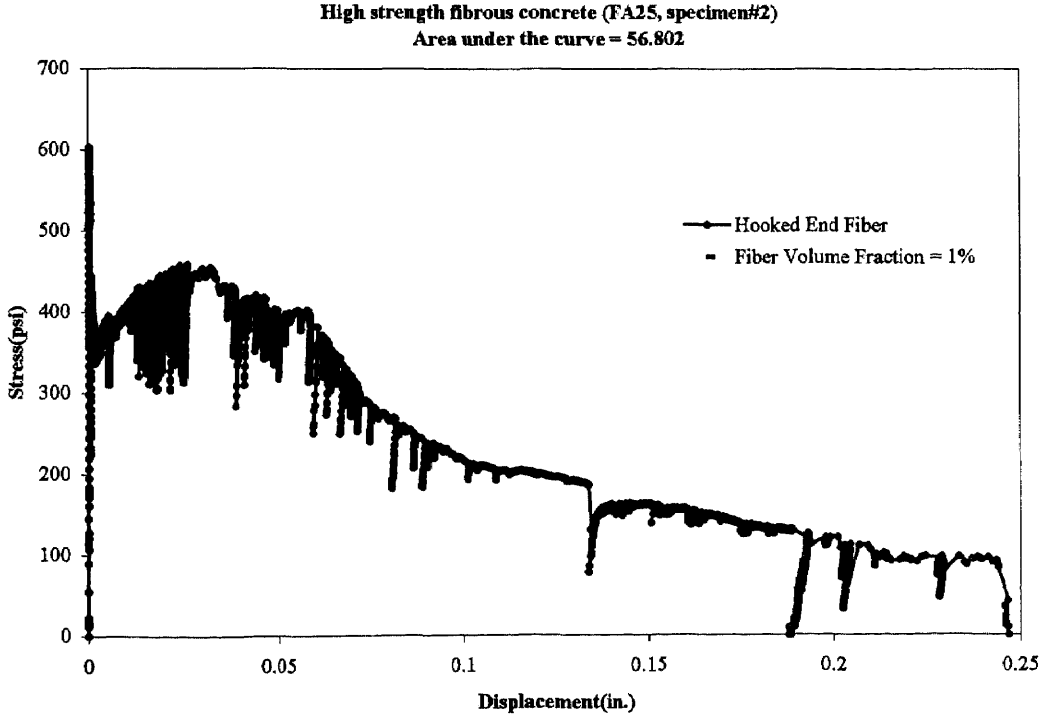
High strength fibrous concrete (FA25, specimen#2)
Area under the curve = 56.802
Stress(psi)
Displacement(in.)
Hooked End Fiber
Fiber Volume Fraction = 1%
0
100
200
300
400
500
600
700
0
0.05
0.1
0.15
0.2
0.25

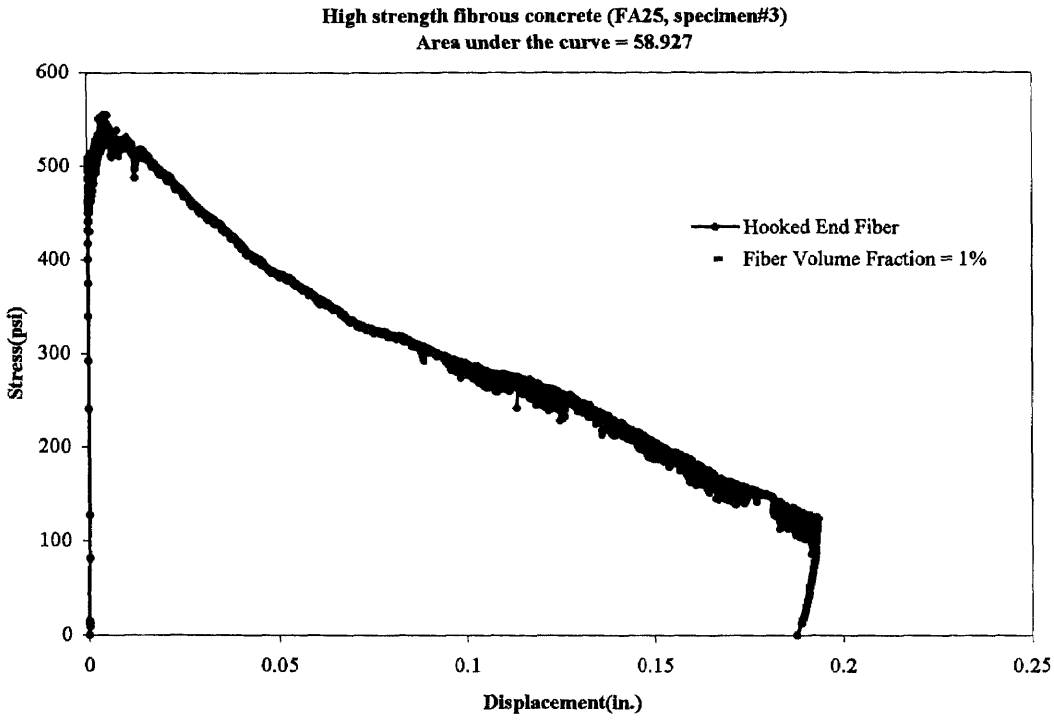
High strength fibrous concrete (FA25, specimen#3)
Area under the curve = 58.927
600
500
400
300
200
100
0
Stress(psi)
0
0.05
0.1
0.15
0.2
0.25
Displacement(in.)
Hooked End Fiber
Fiber Volume Fraction = 1%

APPENDIX C

EXPERIMENTAL RESULTS OF FLEXURAL BEAM TESTS

Load-Deflection Curve for Beam No. A001

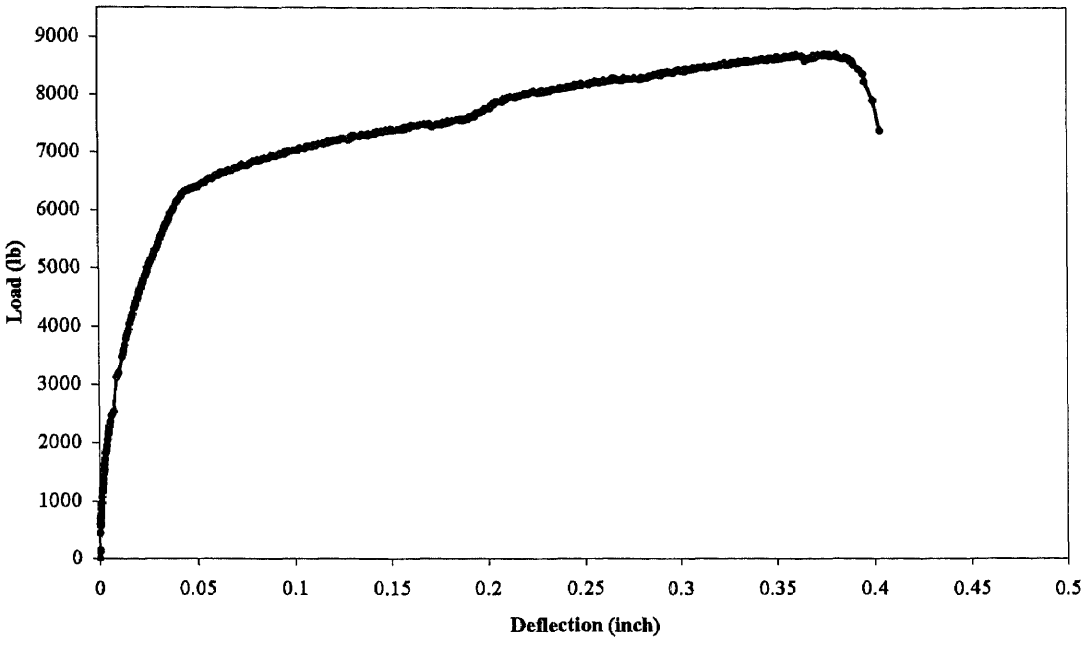

Load-Deflection Curve for Beam No. A002

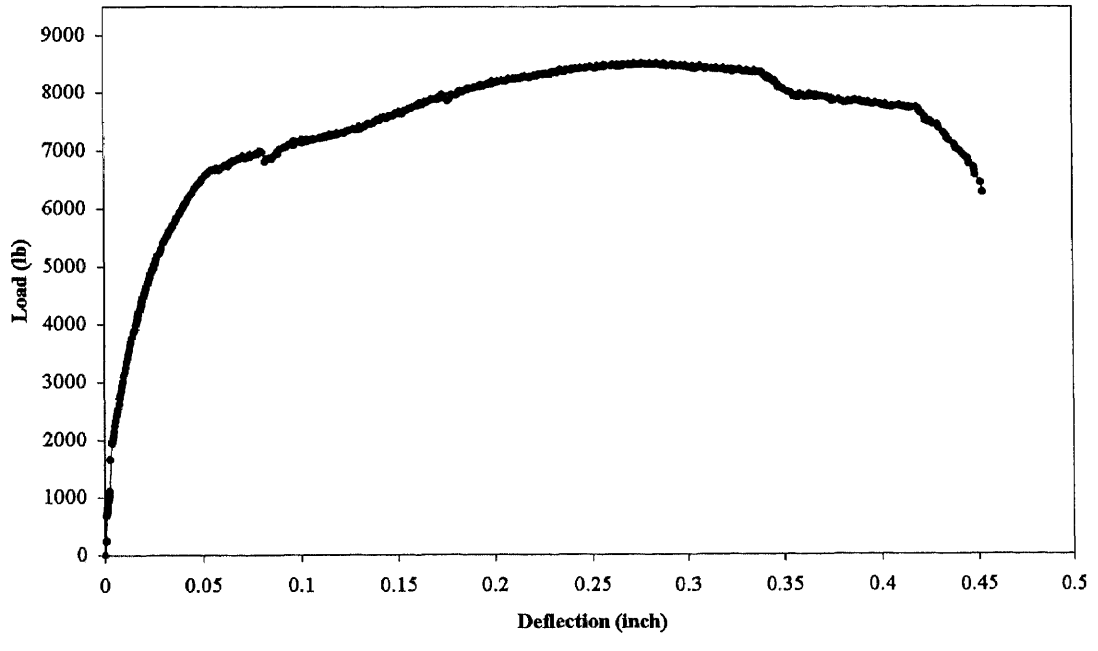

Load-Deflection Curve for Beam No. B101

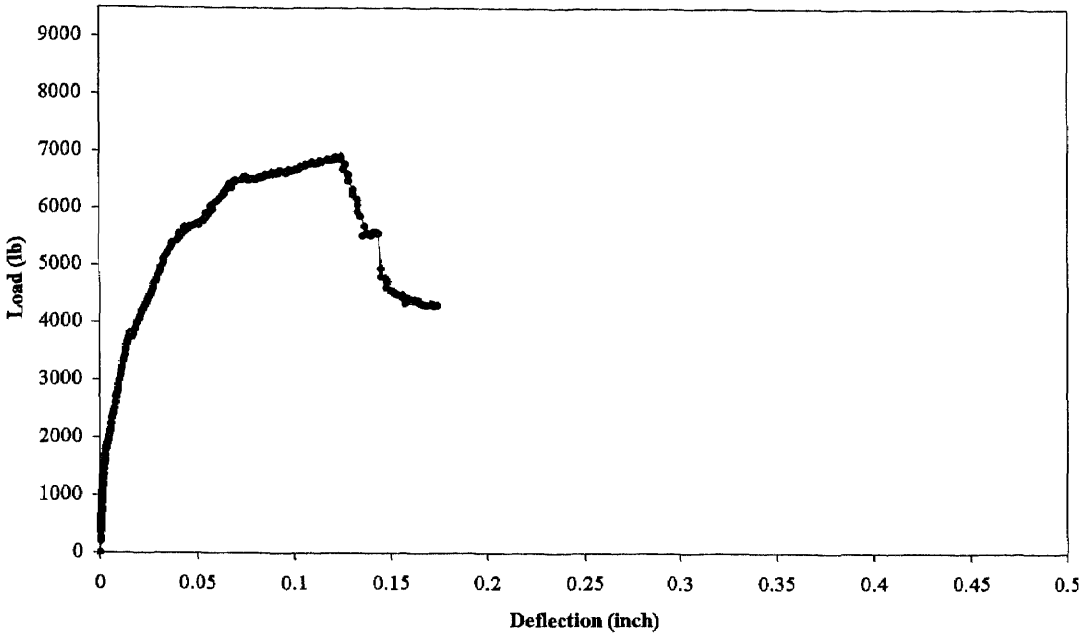

Load-deflection Curve for Beam No.B102

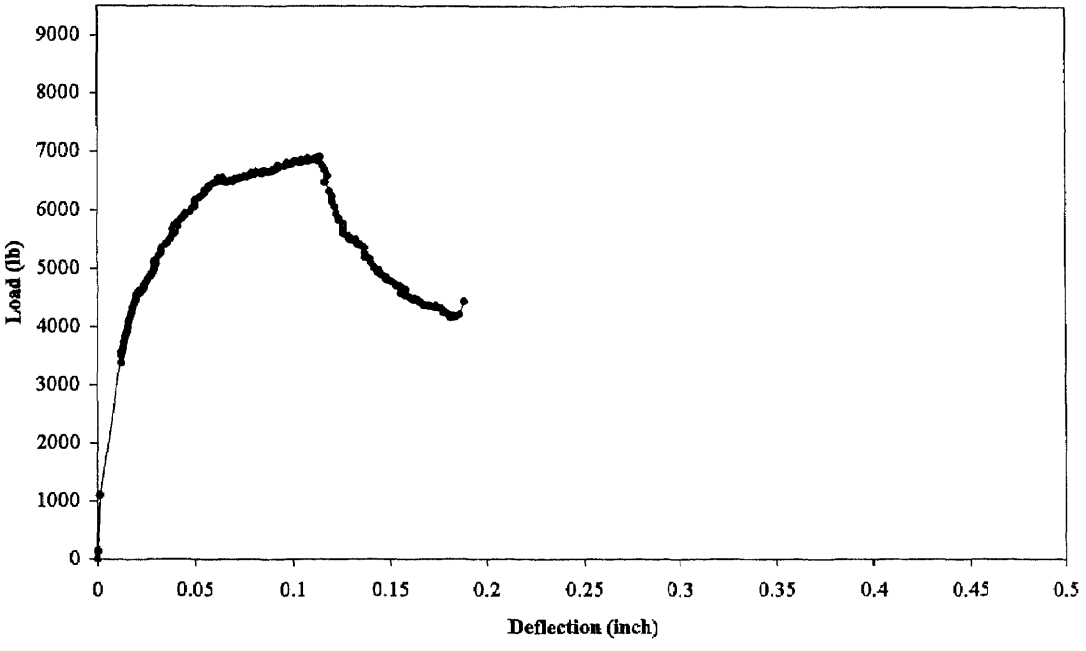

Load-Deflection Curve for Beam No.C201

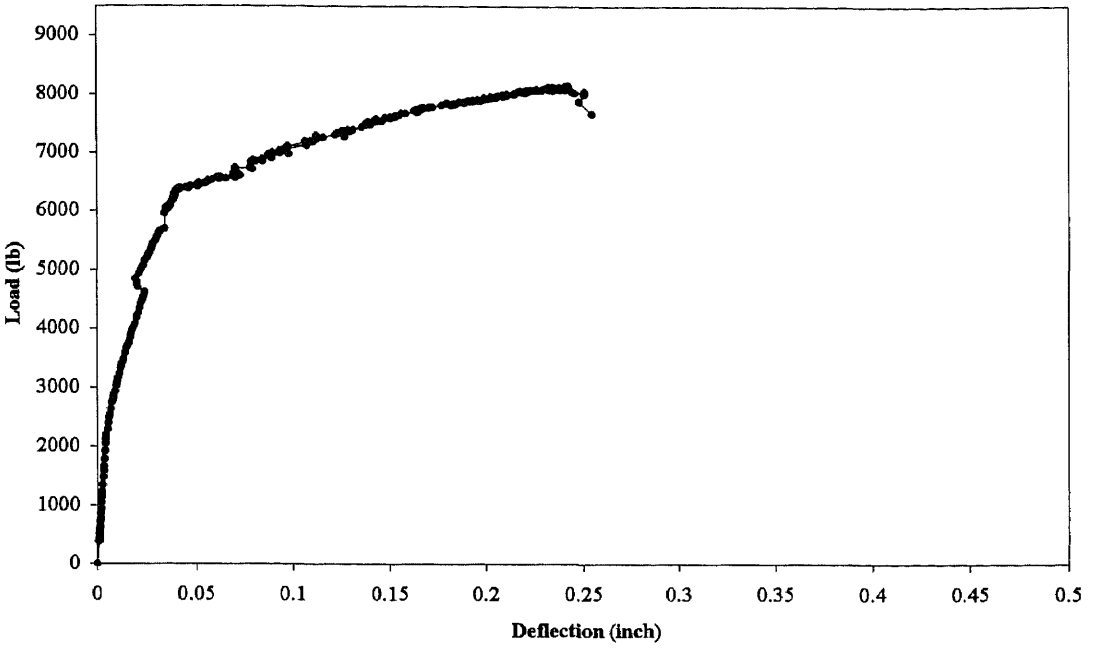

Load-Deflection Curve for Beam No.C202

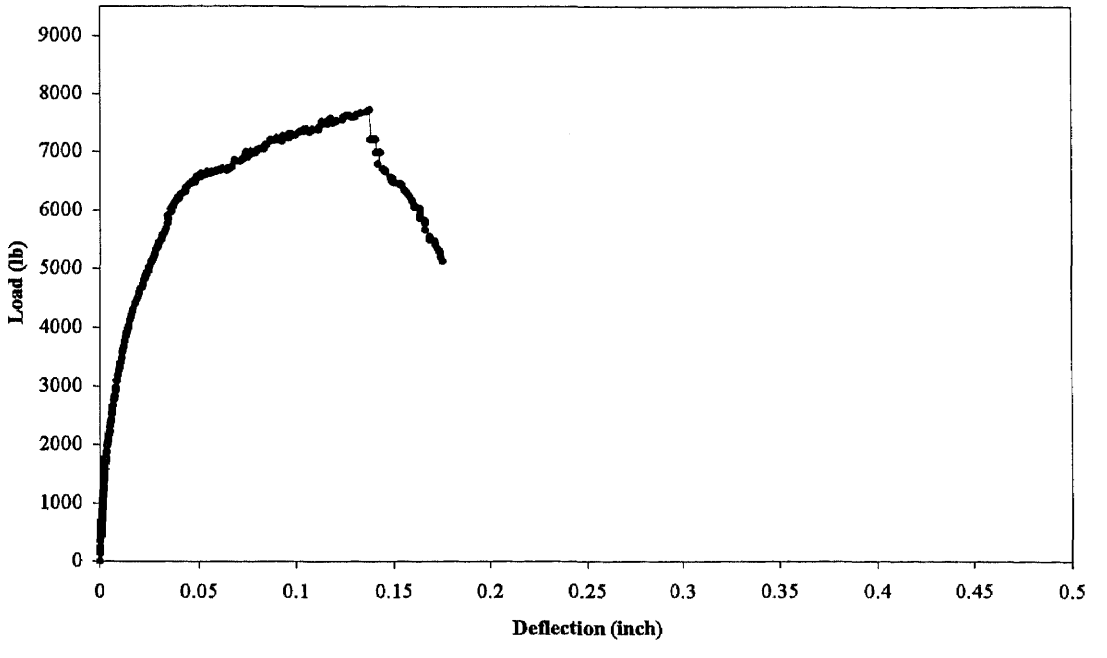

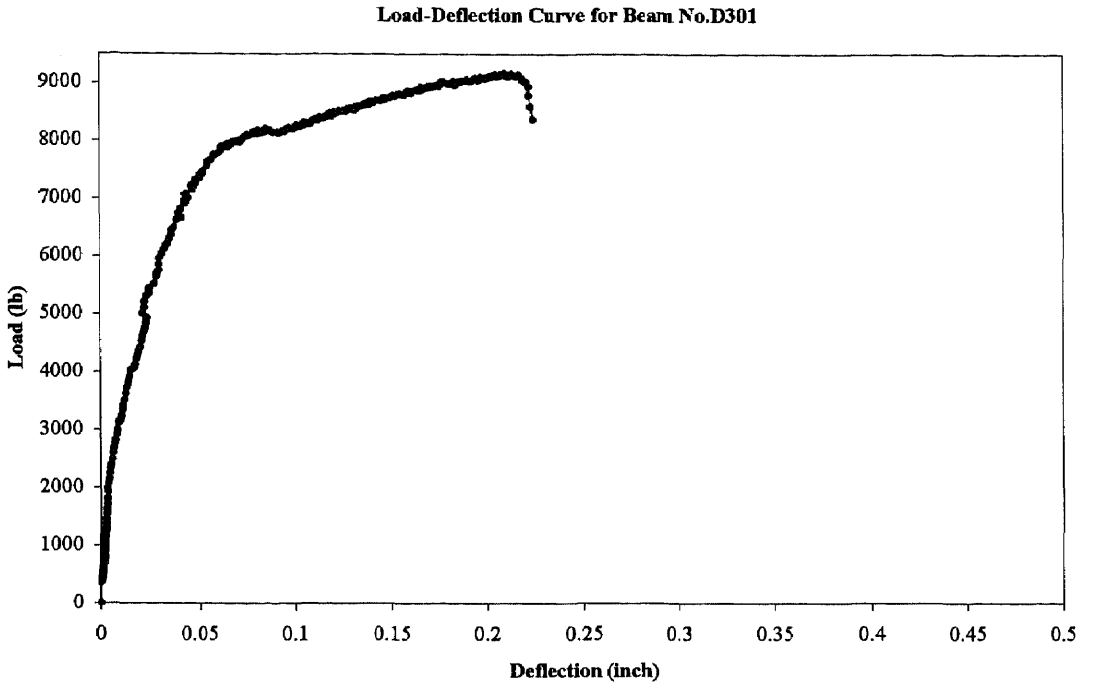
Load-Deflection Curve for Beam No.D301
Load (lb)
9000
8000
7000
6000
5000
4000
3000
2000
1000
0
0
0.05
0.1
0.15
0.2
0.25
0.3
0.35
0.4
0.45
0.5
Deflection (inch)

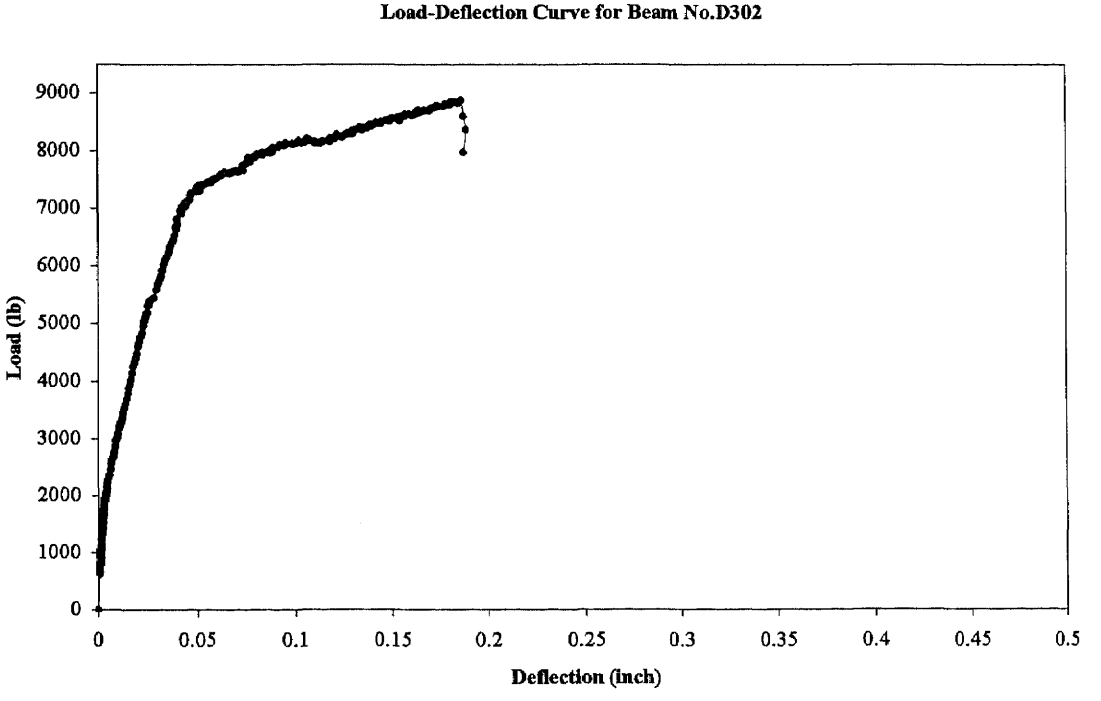
Load-Deflection Curve for Beam No.D302
Load (lb)
9000
8000
7000
6000
5000
4000
3000
2000
1000
0
0
0.05
0.1
0.15
0.2
0.25
0.3
0.35
0.4
0.45
0.5
Deflection (inch)

REFERENCES

ACI committee 363, 1984. "State-of-the-art Report on High-Strength Concrete" *Journal of American Concrete Institute,* July-August, pp.364-411.

Baalbaki, M., Sarkar, S.L., Aitcin, P. -C., and Isabelle, H., 1992."Properties and Microstructure of High-performance Concrete Containing Silica Fume and Fly Ash." *Fly Ash, Silica Fume, Slag and Natural Pozzolans in Concrete,* SP-132, *ACI,* Detroit, pp.121-142.

Bazant, Z.P., and Oh, B.H., 1984. "Deformations of Progressively Cracking Reinforced Concrete." *ACI Structural Journal,* May, V. 81, pp.268-278.

Cedolin, L., Sandro, D.P., and Iori I., 1987. " Tensile Behavior of Concrete." *Journal of Engineering Mechanics,* ASCE, V.113, No.3, March, pp.431-439.

Chimamphant, S., 1989. "Bond And Fatigue Characteristics of High Strength Cement-Based Composites." *Ph.D. Dissertation,* Department of Civil and Environmental Engineering, New Jersey Institute of Technology, Newark, NJ 07102, 312p.

Cintora, T., 1987. "Softening Response of Concrete in Direct Tension." *M.S. Thesis* Department of Civil and Environmental Engineering, New Jersey Institute of Technology, Newark, NJ 07102, 79p.

Djellouli, H., Aitcin, P. -C., and Chaallal, O., 1990. "The Use of Ground Granulated Slag in High-performance Concrete." *Utilization of High-Strength Concrete-Second, International Symposium, SP-121, ACI,* Detroit, pp.351-368.

Dugdale, D.S., 1960. "Yielding of Steel Sheets Containing Slits." *Journal of Mechanics and Physics of Solids,* V.8, pp.100-108.

Evans, R.H., and Marathe M.S., 1968. "Microcracking and Stress-Strain Curves for Concrete in Tension." *Material and Structure,* V.1, pp.61-64.

Gajanan, M.S., Harry, G.H., and Richard N.W., 1983. " Structural Modeling and Experimental Techniques." *Structural Modeling and Experimental Techniques* Prentice-Hall Civil Engineering and Engineering Mechanics Series, pp. 8-12.

Gopalaratnum, V.S., and Shah, S.P., 1985. "Softening Response of Plain Concrete in Direct Tension." *ACI Journal,* Proceedings V.82, No.3, May-June, pp.310-323.

Griffifth, A., 1924. "Theory of Rupture." *Proceedings, 1st International Congress on Applied Mechanics,* Delft, Australia: pp.55-63.

Hillerborg, A., 1985. " The theoretical basis of a method to determine the fracture energy G_f of concrete." *Rilem Technical Committees 50,* pp. 291-296.

Hillerborg, A., 1988. "Existing Methods to determine and evaluate fracture toughness of aggregate material-Rilem recommendation on concrete." *International Workshop on Fracture Toughness and Fracture Energy; Test Methods for Concrete and Rock,* October12-14, pp.121-127.

Hordijik, D.A., 1992. "Tensile and tensile fatigue behavior of concrete; experiments, modeling and analyses." *Heron,* V.37, No.1, 79p.

Hordijik, D.A., Reinhardt, H.W., 1988. "Influence of Load history on mode I fracture of Concrete." *International Workshop on Fracture Toughness and Fracture Energy; Test Methods for Concrete and Rock,* October 12-14, pp 26-36.

Hsu, L.S.M., and Hsu, C. -T. T., 1994. "Complete Stress-Strain Behavior of High Strength Concrete Under Compression." *Magazine of Concrete Research,* V. 46, No.169, pp.301-312.

Hughes, B.P., and Chapman, G.P., 1966. "The Complete Stress-Strain Curve for Concrete in Direct Tension." *Bulletin RILEM,* No. 30, pp.95-97.

John, R., and Shah, S.P., 1989. "Fracture Mechanics Analysis of High Strength Concrete." *Journal of Material in Civil Engineering, ASCE,* V.1, No.4, pp.185-198.

Kaplan, M.F., 1961. "Crack propagation and the Fracture of Concrete." *ACI Journal,* V. 58, No.11, pp.591-610.

Kasperkiewicz, J., 1986. "Fracture and Crack propagation energy in plain concrete." *Heron,* V.31, No.2, pp.5-14.

Li, Z., Li, F., Chang, T. -Y.P., and Mai, Y. -W., 1998. "Uniaxial Tensile Behavior of Concrete Reinforced with randomly distributed short fibers." *ACI Material Journal*, V. 95, No.5, September-October, pp.564-574.

Loland, K.E., and Gjorv, O.E., 1985. "Ductility of concrete and tensile behavior." *Nordic Concrete Research,* No.4, December, pp. 122-135.

Montgomery, D., and Diamond, S., 1984. "The influence of fly ash on the details of cracking in fly ash-bearing cement pastes." *Cement and Concrete Research,* V1.4, pp. 767-775.

Navalurkar, R.K., 1996. "Fracture Mechanics of High Strength Concrete Members." *Ph.D. Dissertation,* Department of Civil and Environmental Engineering, New Jersey Institute of Technology, Newark, NJ 07102, p203.

Navalurkar, R.K., Hsu, C. -T.T, Kim, S.K., and Wecharatana, M., 1999. "True Fracture Energy of Concrete." *ACI Material Journal*, V. 96, No.2, March-April, pp.213-225.

Rammel, G., 1990. "Study on Tensile Fracture Behavior by means of Bending Tests on High-Strength Concrete (HSC)." *Darmstadt Concrete,* Annual Journal on Concrete And Concrete Structures, V.5, pp.155-162.

Raphael, M. 1984. "Tensile strength of concrete." *ACI Journal*, V. 81, March-April, pp.158-165.

Reinhardt, H.W., 1984. "Fracture Mechanics of an Elastic Softening Material like Concrete." *Heron,* V.29, No.2, p42.

Reinhardt, H.W., Cornelissen, H.A.W., and Hordijik, D.A., 1986. "Tensile Tests and Failure Analysis of Concrete." *Journal of Structural Engineering,* ASCE, V.112, No.11, November, pp.2462-2477.

Roy, H.E.H., and Meta, A.Z, 1964. " Ductility of concrete." *Flexural Mechanics of Reinforced Concrete; Proceedings of the International Symposium*, ASCE-ACI, November10-12, pp. 213-236.

Ryell, J., and Bickley, J.A., 1987."Scotia Plaza: High-Strength Concrete for Tall Buildings." *Proceeding on the Utilization of High-Strength Concrete,* Stavanger, Norway, pp.641-653.

Saucier, K. L., 1979. " High-Strength Concrete, Past, Present, Future" *Paper presented at the 1979 Annual Convention,* ACI, Milwaukee, Wisconsin, March 18-23, pp. 239-251.

Shin, S. -W., Kamara, M., and Ghosh S.K., 1990. " Flexural Ductility, Strength Prediction, and Hysteric Behavior of Ultra-High-Strength Concrete Members." *High-Strength Concrete; Second International Symposium 121*, ACI, pp. 239-251.

Shin, S. -W., Satyendra, K.G., and Jaime, M., 1989. " Flexural Ductility of Ultra High-Strength Concrete Members." *ACI Structural Journal,* July-August, V. 86, pp.394-400.

Toutanji, H.A., and El-Korchi, T. 1994. "Uniaxial Tensile Strength of Cementitious Composites." *Journal of Testing and Evaluation, JTEVA*, V.22, No.3, May, pp.226-232.

Van, Mier., J.G.M., 1995. "Fracture Mechanics Application: will applications start to emerge." *Heron,* V.40 No.2, pp.147-162

Wecharatana, M., 1986. "Specimen Size Effects on Non-linear Fracture Parameters in Concrete." *Fracture Toughness and Fracture Energy of Concrete*, Elsevier Science Publishers B.V., New York., pp.437-441.

Wecharatana, M., 1990. "Brittleness Index of Cementitious Composites." *Serviceability And Durability of Construction Materials: Proceedings of the First Materials Engineering Congress,* ASTM, pp.966-975.